

การปลูกผลึก สารอินทรีย์ สารอินทรีย์ และสารกึ่งอินทรีย์ แบบไม่เป็นเชิงเส้น  
โดยวิธี สานครานรายนาน รามาชามี และการกำหนดลักษณะเฉพาะ

นายอุฤทธิ์ เจริญอินทร์

วิทยานิพนธ์นี้เป็นส่วนหนึ่งของการศึกษาตามหลักสูตรปริญญาวิทยาศาสตรดุษฎีบัณฑิต  
สาขาวิชาฟิสิกส์  
มหาวิทยาลัยเทคโนโลยีสุรนารี  
ปีการศึกษา 2553

**GROWTH OF SOME INORGANIC, ORGANIC AND  
SEMI-ORGANIC NONLINEAR OPTICAL CRYSTALS  
BY SANKARANARAYANAN-RAMASAMY METHOD  
AND THEIR CHARACTERIZATION**

**Urit Charoen-In**

**A Thesis Submitted in Fulfillment of the Requirements for the  
Degree of Doctor of Philosophy in Physics  
Suranaree University of Technology  
Academic Year 2010**

**GROWTH OF SOME INORGANIC, ORGANIC AND  
SEMI-ORGANIC NONLINEAR OPTICAL CRYSTALS  
BY SANKARANARAYANAN-RAMASAMY METHOD  
AND THEIR CHARACTERIZATION**

Suranaree University of Technology has approved this thesis submitted in partial fulfillment of the requirements for the Degree of Doctor of Philosophy.

Thesis Examining Committee

\_\_\_\_\_  
(Asst. Prof. Dr. Chinorat Kobdaj)

Chairperson

\_\_\_\_\_  
(Assoc. Prof. Dr. Prapun Manyum)

Member (Thesis Advisor)

\_\_\_\_\_  
(Dr. Hideki Nakajima)

Member

\_\_\_\_\_  
(Asst. Prof. Dr. Rattikorn Yimnirun)

Member

\_\_\_\_\_  
(Dr. Saroj Rujirawat)

Member

\_\_\_\_\_  
(Prof. Dr. Sukit Limpijumnong)

Vice Rector for Academic Affairs

\_\_\_\_\_  
(Assoc. Prof. Dr. Prapun Manyum)

Dean of Institute of Science

อุทุทธิ์ เจริญอินทร์ : การปลูกผลึก สารอนินทรีย์ สารอินทรีย์ และสารกึ่งอินทรีย์ แบบไม่  
เป็นเชิงเส้น โดยวิธีसानครานรายานาน รามาซามี และการกำหนดลักษณะเฉพาะ  
(GROWTH OF SOME INORGANIC, ORGANIC AND SEMI-ORGANIC  
NONLINEAR OPTICAL CRYSTALS BY SANKARANARAYANAN-RAMASAMY  
METHOD AND THEIR CHARACTERIZATION) อาจารย์ที่ปรึกษา: รองศาสตราจารย์  
ดร.ประพันธ์ แม่นยำ. 168 หน้า.

ผลึกเดี่ยวของสารอนินทรีย์ กรดซัลฟามิก (Sulphamic acid) สารอินทรีย์ เอล อลานินเนียม  
มาเลต (L-alaninium maleate) เอล อาจีนิน มาเลต ไดไฮเดต (L-arginine maleate dihydrate) และ  
สารกึ่งอินทรีย์ เอล โพลีน ซิงค์ คลอไรด์ (L-proline zinc chloride) ปลูกขึ้น โดยวิธีการปลูกผลึก  
แบบ สานครานรายานาน รามาซามี และวิธีการปลูกผลึกแบบดั้งเดิม ผลึกที่ได้จากการทดลอง ถูก  
นำมาศึกษาสมบัติเฉพาะด้านต่างๆ โดยเทคนิคที่ใช้ในการศึกษาสมบัติเฉพาะของสาร ได้แก่  
การศึกษาการเลี้ยวเบนของรังสีเอกซ์แบบผลึกเดี่ยว การศึกษาการเลี้ยวเบนของรังสีเอกซ์ แบบความ  
เข้มสูง การศึกษาลักษณะการเกิดมลทินเมื่อพื้นผิวของผลึกถูกละลายโดยตัวทำละลาย การศึกษา  
สมบัติไดอิเล็กตริก การศึกษาสมบัติเพียโซอิเล็กตริก การศึกษาสมบัติทางความร้อน การศึกษาการ  
ส่องผ่านของแสง การศึกษาความแข็ง และการศึกษาพฤติกรรมการเกิดฮาโมนิกที่สอง และได้นำผล  
การศึกษามาวิเคราะห์และเปรียบเทียบ ถึงลักษณะของผลึกที่ได้จากการปลูกทั้งสองวิธี การศึกษา  
การเลี้ยวเบนของรังสีเอกซ์แบบผลึกเดี่ยว ข้อมูลที่ได้สามารถยืนยัน โครงสร้างของผลึกที่ได้จาก  
ทดลอง มีลักษณะเหมือนกับที่เคยมีการรายงานมาแล้ว ความสมบูรณ์ของผลึกได้รับการยืนยัน จาก  
การศึกษาเลี้ยวเบนของรังสีเอกซ์แบบความเข้มสูง จำนวนความหนาแน่นของมลทินในผลึก ถูก  
คำนวณจากการกระจายตัวของมลทินที่เกิดขึ้นหลังจากการละลายผิวหน้าของผลึก ค่าคงที่ไดอิเล็ก-  
ตริกและไดอิเล็กตริก ลอส วัดอยู่ในรูปฟังก์ชันของอุณหภูมิ ที่อุณหภูมิในช่วง 40 ถึง 140 องศา  
เซลเซียส สัมประสิทธิ์ประจุ เพียโซอิเล็กตริก ของผลึกคำนวณจากแรงที่กระทำกับผลึก การทน  
ความร้อนของผลึกวัดจากการศึกษาสมบัติทางความร้อนของผลึก การส่องผ่านของแสงแสดงใน  
รูปแบบการบันทึกค่า UV-Vis-NIR ความแข็งของผลึกวิเคราะห์จากการทดสอบ Vickers  
microhardness การวัดฮาร์โมนิกที่สองของผลึกที่ความยาวคลื่นพื้นฐาน 1064 นาโนเมตร ได้นำมา  
เปรียบเทียบกับค่าฮาร์โมนิกที่สองของผลึก KDP

สาขาวิชาฟิสิกส์  
ปีการศึกษา 2553

ลายมือนักศึกษา \_\_\_\_\_  
ลายมืออาจารย์ที่ปรึกษา \_\_\_\_\_

URIT CHAROEN-IN : GROWTH OF SOME INORGANIC, ORGANIC  
AND SEMI-ORGANIC NONLINEAR OPTICAL CRYSTALS BY  
SANKARANARAYANAN-RAMASAMY METHOD AND THEIR  
CHARACTERIZATION. THESIS ADVISOR : ASSOC. PROF.  
PRAPUN MANYUM, D.Phil. 168 PP.

GROWTH FROM SOLUTION/SINGLE CRYSTAL GROWTH/HIGH  
RESOLUTION X-RAY DIFFRACTION/ DEFECT/OPTICAL MICROSCOPY  
/DIELECTRIC MATERIALS

Single crystals of some inorganic, sulphamic acid (SA) organic, L-alaninium maleate (LAM), L-arginine maleate dihydrate (LAMD) and semiorganic, L-proline zinc chloride (LPZ) were successfully grown by Sankaranarayanan-Ramasamy (SR) method and conventional slow evaporation solution technique. The grown SA, LAM, LAMD and LPZ crystals were subjected to single crystal X-ray diffraction, high resolution X-ray diffraction (HRXRD), chemical etching, dielectric, piezoelectric, Thermo gravimetric-differential thermal analysis, UV-Vis-NIR Vickers microhardness and second harmonic generation (SHG) efficiency study and their results were discussed. Single crystal X-ray diffraction confirmed the lattice parameters of the grown crystals. Crystalline perfection was observed from HRXRD analysis. Etch pit density of the grown crystals were calculated and the distribution of structural defect was observed in chemical etching studies. The dielectric constant and loss measurements were made as function of temperature in the range of 40-140 degree celsius. Piezoelectric charge coefficients of the grown crystal have been determined. From thermo gravimetric-differential thermal analysis of the grown

crystals the thermal stability was investigated. The range and percentage of optical transmission were represented by recording UV-Vis-NIR analysis. Mechanical strength of the grown crystals was analyzed by Vickers microhardness. SHG measurements indicated that the SHG efficiency of the grown crystals at a fundamental wavelength of 1064 nm was compared with that of KDP crystal.

School of Physics

Academic Year 2010

Student's Signature \_\_\_\_\_

Advisor's Signature \_\_\_\_\_

## ACKNOWLEDGEMENTS

The author places on record his deep sense of gratitude and indebtedness to his research supervisor Assoc. Prof. Dr. Prapun Manyum, Dean of Science, Suranaree University of Technology for having introduced him to this research field, concerted guidance and personal interest.

The author is beholden to his co-supervisor Prof. P. Ramasamy, Former CSIR-Emeritus Scientist, Centre for Crystal Growth SSN College, for his inspiring guidance, illimitable encouragement, passionate support, soaring scientific proficiency and profuse personal interest.

The authors are thankful to Dr. G. Bhagavannarayana, Head of Material Characterization Division, National Physical Laboratory, Dr. C.K. Mahadevan, Physics Research Centre, S.T. Hindu College, Dr. Binay Kumar, Department of Physics Astrophysics, University of Delhi and Prof. K. Kishan Rao, Department of Physics, Kakatiya University for their help and encouragement.

Profound thanks are due to Mr. Nakarin Pattanaboonme, Mr. Yuttapong Inkkong, Crystal Growth Laboratory Suranaree University of Technology, Mr. A. Senthil, Mr. P. Rajesh, Mr. M. Senthil Pandian, Mr. Senthil Murugun, Dr. G. Anandha Babu and other research scholar of Centre for Crystal Growth SSN College of Engineering for their timely help and support. The author is also thankful to University Staff Developme Scholarships from Mahasarakham University for financial support.

Urit Charoen-In

# CONTENTS

|  | <b>Page</b> |
|--|-------------|
| ABSTRACT IN THAI . . . . .                               | I           |
| ABSTRACT IN ENGLISH . . . . .                            | II          |
| ACKNOWLEDGEMENTS . . . . .                               | IV          |
| CONTENTS . . . . .                                       | V           |
| LIST OF TABLES . . . . .                                 | XI          |
| LIST OF FIGURES . . . . .                                | XII         |
| LIST OF ABBREVIATIONS . . . . .                          | XVI         |
| <b>CHAPTER</b>   |             |
| <b>I INTRODUCTION . . . . .</b>                          | <b>1</b>    |
| 1.1 Rationale of study . . . . .                         | 1           |
| 1.2 Research objective . . . . .                         | 6           |
| 1.3 Scope and limitation of the study . . . . .          | 7           |
| 1.4 References . . . . .                                 | 7           |
| <b>II REVIEW OF THE LITERATURE . . . . .</b>             | <b>10</b>   |
| 2.1 Crystal growth phenomena . . . . .                   | 10          |
| 2.1.1 Introduction . . . . .                             | 10          |
| 2.1.2 Nucleation . . . . .                               | 11          |
| 2.2 Crystal growth techniques . . . . .                  | 15          |
| 2.2.1 Low temperature solution growth . . . . .          | 16          |
| 2.2.2 Solution, solubility and supersolubility . . . . . | 16          |
| 2.2.3 Crystallization by slow cooling . . . . .          | 19          |

## CONTENTS (Continued)

|   | <b>Page</b> |
|---|-------------|
| 2.2.4 Crystallization by solvent evaporation . . . . .                            | 19          |
| 2.2.5 Material purification . . . . .   | 20          |
| 2.2.6 Solvent selection . . . . .   | 21          |
| 2.2.7 Preparation of solutions . . . . .  | 21          |
| 2.2.8 Seed preparation . . . . .  | 22          |
| 2.2.9 Cooling rate . . . . .  | 22          |
| 2.2.10 Harvesting of the grown crystals . . . . .                                 | 23          |
| 2.2.11 Crystal growth system . . . . .  | 23          |
| 2.3 Sankaranayanan-Ramasamy (SR) method . . . . .                                 | 24          |
| 2.3.1 SR method experimental setup . . . . .                                      | 25          |
| 2.3.2 Crystal quality analysis of SEST and SR methods grown<br>crystals . . . . . | 28          |
| 2.4 Nonlinear optical materials . . . . .   | 29          |
| 2.5 Classification of nonlinear optical crystal . . . . .                         | 33          |
| 2.5.1 Inorganic crystals . . . . .  | 33          |
| 2.5.2 Organic crystals . . . . .  | 33          |
| 2.5.3 Semi-organic crystals . . . . .   | 36          |
| 2.6 Characterization . . . . .  | 38          |
| 2.6.1 Single-crystal X-ray diffraction . . . . .                                  | 38          |
| 2.6.2 High resolution X-ray diffraction . . . . .                                 | 42          |
| 2.6.3 Etching studies . . . . .   | 44          |
| 2.6.4 Thermal analysis . . . . .  | 45          |
| 2.6.5 Dielectric measurement . . . . .  | 47          |

## CONTENTS (Continued)

|  | Page      |
|--|-----------|
| 2.6.6 Piezoelectric measurement . . . . .                        | 54        |
| 2.6.7 UV-Vis spectrophotometry . . . . .                         | 56        |
| 2.6.8 Microhardness . . . . .                                    | 58        |
| 2.6.9 Nonlinear optical measurement technique . . . . .          | 61        |
| 2.7 References . . . . .   | 65        |
| <br><b>III UNIDIRECTIONAL GROWTH OF SULPHAMIC ACID</b>           |           |
| <b>SINGLE CRYSTAL AND ITS QUALITY ANALYSIS . . . . .</b>         | <b>70</b> |
| 3.1 Abstract . . . . .   | 70        |
| 3.2 Introduction . . . . .                                       | 71        |
| 3.3 Crystal growth . . . . .                                     | 72        |
| 3.4 Results and discussions . . . . .                            | 74        |
| 3.4.1 Chemical etching analysis . . . . .                        | 74        |
| 3.4.2 Mechanical strength analysis . . . . .                     | 75        |
| 3.4.3 High resolution X-ray diffraction analysis . . . . .       | 78        |
| 3.4.4 Optical studies . . . . .                                  | 80        |
| 3.4.5 Thermo gravimetric-Differential thermal analysis . . . . . | 83        |
| 3.5 Conclusions . . . . .  | 84        |
| 3.6 Acknowledgements . . . . .                                   | 85        |
| 3.7 References . . . . .   | 85        |
| <br><b>IV COMPARATIVE STUDY ON L-ALANINIUM MALEATE</b>           |           |
| <b>SINGLE CRYSTAL GROWN BY SANKARANARAYANAN-</b>                 |           |
| <b>RAMASAMY METHOD AND CONVENTIONAL SLOW</b>                     |           |
| <b>EVAPORATION SOLUTION TECHNIQUE . . . . .</b>                  | <b>90</b> |

## CONTENTS (Continued)

|  | <b>Page</b> |
|--|-------------|
| 4.1 Abstract . . . . .   | 90          |
| 4.2 Introduction . . . . .   | 91          |
| 4.3 Experiments . . . . .  | 92          |
| 4.3.1 Conventional method . . . . .  | 92          |
| 4.3.2 SR method . . . . .  | 94          |
| 4.4 Results and discussions . . . . .  | 96          |
| 4.4.1 Single crystal X-ray diffraction . . . . .   | 96          |
| 4.4.2 High resolution X-ray diffraction . . . . .  | 96          |
| 4.4.3 Chemical etching analysis . . . . .  | 99          |
| 4.4.4 Dielectric measurements . . . . .  | 101         |
| 4.4.5 Thermo gravimetric and differential thermal analysis . . . . .   | 104         |
| 4.4.6 UV-Vis NIR analysis . . . . .  | 106         |
| 4.4.7 Vickers microhardness test . . . . .   | 108         |
| 4.5 Conclusions . . . . .  | 111         |
| 4.6 Acknowledgements . . . . .   | 112         |
| 4.7 References . . . . .   | 112         |
| <b>V UNIDIRECTIONAL GROWTH OF L-ARGININE<br/>MALEATE DIHYDRATE SINGLE CRYSTAL AND ITS<br/>CHARACTERIZATION . . . . .</b> | <b>118</b>  |
| 5.1 Abstract . . . . .   | 118         |
| 5.2 Introduction . . . . .   | 119         |
| 5.3 Experimental procedures . . . . .  | 120         |
| 5.3.1 Synthesis and crystal growth . . . . .   | 120         |

## CONTENTS (Continued)

|  | <b>Page</b> |
|--|-------------|
| 5.4 Characterization . . . . .                       | 124         |
| 5.5 Results and discussions . . . . .                | 124         |
| 5.5.1 Single crystal X-ray diffraction . . . . .     | 124         |
| 5.5.2 Crystalline perfection . . . . .               | 125         |
| 5.5.3 Piezoelectric measurement . . . . .            | 127         |
| 5.5.4 Dielectric studies . . . . .                   | 127         |
| 5.5.5 Transmittance . . . . .                        | 129         |
| 5.5.6 Microhardness study . . . . .                  | 130         |
| 5.5.7 SHG study . . . . .                            | 132         |
| 5.6 Conclusions . . . . .                            | 134         |
| 5.7 Acknowledgements . . . . .                       | 135         |
| 5.8 References . . . . .                             | 135         |
| <b>VI GROWTH OF DICHLORO BIS(L-PROLINE) ZINC(II)</b> |             |
| <b>SINGLE CRYSTAL BY SANKARANARAYANAN-</b>           |             |
| <b>RAMASAMY METHOD AND ITS CHARACTERIZATION</b> 139  |             |
| 6.1 Abstract . . . . .                               | 139         |
| 6.2 Introduction . . . . .                           | 140         |
| 6.3 Experiment . . . . .                             | 141         |
| 6.3.1 Crystal growth . . . . .                       | 141         |
| 6.3.2 Characterization . . . . .                     | 144         |
| 6.4 Results and discussions . . . . .                | 146         |
| 6.4.1 Singly crystal X-ray diffraction . . . . .     | 146         |
| 6.4.2 High resolution X-ray diffraction . . . . .    | 146         |

## CONTENTS (Continued)

|  | <b>Page</b> |
|--|-------------|
| 6.4.3 Etching study . . . . .                  | 148         |
| 6.4.4 Dielectric studies . . . . .             | 150         |
| 6.4.5 Piezoelectric measurement . . . . .      | 152         |
| 6.4.6 Transmittance spectral studies . . . . . | 155         |
| 6.4.7 Measurement of microhardness . . . . .   | 157         |
| 6.4.8 SHG conversion efficiency . . . . .      | 159         |
| 6.5 Conclusions . . . . .                      | 159         |
| 6.6 Acknowledgements . . . . .                 | 160         |
| 6.7 References . . . . .                       | 160         |
| <b>VII CONCLUSIONS . . . . .</b>               | <b>165</b>  |
| <b>CURRICULUM VITAE . . . . .</b>              | <b>168</b>  |

## LIST OF TABLES

| Table |  | Page |
|-------|--|------|
| 2.1   | Comparison of various classes of NLO crystal . . . . .   | 37   |
| 4.1   | Comparative thermal stability of organic NLO materials. . . . .                                  | 106  |
| 4.2   | Comparative results of characterization on LAM crystals grown by<br>SEST and SR methods. . . . . | 111  |

## LIST OF FIGURES

| Figure |   | Page |
|--------|---|------|
| 1.1    | Estimated shares of word crystal production . . . . .   | 3    |
| 2.1    | Change in free energy due to the formation of nucleus . . . . .                               | 13   |
| 2.2    | Classification of nucleation . . . . .  | 14   |
| 2.3    | Meirs solubility curve . . . . .  | 18   |
| 2.4    | Constant temperature bath. . . . .  | 24   |
| 2.5    | Schematic of the SR method . . . . .  | 26   |
| 2.6    | Experimental setup of the SR method. . . . .  | 27   |
| 2.7    | A typical SHG active molecule . . . . .   | 34   |
| 2.8    | Schematic of 4-circle diffractometer . . . . .  | 40   |
| 2.9    | Image courtesy of Bruker-Axs . . . . .  | 41   |
| 2.10   | Schematic diagram of multi crystal X-ray diffractometer . . . . .                             | 44   |
| 2.11   | Schematic diagram of TGA . . . . .  | 47   |
| 2.12   | Schematic diagram of ultra micro-furnace and sample holder . . . . .                          | 48   |
| 2.13   | Dielectric measuerment . . . . .  | 51   |
| 2.14   | LCR meter . . . . .   | 54   |
| 2.15   | Example of the piezoelectric effect . . . . .   | 55   |
| 2.16   | UV-Vis-NIR spectrophotometer . . . . .  | 57   |
| 2.17   | Schematic diagram of Vickers diamond pyramid indenter and in-<br>dentation produced . . . . . | 61   |
| 2.18   | Apparatus used for study of second harmonic generation in powders                             | 63   |
| 3.1    | Conventional method grown SA crystals. . . . .  | 73   |

## LIST OF FIGURES (Continued)

| <b>Figure</b> | <b>Page</b>   |
|---------------|---|
| 3.2           | (a) As grown and (b) Cut and polished SR grown Sulphamic acid crystal. . . . . 74   |
| 3.3           | Etch pattern produced on the (100) plane of (a) conventional and (b) SR grown SA crystals by water after etching for 5 sec. Surface of (c) conventional and (d) SR grown SA crystals by methanol after etching for 20 sec. . . . . 76 |
| 3.4           | Vicker's microhardness analysis of SA. . . . . 78   |
| 3.5           | HRXRD curve of SR grown sulphamic acid crystal. . . . . 81  |
| 3.6           | HRXRD curve of conventional grown sulphamic acid crystal. . . . . 82  |
| 3.7           | UV-Vis NIR analysis of SA. . . . . 83   |
| 3.8           | TG-DTA analysis of SA. . . . . 84   |
| 4.1           | (a) Conventional method grown LAM crystal and (b) Morphology of LAM crystal. . . . . 93   |
| 4.2           | (a) SR-grown LAM crystal, (b) Cut and polished LAM crystals with various diameters. . . . . 95  |
| 4.3           | High-resolution X-ray diffraction curves recorded for (005) diffracting planes of LAM crystals grown by (a) conventional and (b) SR methods. . . . . 97   |
| 4.4           | Etching study on (011) face of LAM crystals grown by (a) conventional and (b) SR methods. . . . . 100   |

## LIST OF FIGURES (Continued)

| <b>Figure</b> | <b>Page</b>  |
|---------------|--|
| 4.5           | (a) Dielectric permittivity, (b) dielectric loss curve of LAM crystals and (c) dielectric tensor long a-,b-and c-directions as a function of temperature at 1 kHz frequency. . . . . 102 |
| 4.6           | TG-DTA measurement of LAM. . . . . 105   |
| 4.7           | UV-Visible analysis of LAM. . . . . 107  |
| 4.8           | Vickers microhardness analysis of LAM. . . . . 109   |
| 5.1           | (a) Conventional method grown LAMD crystal and (b) Morphology of LAMD crystal. . . . . 122   |
| 5.2           | (a) SR-grown LAMD crystal, (b) Cut and polished SR-grown LAMD crystals. . . . . 123  |
| 5.3           | High-resolution X-ray diffraction curves recorded for (100) diffracting planes of LAMD crystals grown by (a) conventional and (b) SR methods. . . . . 126                                |
| 5.4           | (a) Dielectric constant and (b) Dielectric loss curve as function of temperature at 1 kHz frequency of LAMD. . . . . 128   |
| 5.5           | UV-Visible analysis of LAMD. . . . . 131   |
| 5.6           | Vickers microhardness analysis of LAMD. . . . . 133  |
| 6.1           | (a) Conventional grown LPZ crystal and (b) Morphology of LPZ crystal. . . . . 143  |
| 6.2           | SR-grown LPZ crystal. . . . . 144  |
| 6.3           | High-resolution X-ray diffraction curves recorded for (024) diffracting planes: (a) SEST and (b) SR-grown single crystals of LPZ. . . 147  |

## LIST OF FIGURES (Continued)

| <b>Figure</b> |   | <b>Page</b> |
|---------------|---|-------------|
| 6.4           | Etching study on (010) face of LPZ crystals grown by (a) conventional and (b) SR methods. . . . .                                     | 151         |
| 6.5           | (a) Dielectric constant and (b) dielectric loss as function of frequency with temperature for SR-grown LPZ crystal. . . . .           | 153         |
| 6.6           | (a) Dielectric constant and (b) Dielectric loss curve of LPZ crystals grown by conventional and SR method at 1 kHz frequency. . . . . | 154         |
| 6.7           | UV-Visible analysis of LPZ. . . . .   | 156         |
| 6.8           | Vickers microhardness analysis of LPZ. . . . .  | 158         |

## LIST OF ABBREVIATIONS

|                 |   |
|-----------------|---|
| $A$             | Area of parallel plate capacitor  |
| $C$             | Capacitance   |
| <i>c.c.</i>     | Complex conjugate   |
| $\chi^{(n)}$    | n-th order susceptibility   |
| <b>D</b>        | Electric field displacement vector                                      |
| $d$             | Thickness of the sample   |
| $d_{hkl}$       | d-spacing   |
| <b>E</b>        | Electric field  |
| $E$             | Evaporation rate of solvent   |
| $E_1, E_2$      | Electric field components   |
| $E_1^*, E_2^*$  | Complex electric field components                                       |
| $E(t)$          | Electric field as a function of time                                    |
| $\varepsilon'$  | Dielectric constant   |
| $\varepsilon''$ | Dielectric loss   |
| $\varepsilon_0$ | Permittivity of free space ( $8.8542 \times 10^{-14} \text{Fcm}^{-1}$ ) |
| $\varepsilon_r$ | Relative permittivity   |
| $H_v$           | Vickers hardness  |
| $\lambda$       | Wavelength  |
| <b>P</b>        | Polarization  |
| $P^{(n)}$       | n-th order polarization   |
| $P(t)$          | Polarization as a function of time                                      |

**LIST OF ABBREVIATIONS (Continued)**

|               |                                     |
|---------------|-------------------------------------|
| $\theta$      | Scattering angle (or Bragg angle)   |
| R             | Growth rate                         |
| r             | Radius of the vessel                |
| S             | Solubility                          |
| T             | Temperature (Kelvin)                |
| t             | Time                                |
| $\tan \theta$ | Dielectric loss tangent             |
| $\omega$      | Angular frequency                   |
| AR            | Analytical reagent                  |
| DFG           | Difference frequency generation     |
| DTA           | Differencial Temperatuer Analysis   |
| KDP           | Potassium dihydrogen orthophosphate |
| LAM           | L-Alaninium Maleate                 |
| LAMD          | L-Arginine Maleate Dihydrate        |
| LPZ           | L-Proline Zinc Chloride             |
| NLO           | Nonlinear optics                    |
| OR            | Optically rectified                 |
| SA            | Sulphamic Acid                      |
| SEST          | Slow Evaporation Solution Technique |
| SHG           | Second harmonic generation          |
| SFG           | Sum frequency generation            |

**LIST OF ABBREVIATIONS (Continued)**

SR Sankaranarayanan-Ramasamy

TGA Thermogravimetric analysis

XRD X-ray diffraction

# CHAPTER I

## INTRODUCTION

### 1.1 Rationale of study

Crystal growth has prominent role to play in the era of immense technological excellence attributing to the usefulness of many crystals in important areas of service to the humanity namely science, medicine, engineering, technology and also strategic areas of defence and space science. In addition, many crystals be as useful as elements in piezoelectric, accousto-optic, photo-refractive, photo-elastic, elasto-optic applications and also as radiation detectors, laser hosts, parametric amplifiers, transducers, harmonic generators, bragg cells etc., (Junaidah Osman et al., 1998; Wenhua Jiang, 2003; Mackay Salley, 2002). Crystals grown nowadays find places ranging from microelectronics, optoelectronics, medical instruments, radar systems, communication systems, defence, laser sources upto the space age viz. satellites. Progress in crystal growth and epitaxy technology is highly demanded in view of its essential role for the development of several important areas such as production of high efficiency photovoltaic cells and detectors for alternative energy and the fabrication of bright long-lifetime light emitting diodes, for saving energy by wide use in illumination and traffic lights. The success of laser fusion energy depends on the timely development of high-power laser crystals and radiation-resistant frequency multiplying crystals of oxide compounds. Furthermore, the great and wide potential of oxide superconductors with high transition temperatures could not be explored so far because proper crystal growth and materials technology development was neglected (Santhanaraghavan and Ramasamy,

2001).

Single crystal forms foundation for modern technology. The ordered array of atoms in repeated groups, showing characteristic symmetry elements, by which entire block of the material is built is called single crystal. Single crystal growth helps to study many physical properties of solids and effects of grain boundaries. The full range of tensor relationship between applied physical cause and observed effect (property) can be obtained only if the full internal symmetry of the crystal structure is maintained throughout the specimen. The grain boundaries present in the crystal and the part played by imperfection are helpful in determining the physical and chemical properties of solids (Basset, 1968).

Crystal growth is a vital and fundamental part of materials science and engineering, since crystal of suitable size and perfection are required for fundamental data acquisition and for practical devices such as detectors, integrated circuits and for other millions and millions of applications. Due to large requirement of crystals to fulfill the needs of information world and emerging field of research, many methods for the growth of crystals have been a part of research for more than a century and crystals are wonders for many thousand years. The aim of crystal growth is also to understand the fundamental properties of the crystal and material. Lot of basic science owing to the property of the crystal depends on the production of high quality crystals with reasonable size. Crystal growth is more often an art than a science and many trials are often necessary before good crystals of a given material may be produced. Buckley (1951) has elegantly put the matter, "It should be remembered that, in the preparation of large crystals, the touch of the artist is about as important as the application of established scientific principles".

The following pie chart (Figure 1.1) shows the overview of the worldwide

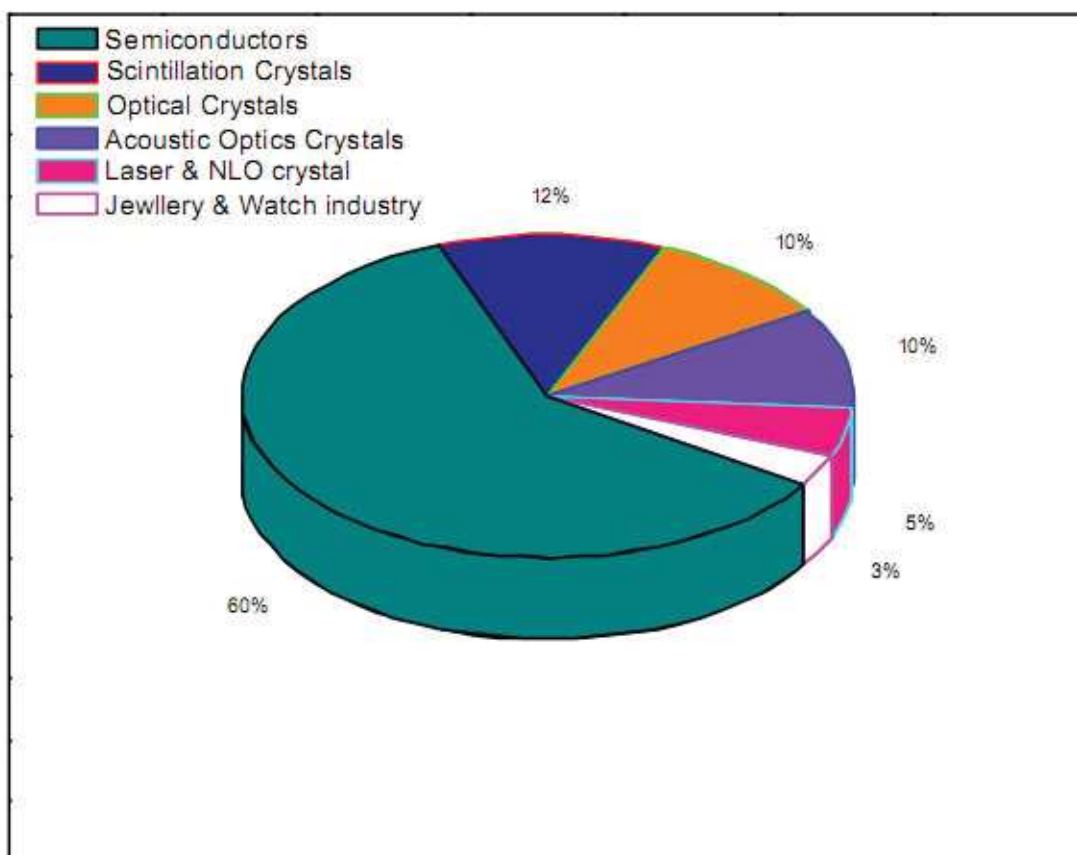


**Figure 1.1** Estimated shares of world crystal production (Santharaghavan and Ramasamy, 2001).

crystal production. Many of present-day instruments and devices used in various areas of science and technology, e.g. in electronics, optics, acoustics, and lasers incorporate single crystals of various materials in the shape of plates, fibers, tubes or rods of different cross sections. Cutting and machine working of single crystals result in the appearance of structural defects and, what is most important, in these processes the expensive material ends up as scraps. Hence, growth of single crystal with single direction in a desired shape has become inevitable for further research and technology. Nonlinear optic (NLO) is a new frontier of science and technology playing a major role in the emerging era of photonics. Photonics involves the application of photons for information and image processing and is branded to be

the technology of the 21st century wherein nonlinear optical processes have applications in the vital functions such as frequency conversion and optical switching (Dhanuskodi and Mary, 2003; Prasad and Williams, 1991). Potassium dihydrogen phosphate ( $\text{KH}_2\text{PO}_4$ ) or KDP is a suitable crystal for higher harmonic generation of huge laser system for fusion experiments because it can be grown to larger sizes and also KDP has a high laser damage threshold. Potassium titanyl phosphate ( $\text{KTiOPO}_4$ ) or KTP is a useful nonlinear optical crystal to get efficient green light by the frequency doubling of Neodymium Yttrium Aluminum Garnet (Nd:YAG) laser. It has high optical nonlinearity, large temperature and angular allowance and it is non hygroscopic and mechanically hard.

Search for new materials with enhanced NLO properties has increased considerably over the recent year as a result of potentially wide range of applications in optical communication and computation. Efforts have been made on amino acid with organic and inorganic complexes, in order to improve the chemical stability, laser damage threshold, and linear and non-linear optical properties. The importance of amino acid for NLO application lies on the fact that almost all amino acids contain an asymmetric carbon atom and crystallize in non-centro symmetric space group. In solid state, many amino acids contain a deprotonated carboxylic acid group ( $\text{COO}^-$ ) and protonated amino groups ( $\text{NH}_3^+$ ). This dipolar nature exhibits peculiar physical and chemical properties in amino acid, thus making them ideal candidate for NLO application.

Among the materials producing NLO effects, in particular the second harmonic generation (SHG), the organic materials have been identified to be of considerable importance owing to their synthetic flexibility to design and produce many novel materials (Bosshard et al., 1997). The added advantages of organic materials are their large optical susceptibilities, inherent ultrafast response times,

and high laser damage thresholds. Moreover, their lower cutoff wavelengths and a wide optical transparency window in the visible region makes these materials subject for extensive investigations. Organic molecules with remarkable nonlinear activity mostly consist of a  $\pi$ -electron conjugated moiety with an electron donor group and acceptor group at the extreme ends of a conjugated structure. The donor and acceptor groups provide the infrastructure to introduce the charge asymmetry required for second order nonlinearity. Example of a series of organic compounds are Alaninium maleate (LAM) (Natarajan et al., 2006) and Arginine maleate dihydrate (LAMD) (Kalaiselvi et al., 2008).

Semi-organic NLO crystals have also attracted attention because they have been proposed as a new approach for materials with fascinating NLO properties which have the combined properties of both inorganic and organic crystals like high damage threshold, wide transparency range, less deliquescence and high nonlinear coefficients which make them suitable for device fabrication (Jiang and Fang, 1999). Example of a series of studies on semiorganic amino acid compounds are L-proline zinc chloride (LPZ) (LydiaCaroline et al., 2009), L-arginine phosphate (LAP) (Monaco et al., 1987), L-arginine hydrobromide (L-AHBr) (Mukerji and Kar, 1998), L-histidine nitrate (LHN) (Yun Zhang, 2008), L-arginine hydrochloride (L-HCl) (Meeraa, 2001), and glycine sodium nitrate (GSN) (Narayan Bhat, 2002).

Most of these crystals have been grown by slow evaporation solution growth technique (SEST). Due to the inherent limitations of these techniques, the size of the crystals grown by these methods is small. Large size crystals of the above are necessary for device purposes. Orientation control during bulk crystal growth is one of the important development targets for crystal growers. Effective control of growth direction (orientation control) has attracted a great deal of attention. It is obvious that new functions can be created through the orientation control of

molecules in the fields such as semiconductors, light-emitting devices, NLO materials, and photonic crystals. Therefore, technology for preparing bulk materials with effective orientation control has been required for achieving significant applications in the field of optoelectronics. In crystal growth literature, the discovered uniaxially solution-crystallization method of Sankaranarayanan-Ramasamy (SR) (Sankaranarayanan and Ramasamy, 2005) is a suitable method to effectively control the orientation of molecules during the bulk crystal growth from solution at room temperature with almost 100% solute-crystal conversion efficiency. This method can be used to grow single crystals along a selected crystal direction, which is very important for the preparation of functional crystals. For example, as the conversion efficiency of SHG is always highest along the phase-match direction for nonlinear optical crystals, the unidirectional crystal growth method is most suitable for the crystal growth along that direction. In addition, the unidirectional solution crystallization usually occurs at around room temperature; much lower thermal stress is expected in these crystals over those grown at high temperatures (Jingran Su et al., 2009). From this point of view, we have attempted to grow unidirectional, bulk, good quality single crystals of organic and semiorganic NLO from its aqueous solution by SR method.

## 1.2 Research objective

The objectives of this thesis are as follow:

1.2.1 Growth of inorganic SA crystals which have a good quality, large size by using both conventional SEST and uniaxially solution crystallization Sankaranarayanan-Ramasamy method.

1.2.2 Growth of organic LAM and LAMD crystals which have a good quality, large size by using both conventional SEST and uniaxially solution crystalliza-

tion Sankaranarayanan-Ramasamy method.

1.2.3 Growth of semi-organic LPZ crystals which have a good quality, large size by using both conventional SEST and uniaxially solution crystallization Sankaranarayanan-Ramasamy method.

1.2.4 Characterization of the grown crystals.

### 1.3 Scope and limitation of the study

1.3.1 Synthesis and growth of SA, LAM, LAMD and LPZ seed crystals were carried out using the conventional slow evaporation method.

1.3.2 Growth of larger size crystals was carried out using the uniaxially solution-crystallization Sankaranarayanan-Ramasamy method.

1.3.3 Characterization of the grown crystals were made by single crystal X-ray diffraction, HRXRD, TG-DTA, dielectric measurement, piezoelectric measurement, UV-Vis NIR analysis, Vickers microhardness measurement and SHG conversion efficiency.

### 1.4 References

Basset D.C. (1968). The growth of polymer crystals. **Journal Crystal of Growth.** 3(4): 92.

Bosshard, Ch., Sutter, K., Pretre, Ph., Hulliger, J., Florsheimer, M., Kaatz, P. and Gunter, P.(1997). **Organic Non-linear Optical Materials.** Gordon and Breach. Switzerland.

Buckley, H.E. (1951). **Crystal Growth.** New York, John Wiley sons, Inc, London. Chapman Hall. Ltd. p44.

- Dhanuskodi, S., Mary, P.A.A. (2003). **Journal of Crystal Growth**. 253: 424.
- Jiang, M.H., Fang, Q. (1999). **Advance Materials**. 13: 1147.
- Jingran Su, Youting Song, Daofan Zhang and Xinan Chang. (2009). **Powder diffraction** 24: 234.
- Junaidah Osman, Siew-Choo Lim, Tilley, D. R. and Ishibashi, Y. (1998). Nonlinear Optic Co-efficients in the Ferroelectric Phase. **Journal of the Korean Physical Society**., 32: 446.
- Kalaiselvi, D., Mohan Kumar, R. and Jayavel, R. (2008). Growth and characterization of nonlinear optical l-arginine maleate dihydrate single crystals. **Materials Letters**. 62(4-5): 755.
- LydiaCaroline, M., Kandasamy, A., Mohan, R. and Vasudevan, S.(2009). Growth and characterization of dichlorobis L-prolineZn(II) : A semiorganic non-linear optical single crystal. **Journal Crystal of Growth**. 311: 1161.
- Mackay Salley G, Oliver S. Wenger, Karl W. Kramer and Hans U. Gudel. (2002). Inorganic solid state optical materials:Major recent advances **Current Opinion in Solid State and Materials Science**. 6: 487.
- Monaco, S. B., Davis, L. E., Velsko, S. P., Wang, F. T., Eimerl, D. and Zalkin, A. (1987). **Journal Crystal of Growth**. 85: 252.
- Mukerji, S., Kar, T. (1998). Structural,thermal and spectroscopic investigation of nonlinear optical cryastal L-arginine hydrobromide monohydrate. **Materials Research Bulletin**. 33(4): 619.
- Meeraa, K., Muralidharana R., Dhanasekarana R., Prapun Manyum and Ramasamy, P. (2004) P. Growth of nonlinear optical material: L-arginine

- hydrochloride and its characterisation. **Journal Crystal of Growth.** 263: 510.
- Narayan Bhat, M., Dharmaprakash, S.M. (2002). New nonlinear optical material: glycine sodium nitrate. **Journal Crystal of Growth.** 235: 511.
- Natarajan, S., Martin Britto Dhas, S.A. and Ramachandran, E. (2006). Growth, Thermal, Spectroscopic, and Optical Studies of L-Alaninium Maleate, a New Organic Nonlinear Optical Material. **Crystal Growth and Design.** 6(1): 137.
- Prasad, P. N., Williams, D.J. (1991). **Introduction to Nonlinear Optical Effects in Molecules and Polymers.** John-Wiley Sons Inc., New York. p1.
- Sankaranarayanan, K., Ramasamy, P. (2005). Unidirectional seeded single crystal growth from solution of benzophenone. **Journal Crystal of Growth.** 280(3-4): 467.
- Santhanaraghavan, P., Ramasamy, P. (2001). **Crystal growth process and method.** India, KRU publications.
- Wenhua Jiang, Rui Zhang, Bei Jiang and Wenwu Cao. (2003). Characterization of piezoelectric materials with large piezoelectric and electromechanical coupling coefficients. **Ultrasonics.** 41: 55.
- Yun Zhang, Hua Li, Bin Xi, Yunxia Che. and Jimin Zheng. (2008). Growth and characterization of l-histidine nitrate single crystal, a promising semiorganic NLO material. **Materials Chemistry and Physics.** 108: 192.

# CHAPTER II

## REVIEW OF THE LITERATURE

### 2.1 Crystal growth phenomena

#### 2.1.1 Introduction

People grow crystals for two main reasons, to understand how crystals grow (aesthetic) and for the utility (scientific or technological application of the grown crystals); for either of these one must evaluate the quality of the crystals grown (Laudise et al., 1975). The responsibility for the exquisiteness of the crystal is due to their structural simplicity, symmetry and purity. These characteristics endow crystals with unique physical and chemical properties which caused major transformation in the electronics industry.

Initially natural crystals were adored as gems and museum pieces. Later a transition of crystals from museum to technology have occurred which stimulated crystal growing community to produce large crystals artificially. Finally, crystal production and fabrication became a major commercial activity when transistor was invented (Gilman, 1963). Crystal growth is rather an art than a science (Stringfellow, 1979) and very many attempts have been made for a long time to produce good crystals of desired materials. Incidentally the essential work of the crystal grower is to produce a single crystal in large size from its poly-crystalline form by adopting appropriate technique. It remains for the crystal growers to collate the physical and chemical properties, supplement these measurements with analytical, optical and other physical instrumental measurements to deduce things

relevant to the identity and position of the atoms in the crystal to characterize it (Laudise et al., 1975).

### 2.1.2 Nucleation

Nucleation is an important phenomenon in crystal growth and is the precursor of crystal growth and of the overall crystallization process. The condition of supersaturation alone is not sufficient cause for a system to begin to crystallization. Before crystals can grow, there must exist in the solution a number of minute solid bodies known as centers of crystallization, seeds, embryos or nuclei (Santhanaraghavan and Ramasamy, 2001). The formation of stable nuclei occurs only by the addition of a number of molecules ( $A_1$ ) until a critical cluster is formed. In general,



Any further addition to the critical nucleus results in nucleation followed by growth. Once these nuclei grow beyond a certain critical size, they become stable under the average condition of supersaturation of the solution. Further, the creation of a new phase in the homogeneous solution demands for the expenditure of certain quantity of energy.

The total Gibbs free energy change,  $\Delta G$  of the embryo between the two phases associated with this process is then given as

$$\Delta G = \Delta G_s + \Delta G_v, \quad (2.2)$$

where  $\Delta G_s$  is the surface free energy and  $\Delta G_v$  is the volume free energy. For a

spherical nucleus of radius  $r$ ,

$$\Delta G = 4\pi r^2 \gamma + (4/3)\pi r^3 \Delta G_v. \quad (2.3)$$

Where  $\gamma$  is the interfacial tension and  $\Delta G_v$  is the free energy change per unit volume and is a negative quantity. The quantities  $\Delta G$ ,  $\Delta G_s$ , and  $\Delta G_v$  are represented in Figure 2.1. Since surface free energy increases with  $r^2$  and the volume free energy decreases with  $r^3$ , the total net free energy change increases with increase in size, attains a maximum and decreases for further increase in the size of the nucleus. The size corresponding to the maximum free energy change is called critical nucleus. The radius of the critical nucleus is obtained by setting the condition

$$\frac{d\Delta G}{dr} = 0 \quad (2.4)$$

and the expression for critical radius is given by

$$r^* = \frac{-2\gamma}{\Delta G_v}. \quad (2.5)$$

Substituting the values of  $r^*$  in the above equation the free energy change associated with the critical nucleus is

$$\Delta G^* = \frac{16\pi\gamma^3}{3\Delta G_v^2}. \quad (2.6)$$

The number of molecules in the critical nucleus is expressed as

$$i^* = (4/3)\pi r^*(r^*)^3. \quad (2.7)$$

The interfacial tension  $\gamma$  has been determined experimentally (Santhanaraghavan

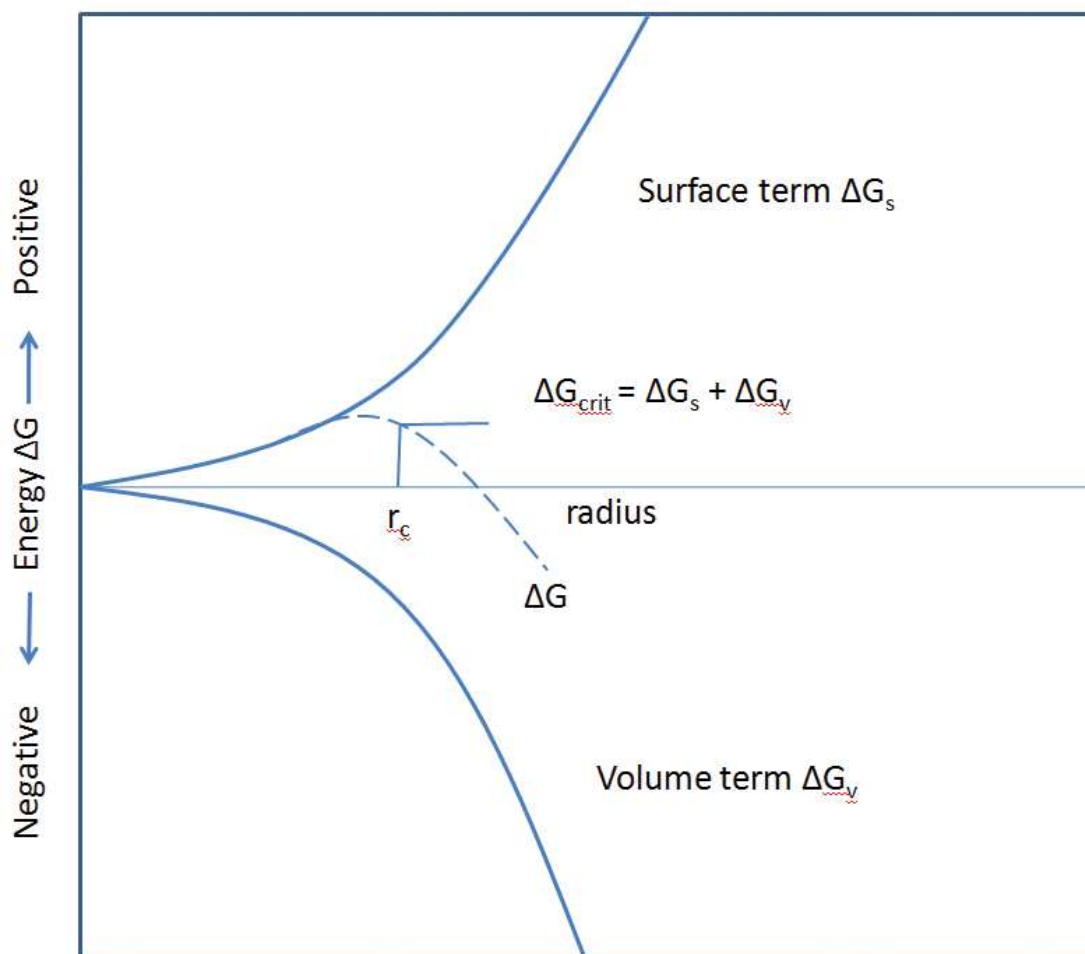


**Figure 2.1** Change in free energy due to the formation of nucleus (Santharaghavan and Ramasamy, 2001).

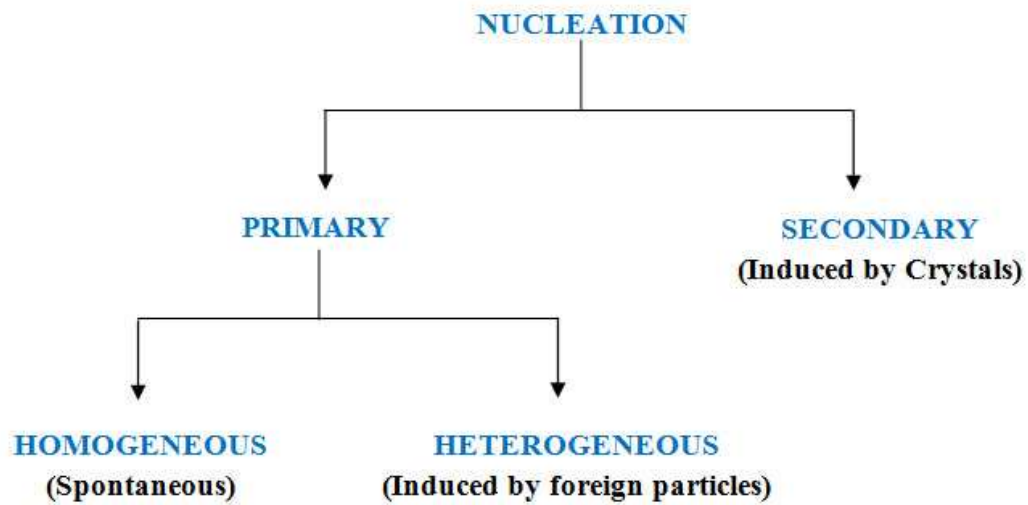


**Figure 2.2** Classification of nucleation (Claude, 2006).

and Ramasamy, 2001).

Nucleation may occur spontaneously or it may be induced artificially and they are usually referred to as homogeneous and heterogeneous nucleations respectively. As shown in Figure 2.2, The term primary is used for both homogeneous and heterogeneous nucleation even in systems that do not contain crystalline matter. On the other hand, during secondary nucleation, nuclei are often generated in the vicinity of the crystals present in the supersaturated system. This process involves the dislodgement of the nuclei from the parent crystal at supersaturation in which primary homogeneous nucleation cannot occur. When a supersaturated solution is disturbed by agitation, friction or mechanical stimulus in the presence of the crystalline substance of the solute, embryos are formed at the surfaces of the parent crystal. These embryos give rise to secondary nucleation.

If the nuclei form homogeneously in the interior of the phase, it is called homogeneous nucleation. If the nuclei form heterogeneously around ions, impurity molecules or on dust particles, on surfaces or at structural singularities such as

imperfections or dislocations, it is known as heterogeneous nucleation (Claude, 2006).

In general, the crystallization process takes place by three steps:

1. achievement of supersaturation or super cooling
2. formation of crystal nuclei and
3. growth of crystal.

## 2.2 Crystal growth techniques

There are several techniques for crystallization which can be classified according to their phase transformation as

Growth from solid solid → solid phase transformation

Growth from liquid liquid → solid phase transformation

Growth from vapor vapor → solid phase transformation

The crystal growth from liquid falls into two categories namely,

1. Melt growth,
2. Solution growth.

Growth from solution, in particular the low temperature solution growth, occupies an outstanding position due to its versatility and simplicity. Growth from solution occurs close to equilibrium conditions and hence crystals of high perfection can be grown. Since this thesis involves the work on growing crystals from low temperature solutions, the processes of low temperature solution growth methods are briefly discussed.

### **2.2.1 Low temperature solution growth**

Growth of crystals from aqueous solution is one of the ancient methods of crystal growth. The method of crystal growth from low temperature aqueous solutions is extremely popular in the production of many technologically important crystals. Materials having moderate to high solubility in temperature range, ambient to 100 °C at atmospheric pressure can be grown by low-temperature solution method. The mechanism of crystallization from solutions is governed, in addition to other factors, by the interaction of ions or molecules of the solute and the solvent which is based on the solubility of substance on the thermodynamical parameters of the process; temperature, pressure and solvent concentration (Chernov, 1984).

### **2.2.2 Solution, solubility and supersolubility**

Solution is a homogeneous mixture of a solute in a solvent. Solute is the component, which is present in a smaller quantity. Solubility of the material in a solvent decides the amount of the material, which is available for the growth and hence defines the total size limit. Solubility gradient is another important parameter, which dictates the growth procedure. Neither a flat nor a steep solubility curve will enable the growth of bulk crystals from solution, while the level of supersaturation could not be varied by reducing the temperature in the former. Even a small fluctuation in the temperature will affect the supersaturation to grow the good quality bulk crystals in both cases. If the solubility gradient is very small, slow evaporation of the solvent is the best option for crystal growth in order to maintain a constant supersaturation in the solution.

Growth of crystals from solution is mainly a diffusion-controlled process. The medium must be viscous enough to enable faster transference of the growth units from the bulk solution by diffusion. Hence, a solvent with less viscosity is

preferable. Supersaturation is an important parameter for the solution growth process. The crystal grows by the access of the solute in the solution where the degree of supersaturation is maintained. The solubility data at various temperatures are essential to determine the level of supersaturation. Hence, the solubility of the solute in the chosen solvent must be determined before starting the growth process. The diagram is divided into three zones, which are termed as region I, region II and region III. Region I corresponds to the under saturated zone, where crystallization is impossible. This region is thermodynamically stable. The region II between the super solubility curve and the solubility curve is termed as metastable zone where spontaneous crystallization is improbable. Seeded crystal growth can be achieved in this region. The unstable or labile zone occurs at region III where the spontaneous nucleation is more probable (Figure 2.3). Many crystals grown for basic and advanced research having technological applications are from low temperature solution growth. This method is executable not only for water soluble materials, but also for insoluble materials which can be brought into solution by forming complexes (Santharaghavan and Ramasamy, 2001).

Growth rate of a growing crystal is accompanied by a concentration gradient around the growth face. Those growth faces are inherently unstable with respect to supersaturation. Hence in solution growth stable faces are always singular, whereas non-singular faces occur around seeds cut from crystals. This veil can be reduced, but seldom eliminated by dissolving the little of the surface of the cut seed prior to growth (Brice, 1986). This intrinsic instability of the growth faces accounts for the slow rate of growth. Growth rate of solution falls in the range 0.1 - 10 mm per day, much smaller than the comparative fast growth rates from melt growth.

Low temperature solution growth can be further subdivided as

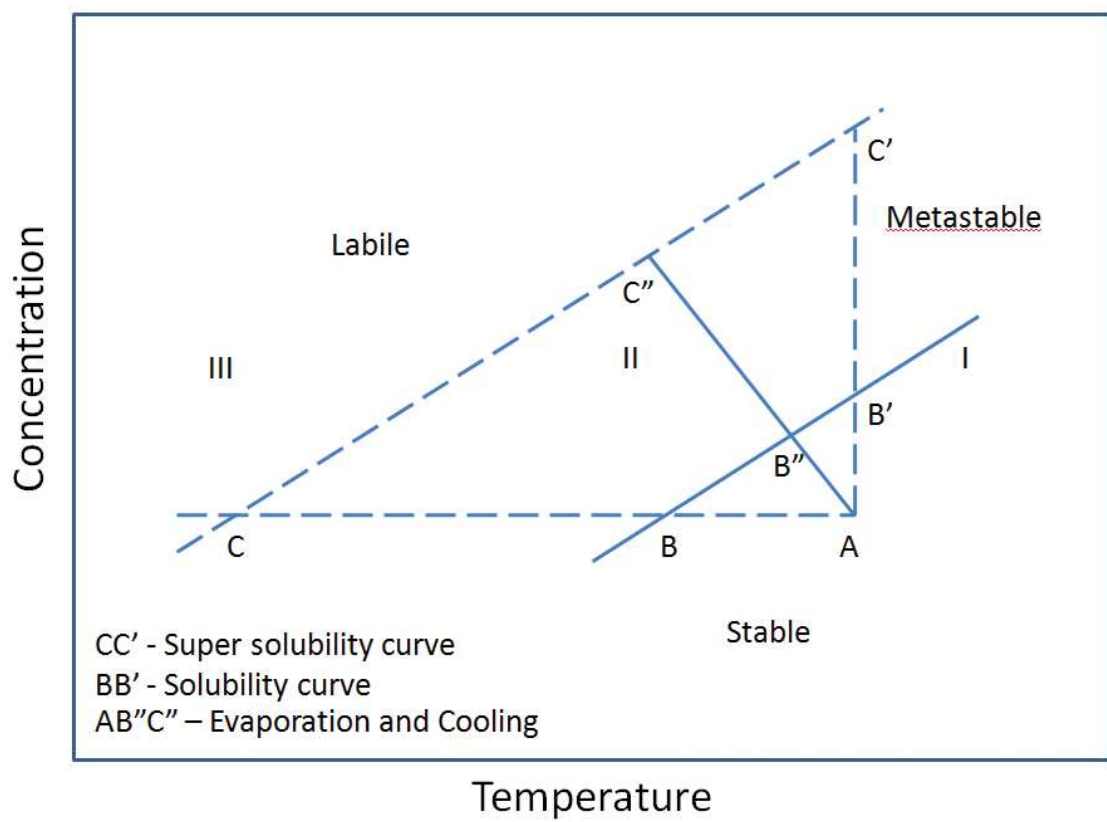


**Figure 2.3** Meir's solubility curve (Santhanaraghavan and Ramasamy, 2001).

1. Slow cooling method;
2. Slow evaporation method;
3. Temperature gradient method.

### **2.2.3 Crystallization by slow cooling**

This is one of the best suited methods of growing bulk single crystals. In this method, supersaturation is attained by a change in temperature usually throughout the whole crystallizer. The crystallization process is carried out in such a way that the point on the temperature dependence of the concentration moves into the metastable region along the saturation curve in the direction of lower solubility. Since the volume of the crystallizer is finite and the amount of substance placed in it is limited, the supersaturation requires systematic cooling. It is achieved by using a thermostated crystallizer and volume of the crystallizer is selected based on the desired size of the crystals and the temperature dependence of the solubility of the substance. The temperature at which such crystallization can begin is usually within the range of 45 to 75 °C and the lower limit of cooling is the room temperature.

### **2.2.4 Crystallization by solvent evaporation**

In this method, an excess of a given solute is established by utilizing the difference between rates of evaporation of the solvent and the solute. In contrast to the cooling method, in which the total mass of the system remains constant, in the solvent evaporation method, the solution loses particles, which are weakly bound to other components, and, therefore, the volume of the solution decreases. In almost all cases, the vapor pressure of the solvent above the solution is higher than the vapor pressure of the solute and, therefore, the solvent evaporates more

rapidly and the solution becomes supersaturated. Usually, it is sufficient to allow the vapor formed above the solution to escape freely into the atmosphere. This is the oldest method of crystal growth and technically, it is very simple. Typical growth conditions involve temperature stabilization to about  $\pm 0.005$  °C and the rate of evaporation of a few  $\text{mm}^3/\text{hr}$ .

### 2.2.5 Material purification

High purity of material is an essential prerequisite for crystal growth. Therefore the first step in crystal growth is the purification of the material in appropriate solvents. Impurities should be maintained at as low as 10 to 100 ppm. Purification can be attained by repeated crystallization of the substance in an appropriate solvent. Although the chromatographic techniques like high performance liquid chromatography (HPLC) or gas chromatography (GC) can be used for purification, they yield very small quantity of purified product per cycle. In particular, zone refining, sublimation and distillation methods have been frequently used for ultra purification to obtain large quantities of materials. In recrystallization process the material is dissolved in a hot solvent, then gradually cooled down to crystallize. It's importance to say the appropriate selection of solvents used in the recrystallization process. Recrystallization is the most common technique of purifying organic materials. Zone refining method has been found to be the most effective in producing ultra pure materials with impurities at a scale of parts per billion. Sublimation is used for thermally unstable solid materials that possess good volatility at temperatures below their decomposition points. Sublimation is generally performed at vacuum ( $10^{-5}$  to  $10^{-6}$  torr) to avoid decomposition.

### 2.2.6 Solvent selection

In solution growth, suitable choice of solvent is necessary. The solvent must be chosen, taking into account the following factors:

1. good solubility for the given solute;
2. good temperature co-efficient of solute solubility;
3. less viscosity;
4. less volatility;
5. less corrosion and non-toxicity;
6. small vapour pressure; and
7. cost advantage.

It is known that the choice of solvent provides some control over crystal habits and this effect depends on the interaction of the surface of the crystal as it grows and the solvent molecules. Sometimes this is sufficient to result in the precipitation of a new crystalline phase or habit modifications were observed on adding impurities (Buckley, 1951).

### 2.2.7 Preparation of solutions

Preparation of the solution to grow the desired crystal is an important stage in solution growth. The solution is saturated as per the available solubility diagram (accurate solubility-temperature data). The saturated solution is filtered using the filter paper. The filtered solution is transferred into the growth beaker and placed in the constant temperature bath (CTB). The desired supersaturation required is obtained by just lowering the temperature. Extreme care is to be taken to avoid under saturation, which results in the dissolution of seed crystal. Similarly high supersaturation is also to be avoided in order to prevent the formation of spurious nucleation. The growth vessel is hermetically sealed in order to avoid the

evaporation of the solvent. The solution is tested for saturation by suspending small test seed crystal in the solution. If the system is not in equilibrium, the seed crystal either dissolves or the solute will crystallize on the seed. By adjusting the temperature, the necessary equilibrium condition is achieved and the test seed crystal is removed and a fresh seed crystal is introduced for crystal growth.

### **2.2.8 Seed preparation**

The quality of the grown crystal very much depends on the quality of the seed crystal used. Small seed crystals can be obtained by spontaneous nucleation in the labile region of the supersaturated solution. The seed used to grow a large uniform crystal must be a single crystal free of inclusions, cracks, block boundaries, sharp cleaved edges, twinning and any other obvious defects. It should be of minimum size, compatible with other requirements. When larger crystals of the same material are already available, they can be cut in the required orientation to fabricate the seed crystal. Since the growth rate of the crystal depends on the crystallographic orientation, the seed crystal must be cut in such a way that it has larger cross-section in the fast growing direction.

### **2.2.9 Cooling rate**

To obtain the required supersaturation, which is the driving force for the growth of crystal, the temperature of the growth solution is lowered. The cooling rate is to be programmed according to the growth rate of the crystals. A large cooling rate changes the solubility beyond metastable limit and fluctuations in the supersaturation may encourage inclusions. A proper balance between the temperature lowering rate and growth rate will yield a good quality crystal.

### 2.2.10 Harvesting of the grown crystals

The extraction of a crystal from its mother liquor requires enormous care because any damage may destroy completely the scientific value of the crystal or even fracture it altogether. If a crystal is extracted from a solution kept close to room temperature, it can be simply dried by means of filter paper. Filter paper must be used to rub the surface since the majority of crystals prepared from low temperature solutions are easily scratched. The surface of a carelessly treated crystal may immediately acquire many defects.

The quality of the harvested crystal depends on

1. purity of the starting material;
2. quality of the seed crystal and
3. cooling rate employed.

### 2.2.11 Crystal growth system

Since temperature affects the driving force of crystallization very much, highly stable temperature maintenance is essential through out the growth process. To achieve this, an active thermo stating system with fine controlling accuracy is necessary. A general design of a thermostat with a control system, also known as Constant Temperature Bath (CTB) includes a thick walled glass chamber filled with water, heating element, temperature sensor, control relay, temperature indicator, stirrer and illuminating lamp (Figure 2.4). The long periods necessary to grow crystals and the need to avoid any interruption of the temperature control process mean that special measures must be taken to ensure that the control system is reliable.



**Figure 2.4** Constant temperature bath.

### **2.3 Sankaranayanan-Ramasamy (SR) method**

SR method is one of the solution growth methods. In the case of melt, extremely low growth rate and thermal gradients are usually required to grow single crystals having reasonable size and quality. In addition, crystal growth at elevated temperature leads to thermal induced grown- in-defects. The growth of organic crystals with specific orientation has tremendous value in terms of its significance towards device application. Crystallization from the solution is an important process and the driving force for crystallization is the degree of supersaturation, which is attained by slow cooling or slow evaporation. Solution growth is a method of choice when materials

1. melt non congruently or
2. decompose before melting or
3. undergo a solid state phase transformation before melting or
4. have very high melting point.

The basic apparatus for solution growth contains a large thermostat tank heated by the infrared lamp at the base controlled by the contact thermometer

with control accuracy of  $\pm 0.01$  K over long periods of time. In conventional solution growth method large quantity of solution in large container is normally used and only a small fraction of the solute is converted into a bulk single crystal. In the present work, this limitation has been eliminated because the achieved size of the crystal was the size of the growth ampoule. Microbial growth has been causing serious concern in solution growth experiments largely due to aging of the solution (Kavitha et al., 2004). The growth of crystal inside the ampoule facilitates continuous charging of growth solution as crystal growth proceeds; this reduces the problem associated with microbial growth. When a suspension thread is used in crystal growth, the region close to the thread is often of poor quality. This situation is also avoided in this method. In general if the solubility is too high, it is difficult to grow bulk single crystals and too small a solubility restricts the size and growth rate of the crystals. The solubility data at various temperatures are essential to determine the level of supersaturation. Hence, the solubility of the solute in the chosen solvent must be determined before starting the growth process. If the solubility gradient is very small, slow evaporation of the solvent is the other option for crystal growth to maintain the supersaturation in the solution. Growth of crystal from solution is mainly a diffusion-controlled process; the medium must be less viscous to enable faster transference of the growth units from the bulk solution by diffusion. The SR method growth is occurring by solvent evaporation in a specially designed crystallizer.

### **2.3.1 SR method experimental setup**

The schematic diagram of the experimental set up is shown in Figure 2.5. It consists of a growth ampoule made out of glass with seed mounting pad. An outer glass shield tube protects and holds the inner growth ampoule. A ring heater

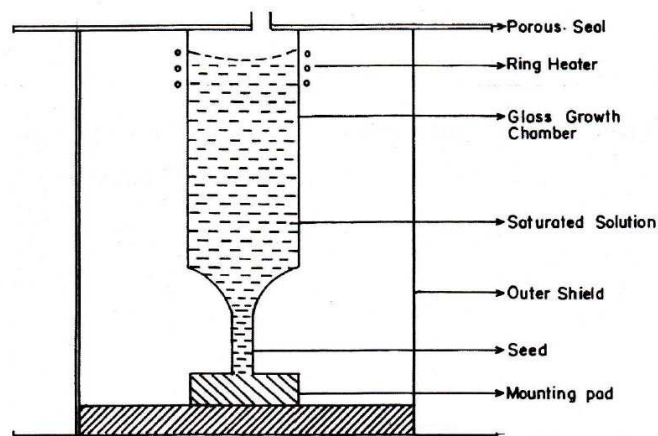


**Figure 2.5** Schematic of the SR method (Sankaranarayanan and Ramasamy, 2005).

positioned at the top of the growth ampoule was connected to the temperature controller and it provides the necessary temperature for solvent evaporation. The temperature around the growth ampoule was selected based on the solvent used and was controlled with the aid of the temperature controller. Depending on the growth rate of the crystal, the ring heater was moved downwards using a translation mechanism (Sankaranarayanan, 2005).

SR method was subjected to many modification in different stages. In the present investigation, a modified SR method setup is shown in Figure 2.6. Once the system attains equilibrium, the growth was initiated with a suitable temperature provided by the ring heater at the top of the solution. Top of the growth ampoule was maintained at 38 °C for solvent evaporation. The temperature around the growth region is maintained at 34 °C for the growing crystals.

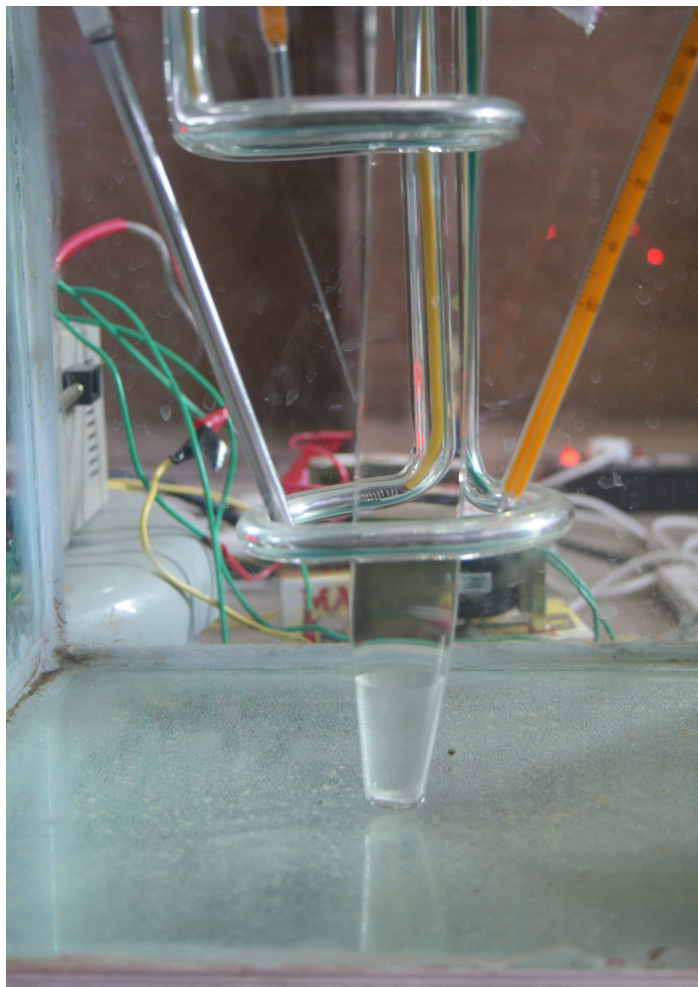


**Figure 2.6** Experimental setup of the SR method.

### 2.3.2 Crystal quality analysis of SEST and SR methods grown crystals

The physical properties of the single crystal may change when the defects are created during growth. Also, the quality of the crystal highly depends on the method (Senthil Pandian, 2008, 2010) and material used for the growth. Two major reasons for the lower crystalline perfection in SEST method grown crystals are inclusions and growth sector boundaries (GSB). Solvent inclusions are potentially a major source of growth induced defects and it is very difficult to avoid the inclusion of solvent at the seed-crystal interface (Hugh et al., 2003). Inclusions are the main sources of dislocations and the generation of dislocations is strongly correlated with the formation of inclusions in the crystals. A variety of factors like,

- i) Variation in supersaturation of the solution,
- ii) Minor fluctuations in temperature during growth,
- iii) Non-uniform growth rates etc., govern the formation of inclusions.

In general it is observed that most of the conventional method grown (ADP, KDP,  $\text{KAlSO}_4$ ) crystals contain inclusions (Senthil Pandian, 2008). For the SR method used in this study, the temperature gradient (at the top portion is 38 °C and down to 34 °C at the bottom portion) creates a concentration gradient along the growth ampoule, with a maximum and stable supersaturation at the bottom of the ampoule and all the solute molecules are directly approaching the one directed crystal face and the surface attracts the atoms without any difficulty. Depending on the temperature at the top and the bottom portions, the rate of evaporation of solvent is controlled effectively. For these reasons, in SR method grown crystal there are

- i) no growth fluctuation,

- ii) uniform supersaturation near the surface of the crystal and
- iii) stable growth rates, the dislocations of these three causes are avoided.

The SEST grown crystals have different facets, growth sectors and growth sector boundaries. In conventional solution method, certain dislocations have a tendency to nucleate at growth sector boundaries (GSB) (Alexandru and Antohe, 2003). But in SR method, since the crystal is growing in selective growth orientation, the growth is on one facet only. There are no growth sector boundaries. Hence the dislocations associated with growth sector boundaries are absent in SR method grown crystal.

This method of growth has been found to be an attractive technique for preparation of single crystals of large size benzophenone (Sankaranarayanan and Ramasamy, 2005; Sankaranarayanan 2005; Sankaranarayanan and Ramasamy, 2006), KDP (Balamurugan and Ramasamy, 2006), ADP (Sethuraman et al., 2006), Sulphamic acid (Lenin et al., 2006), L- glutamic acid (Bairava Ganesh et al., 2006), KAP (Balamurugan et al., 2006).

## 2.4 Nonlinear optical materials

Nonlinear optics is the study of phenomena that occur as a consequence of the modification of the optical properties of a material system by the presence of light. Typically, only laser light is sufficiently intense to modify the optical properties of a material system. In fact, the beginning of the field of nonlinear optics is often taken to be the discovery of second-harmonic generation by Franken et al. in 1961, shortly after the demonstration of the first working laser by Maiman in 1960. Nonlinear optical phenomena are “Nonlinear“ in the sense that they occur when the response of a material system to an applied optical field depends in a nonlinear manner upon the strength of the optical field. For example, Second-

harmonic generation occurs as a result of the part of the atomic response that depends quadratically on the strength of the applied optical field. Consequently, the intensity of the light generated at the second-harmonic frequency tends to increase as the square of the intensity of the applied laser light. Nonlinear optics is a very useful technology because it extends the usefulness of laser by increasing the number of wavelengths available. Wavelengths both longer and shorter than the original can be produced by nonlinear optics. There is one nonlinear optical device that can convert a fixed wavelength laser to a continuously tunable one.

Nonlinear optical effects are analyzed by considering the response of the dielectric material at the atomic level to the electric fields of an intense light beam. For instance, when a dielectric material is subjected to an electromagnetic radiation (em), the propagation of em wave through the material produces changes in spatial and temporal distribution of electric charges due to the interaction between the em wave, electrons and atoms. This perturbation creates electric dipoles whose manifestation is macroscopic polarization  $P(t)$  at time  $t$  in a medium. When the applied electric field  $E(t)$  is very small, the induced polarization is

$$P(t) = \epsilon_0 \chi^{(1)} \cdot E(t), \quad (2.8)$$

where  $\epsilon_0$  is the permittivity of free space. When the applied electric field strength is high enough and comparable to the inter-atomic field, the amplitude of the dipoles does not faithfully reproduce the exact sinusoidal electric field. Indeed, it produces the distorted reradiated wave which contains the induced polarization given by

$$P(t) = \epsilon_0 \chi^{(1)} \cdot E(t) + \epsilon_0 \chi^{(2)} \cdot E(t) \cdot E(t) + \epsilon_0 \chi^{(3)} \cdot E(t) \cdot E(t) \cdot E(t) + \dots \quad (2.9)$$

$$P(t) = P^{(1)} + P^{(2)} + P^{(3)} + \dots, \quad (2.10)$$

where  $\chi^{(1)}, \chi^{(2)}, \chi^{(3)}, \dots$  defines the medium response and are known as nonlinear susceptibilities co-efficients of first, second, third, and higher order respectively. There are tensorial quantities and give a measure of the polarizing effect of the optical field on outer valence electrons. The magnitude of the susceptibilities is dependent on the chemical bonding of the materials. The first term in the expansion is responsible for the material's linear optical properties, and second and third terms give rise to diverse nonlinear three and four wave mixing processes, respectively. Second order susceptibility is non-zero only in non-centro symmetric crystal structure. Here a laser beam whose electric field strength is represented as

$$E(t) = E_1 e^{-i\omega_1 t} + E_2 e^{-i\omega_2 t} + c.c. \quad (2.11)$$

is incident upon a crystal for which the second-order susceptibility  $\chi^{(2)}$  is nonzero (c.c. denotes the complex conjugate). The nonlinear polarization that is created in such a crystal is according to Eq. (2.10) as  $P^{(2)}(t) = \epsilon_0 \chi^{(2)} \cdot E(t) \cdot E(t)$  or as

$$\begin{aligned} P^{(2)}(t) = \chi^{(2)} [ & E_1^2 e^{-2i\omega_1 t} + E_2^2 e^{-2i\omega_2 t} + 2E_1 E_2 e^{-i(\omega_1 + \omega_2)t} \\ & + 2E_1 E_1^* e^{-i(\omega_1 - \omega_2)t} + c.c.] + 2\chi^{(2)} [E_1 E_1^* + E_2 E_2^*]. \end{aligned} \quad (2.12)$$

It is convenient to express this result using the notation

$$P^{(2)}(t) = \sum P(\omega_n) e^{-i\omega_n t}, \quad (2.13)$$

The complex amplitudes of the various frequency component of the nonlinear

polarization are hence given by

$$P_{(2\omega_1)} = \chi^{(2)} E_1^2 \quad (SHG) \quad (2.14)$$

$$P_{(2\omega_1)} = \chi^{(2)} E_2^2 \quad (SHG) \quad (2.15)$$

$$P_{(\omega_1+\omega_2)} = 2\chi^{(2)} E_1 E_2 \quad (SFG) \quad (2.16)$$

$$P_{((\omega_1-\omega_2))} = 2\chi^{(2)} E_1 E_2^* \quad (DFG) \quad (2.17)$$

$$P_{(0)} = 2\chi^{(2)} E_1 E_1^* + E_2 E_2^* \quad (OR). \quad (2.18)$$

Three wave-mixing gives rise to phenomena like second-harmonic generation (SHG), sum-frequency generation (SFG), difference-frequency generation (DFG), and optical rectification (OR), linear electro-optic effect and optical parametric oscillation. Under proper experimental conditions, the process of second-harmonic generation can be so efficient that nearly all of the power in the incident radiation at frequency  $\omega$  is converted to radiation at the second-harmonic frequency  $2\omega$ . One common use of second-harmonic generation is to convert the output of a fixed-frequency laser to a different spectral region. For example, the Nd:YAG laser operates in the near infrared at a wavelength of  $1.06 \mu\text{m}$ . Second-harmonic generation is routinely used to convert the wavelength of the radiation to  $0.53 \mu\text{m}$ , in the middle of the visible spectrum. So, suitable nonlinear crystals are required to have laser sources at new optical wavelengths. The main requirements for non-

linear crystals are large  $\chi^{(2)}$ , wide transmission bandwidth, phase matchability, small walk-off angle and high optical damage thresholds (Boyd, 2003).

## 2.5 Classification of nonlinear optical crystal

On the basis of three types of cohesive forces that bind the charges and polarization together, the NLO materials can be classified into the following cases

1. Inorganic crystals
2. Organic crystals
3. Semiorganic crystals.

### 2.5.1 Inorganic crystals

Inorganic crystals are mostly ionic bonded; it is always easier to synthesize inorganic materials. Often these have high melting point and high degree of chemical inertness. High-temperature oxide materials are well studied for diverse applications like piezoelectric, ferroelectricity and electro-optics. Some of the useful crystals discovered are  $\text{LiNbO}_3$ ,  $\text{KNbO}_3$ , Potassium Dihydrogen Phosphate (KDP) and its analogues, Potassium Titanyl Phosphate (KTP) and its analogues,  $\beta$ -Barium Borate. Many of these materials have been successfully used in commercial frequency doublers, mixers and parametric generators to provide coherent laser radiation at high efficiency in new regions of the spectrum inaccessible by other nonlinear optical crystal and conventional laser sources (Lenin, 2008).

### 2.5.2 Organic crystals

#### Origin of second order NLO effect in organic molecules

Virtually second order NLO effects in organic molecules originate from a



**Figure 2.7** A typical SHG active molecule (Lenin, 2008).

strong donor-acceptor intramolecular interaction. This concept was demonstrated by Davydov and co-workers in 1970s while screening SHG activity in a wide variety of substituted benzenes. They conclude that dipolar aromatic molecules possessing an electron donor group and an electron acceptor group contribute to large second-order optical non-linearity arising from the intramolecular charge transfer between the two groups of opposite nature. Therefore, a typical SHG active molecule can be presented as shown in Figure 2.7 if it lacks a center of symmetry. On the other hand,  $\pi$ -conjugated molecules with a donor and an acceptor will not display SHG activity if they possess a center of symmetry. This symmetry requirement eliminates many materials from being SHG active and at the early stage of designing and synthesizing novel materials, one has to consider ways of introducing noncentrosymmetry in the molecular structures. The large second order optical nonlinearity originates from organic conjugated molecules having an electron acceptor group at one end and a donor group at the opposite end. The  $\pi$ -conjugated systems could be benzene, azobenzene, stilbene, tolans, biphenyl, benzylidene, hetrocycle polyenes etc. The electron acceptor and donor groups that can be attached to a  $\pi$ -conjugated system are as follows: (1) Acceptors groups:  $\text{NO}_2$ ,  $\text{NO}$ ,  $\text{CN}$ ,  $\text{COOH}$ ,  $\text{COO}^-$ ,  $\text{CONH}_2$ ,  $\text{CONHR}$ ,  $\text{CONR}_2$ ,  $\text{CHO}$ ,  $\text{SSI}$ ,  $\text{SO}_2\text{R}$ ,  $\text{SO}_2\text{C}_3\text{F}_7$ ,  $\text{SO}_2\text{CH}_3$ ,  $\text{COR}$ ,  $\text{COCF}^{3+}$ ,  $\text{CF}_3$ ,  $\text{COCH}_3$ ,  $\text{CH}=\text{C}(\text{CN})_2$ ,  $\text{C}_2(\text{CN})_3$ ,  $\text{SO}_2\text{NH}_2$ ,  $\text{N}^{2+}$ ,  $\text{NH}^{3+}$ ,  $\text{N}(\text{CH}_3)^{3+}$  and aromatic, (R is an alkyl group). (2) Donor Groups  $\text{NH}_2$ ,  $\text{NHCH}_3$ ,  $\text{N}(\text{CH}_3)_2$ ,  $\text{NHR}$ ,  $\text{N}_2\text{H}_3$ ,  $\text{F}$ ,  $\text{Cl}$ ,  $\text{Br}$ ,  $\text{I}$ ,  $\text{SH}$ ,  $\text{SR}$ ,  $\text{OR}$ ,  $\text{CH}_3$ ,  $\text{OH}$ ,  $\text{NHCOCH}_3$ ,  $\text{OCH}_3$ ,  $\text{SCH}_3$ ,  $\text{OC}_6\text{H}_5$ ,  $\text{C}(\text{CH}_3)_3$ ,  $\text{COOCH}_3$ ,  $\text{O}^-$ ,  $\text{S}^-$  and aromatic. (R is an alkyl

group) (Hari Shingh Nalwa and Seizo Miyata, 1996).

The electron donor-acceptor groups are of particular interest because they tend to cause bathochromic shifts which also increase the intensity of absorption bands. A donor group can provide additional electrons into the  $\pi$ -conjugated system leading to a strong interaction from a donor-acceptor combination. The donor-acceptor interaction is not only affected by the length of conjugation but also by the relative positions at the  $\pi$ -conjugated system. Because organic structures offer tremendous possibilities of chemical modification, their optical and nonlinear optical properties can be tailored. The strong donor-acceptor charge transfer interactions contribute large  $\beta$  values for organic molecules. For example  $\beta$  is larger for para-nitroaniline molecule because the donor-acceptor charge-transfer intramolecular interactions are prominent by attaining the most desirable resonance structure. The para-nitro aniline exhibits very large first hyperpolarizability due its highly asymmetric charge-correlated excited states of the  $\pi$ - electronic structure of the molecule (Lalama and Garito, 1979).

### **Strength of acceptor and donor groups**

The effects of various factors such as strength of donor and acceptor groups, nature of conjugated systems and  $\pi$ - conjugation length on polarizabilities and hyperpolarizabilities have been investigated using solution-phase dc EFISH and THG techniques (Cheng et al., 1991). The following conclusions can be drawn from these experimental results.

1. The paradisubstituted benzenes show significant increase in  $\beta$  over the sum of mono-substituted benzenes due to charge-transfer;
2. The efficiencies of acceptor groups increase in the order of  $\text{SO}_2\text{CH}_3$ , CN, CHO,  $\text{COCF}_3$ , NO,  $\text{NO}_2$ ,  $\text{CHC}(\text{CN})_2$  and  $\text{C}_2(\text{CN})_2$ ;
3. With nitro acceptor group, relative effectiveness of various donor groups

in an increasing order are :  $\text{OCH}_3 < \text{OH} < \text{Br} < \text{OC}_6\text{H}_5 < \text{OCH}_3 < \text{SCH}_3 < \text{N}_2\text{H}_3 < \text{NH}_2 < \text{N}(\text{CH}_3)_2$ ;

4. The magnitude of optical nonlinearities depends on the strength of donor-acceptor groups and the best combination of donor acceptor groups provides about 10 times enhancement (Nalwa et al., 1997).

### 2.5.3 Semi-organic crystals

The inherent limitation on the maximum attainable nonlinearity in inorganic materials and the moderate success in growing device grade organic single crystals had made scientists adopt newer strategies. The obvious one was to develop hybrid inorganic-organic materials with little trade off in their respective advantages. This new class material has come to be known as the semi-organics (Bhat, 1994). A typical case is the formation of inorganic salts of chiral organic molecules. L-Histidine tetrafluoro borate (L-HBF) monohydrate is an example of this class. The choices of organic molecules to form salts are plenty. For example tartrates, Oxalates and amino acid salts are predominantly NLO active. An alternate approach is to form metal coordination complexes of organic materials. The choice of the ligands is unlimited. In fact, the organic part need not be non-symmetric. This is typified by the example of thiourea, which forms excellent complexes with Zn, Cd and Hg. Thiourea is more polarizable than urea because of the presence of large sulphur atoms while hydrogen bonds in the  $\text{HN}_2$  ensure the lack of center of inversion in many thiourea complexes. The other known choices of ligand are allyl thiourea, guanidium and dithiocarbonate.

**Table 2.1** Comparison of various classes of NLO crystal (Lenin, 2008).

|                              | Inorganic<br>Crystals          | Organic<br>Crystals                         | Semi-organic<br>Crystals                                  |
|------------------------------|--------------------------------|---|---|
| Chemical structure           | Ionic bonded salts.            | Van der waals and hydrogen bonded           | It is formed by salts of organic and inorganic compounds. |
| Solvent                      | Water is the best solvent      | Enormous organic solvents available         | Water is used as a solvent                                |
| Effect of pH                 | Sensitive                      | Insensittive                                | Sensitive   |
| Growth rate                  | Slow and stable                | Fast  | Fast  |
| Growth morphology            | Crystal will grow in all three | Mostly it will grow as needle and platelets | Crystal will grow in all three directions                 |
| Size of the crystal          | No size limit                  | It can be grown to big size                 | It can be grown to big size                               |
| X-ray diffraction quality    | Good                           | Good  | Good  |
| UV transmission lower cutoff | 150 nm                         | 320 nm                                      | 230 nm  |
| Laser damage threshold       | Excellent                      | Moderate                                    | Excellent   |
| NLO efficiency               | High                           | Very high                                   | High  |
| Mechanical strength          | Extremely good                 | Good  | Good  |
| Stability                    | Most stable                    | Volatile                                    | Stable  |

## 2.6 Characterization

### 2.6.1 Single-crystal X-ray diffraction

Single-crystal X-ray Diffraction is a non-destructive analytical technique which provides detailed information about the internal lattice of crystalline substances, including unit cell dimensions, bond-lengths, bond-angles, and details of site-ordering. Directly related is single-crystal refinement, where the data generated from the X-ray analysis is interpreted and refined to obtain the crystal structure.

#### Fundamental principles of single-crystal X-ray diffraction

Max von Laue, in 1912, discovered that crystalline substances act as three-dimensional diffraction gratings for X-ray wavelengths similar to the spacing of planes in a crystal lattice. X-ray diffraction is now a common technique for the study of crystal structures and atomic spacing. X-ray diffraction is based on constructive interference of monochromatic X-rays and a crystalline sample. These X-rays are generated by a cathode ray tube, filtered to produce monochromatic radiation, collimated to concentrate, and directed toward the sample. The interaction of the incident rays with the sample produces constructive interference (and a diffracted ray) when conditions satisfy Bragg's Law ( $n\lambda=2d \sin\theta$ ). This law relates the wavelength of electromagnetic radiation to the diffraction angle and the lattice spacing in a crystalline sample. These diffracted X-rays are then detected, processed and counted. By changing the geometry of the incident rays, the orientation of the centered crystal and the detector, all possible diffraction directions of the lattice should be attained. All diffraction methods are based on generation of X-rays in an X-ray tube. These X-rays are directed at the sample, and the diffracted rays are collected. A key component of all diffraction is the an-

gle between the incident and diffracted rays. Powder and single-crystal diffraction vary in instrumentation beyond this.

### **Interpretation of data**

Typical mineral structures contain several thousand unique reflections, whose spatial arrangement is referred to as a diffraction pattern. Indices (hkl) may be assigned to each reflection, indicating its position within the diffraction pattern. This pattern has a reciprocal Fourier transform relationship to the crystalline lattice and the unit cell in real space. This step is referred to as the solution of the crystal structure. After the structure is solved, it is further refined using least-squares techniques. This procedure is described fully on the single-crystal structure refinement (SREF) page.

### **Single-crystal X-ray diffraction instrumentation**

X-ray diffractometers consist of three basic elements, an X-ray tube, a sample holder, and an X-ray detector as shown in Figure 2.8. X-rays are generated in a cathode ray tube by heating a filament to produce electrons, accelerating the electrons toward a target by applying a voltage, and impact of the electrons with the target material. When electrons have a sufficient energy to dislodge inner shell electrons of the target material, characteristic X-ray spectra are produced. These spectra consist of several components, the most common being  $K_\alpha$  and  $K_\beta$ .  $K_\alpha$  consists, in part, of  $K_{\alpha 1}$  and  $K_{\alpha 2}$ .  $K_{\alpha 1}$  has a slightly shorter wavelength and twice the intensity as  $K_{\alpha 2}$ . The specific wavelengths are characteristic of the target material. Filtering, by foils or crystal monochrometers, is required to produce monochromatic X-rays needed for diffraction.  $K_{\alpha 1}$  and  $K_{\alpha 2}$  are sufficiently close in wavelength such that a weighted average of the two is used. Molybdenum is the most common target material for single-crystal diffraction, with  $\text{Mo}K_\alpha$  radiation = 0.7107 Å. These X-rays are collimated and directed onto the sample. When the

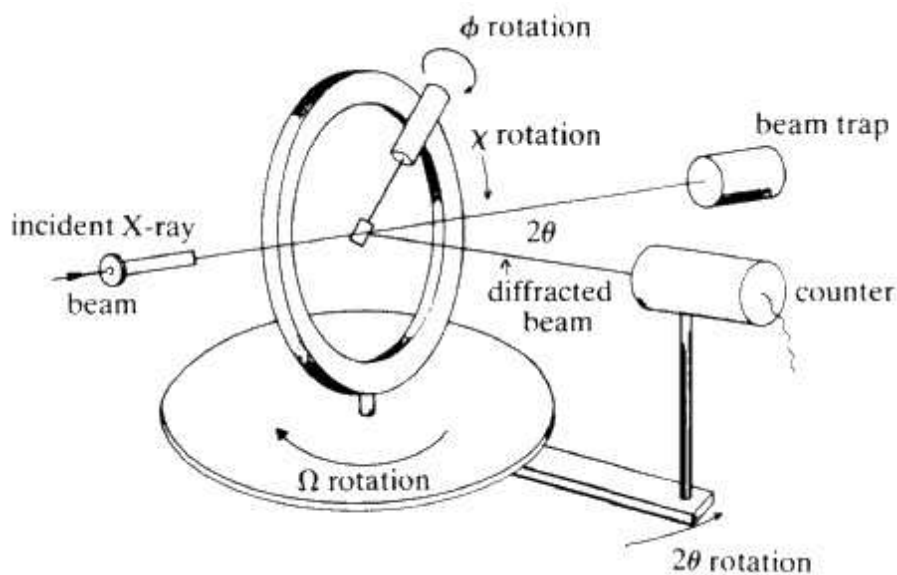


**Figure 2.8** Schematic of 4-circle diffractometer; the angles between the incident ray, the detector and the sample (<http://serc.carleton.edu>).

geometry of the incident X-rays impinging the sample satisfies the Bragg equation, constructive interference occurs. A detector records and processes this X-ray signal and converts the signal to a count rate which is then output to a device such as a printer or computer monitor. X-rays may also be produced using a synchrotron, which emits a much stronger beam. Single-crystal diffractometers use either 3- or 4-circle goniometers. These circles refer to the four angles ( $2\theta$ ,  $\chi$ ,  $\varphi$ , and  $\Omega$ ) that define the relationship between the crystal lattice, the incident ray and detector. Samples are mounted on thin glass fibers which are attached to brass pins and mounted onto goniometer heads as shown in Figure 2.9. Adjustment of the X, Y and Z orthogonal directions allows centering of the crystal within the X-ray beam. X-rays leave the collimator and are directed at the crystal. Rays are either transmitted through the crystal, reflected off the surface, or diffracted by the crystal lattice. A beam stop is located directly opposite the collimator to block transmitted rays and prevent burn-out of the detector. Reflected rays are not picked up by the detector due to the angles involved. Diffracted rays at the correct

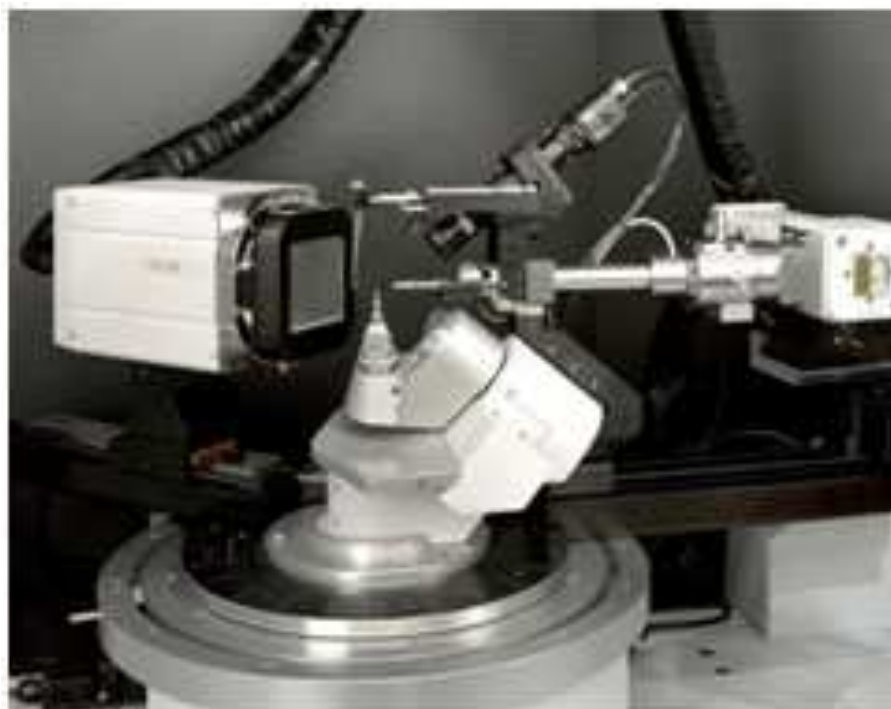


**Figure 2.9** Image courtesy of Bruker-Axs (<http://serc.carleton.edu>).

orientation for the configuration are then collected by the detector. Modern single-crystal diffractometers use CCD (charge-coupled device) technology to transform the X-ray photons into electrical signals which are then sent to a computer for processing.

### **Applications**

Single-crystal X-ray diffraction is most commonly used for precise determination of a unit cell, including cell dimensions and positions of atoms within the lattice. Bond-lengths and angles are directly related to the atomic positions. The crystal structure of a mineral is a characteristic property that is the basis for understanding many of the properties of each mineral. Specific applications of single-crystal diffraction include:

- New mineral identification, crystal solution and refinement
- Determination of unit cell, bond-lengths, bond-angles and site-ordering

- Characterization of cation-anion coordination
- Variations in crystal lattice with chemistry
- With specialized chambers, structures of high pressure and/or temperature phases can be determined
- Determination of crystal-chemical vs. environmental control on mineral chemistry
- Powder patterns can also be derived from single-crystals by using specialized cameras.

([http://serc.carleton.edu/research\\_education/gochemsheets/techniques/SXD.html](http://serc.carleton.edu/research_education/gochemsheets/techniques/SXD.html))

## 2.6.2 High resolution X-ray diffraction

A multicrystal X-ray diffractometer designed and developed at National Physical Laboratory (NPL) (Krishan Lal and Bhagavannarayana, 1989) has been used to study the crystalline perfection of single crystal(s) and was used in the present investigation. Figure 2.10 shows the schematic diagram of the multicrystal X-ray diffractometer. The divergence of the X-ray beam emerging from a fine focus X-ray tube (Philips X-ray Generator; 0.4 mm × 8 mm; 2kW Mo) is first reduced by a long collimator fitted with a pair of fine slit assemblies. This collimated beam is diffracted twice by two Bonse-Hart (Bonse and Hart, 1965) type of monochromator crystals and the thus diffracted beam contains well resolved  $\text{MoK}\alpha_1$  and  $\text{MoK}\alpha_2$  components. The  $\text{MoK}\alpha_1$  beam is isolated with the help of fine slit arrangement and allowed to further diffract from a third (111) Si monochromator crystal set in dispersive geometry (+, -, -). Due to dispersive configuration, though the lattice constant of the monochromator crystal and the specimen are different, the dispersion broadening in the diffraction curve of the specimen does not arise. Such an arrangement disperses the divergent part of the  $\text{MoK}\alpha_1$  beam away from the

Bragg diffraction peak and thereby gives a good collimated and monochromatic MoK $\alpha_1$  beam at the Bragg diffraction angle, which is used as incident or exploring beam for the specimen crystal. The dispersion phenomenon is well described by comparing the diffraction curves recorded in dispersive (+, -, -) and non-dispersive (+, -, +) configurations (Bhagavannarayana, 1994). This arrangement improves the spectral purity ( $\Delta\lambda/\lambda \ll 10^{-5}$ ) of the MoK $\alpha_1$  beam. The divergence of the exploring beam in the horizontal plane (plane of diffraction) was estimated to be  $\ll 3$  arc sec. The specimen occupies the fourth crystal stage in symmetrical Bragg geometry for diffraction in (+, -, -, +) configuration. The specimen can be rotated about a vertical axis, which is perpendicular to the plane of diffraction, with minimum angular interval of 0.5 arc sec. The diffracted intensity is measured by using an in-house (NPL) developed scintillation counter. To provide two-theta ( $2\theta_B$ ) angular rotation to the detector (scintillation counter) corresponding to the Bragg diffraction angle ( $\theta_B$ ), it is coupled to the radial arm of the goniometer of the specimen stage. The rocking or diffraction curves were recorded by changing the glancing angle (angle between the incident X-ray beam and the surface of the specimen) around the Bragg diffraction peak position  $\theta_B$  (taken as zero for the sake of convenience) starting from a suitable arbitrary glancing angle. The detector was kept at the same angular position  $2\theta_B$  with wide opening for its slit, the so-called  $\omega$  scan. Before recording the diffraction curve to remove the non-crystallized solute atoms remained on the surface of the crystal and also to ensure the surface planarity, the specimen was first lapped and chemically etched in a non preferential etchant of water and acetone mixture in 1:2 volume ratio.

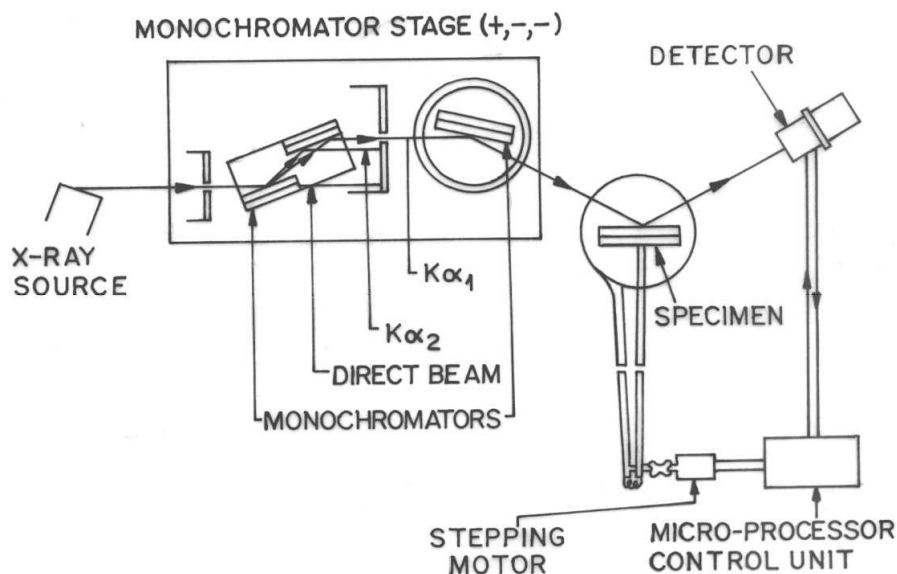


**Figure 2.10** Schematic diagram of multi crystal X-ray diffractometer designed, developed and fabricated at NPL.

### 2.6.3 Etching studies

The basis of etching technique is the fact that the region where dislocations intersect the surface of the crystal is energetically different from the surrounding area. This is reflected as difference in chemical or physical “reactivity“. Reaction or dissolution under careful control can result in enhanced reaction at these points with the consequent development of surface pitting, which defines the positions of the emergent dislocation cores and, hence, the number of these defects which intersect the surface. Such pitting can, of course, occur randomly and it is essential to define that the pits produced do arise from dislocations. Dislocation generally moves from nucleation point or seeding point. Any cleavage will intersect the dislocation lines. The etch patterns observed in the two halves of etched crystal look alike. Some times, continued etching can also be done and it reveals the same pattern with less variation. The etch pits are aligned according to movement of dislocations or mechanical deformation. The continued etching reveals etch pits without distortion. The patterns with well-defined alignment of etch pits

corresponding to the migration of dislocations along slip planes are well observed features of organic crystals.

## 2.6.4 Thermal analysis

### Thermo-gravimetric analysis

Thermal-gravimetric analysis (TGA) includes a group of techniques in which the physical property of the substance is measured as a function of temperature while the substance is subjected to a controlled temperature program. When a sample is heated or cooled at a controlled rate, the weight of substance in an environment is recorded and the change of weight (loss or gain) is measured as a function of temperature or time. The main parts of TGA are

- High sensitive thermobalance
- Micro - furnace
- Furnace temperature programmer or controller
- Recorder or computer with plotter.

The thermobalance is used to measure the weight accurately and the microfurnace to change the temperature in a controlled manner at a specific rate. A schematic diagram of TGA is presented in Figure 2.11. The thermobalance chamber consists of a servo controlled balance arm. At one end of the balance arm, a tare weight is suspended and at the other end, sample pan is hung down by means of a nichrome wire through a quartz link. This pan extends down to micro-furnace chamber through a metallic anti static tube. The thermobalance uses a servo operated balance system in which the electrical signal from an optical null detector is applied directly to control the current in a torque motor. The weight loss as a function of temperature is measured by the principle of null deflection method using a light source, a photosensitive diode. Here the torque exerted by the servo

motor to restore the balance arm to its null position, is directly proportional to the weight of the sample which was calibrated using a standard 100 mg weight (Willard, 1986; Gilson, 1970).

The ultra microwave furnace and the sample holder are shown in Figure 2.12. A unique of an alumina cylinder which is 0.5 inch in diameter and 0.75 inch in length, wound with platinum wire. The furnace is constructed with bifilarly wound platinum wire and plasma sprayed with alumina at high temperature. It is covered with ceramic cement and cured. This coating protects platinum winding from the attack of the corrosive gases evolved during analysis. The platinum wire functions both as a heater and also as a temperature sensor. A platinum sleeve is placed around the platinum wire wound around the mandrel to provide uniform distribution in the furnace. The maximum temperature of the furnace is 1000 °C. This mandrel is held by a mullite stem, which is about four inches long. The mullite stem is supported by short posts at its base and fits into a stainless steel assembly. The whole assembly is enclosed by a pyrex tube provide with a gas outlet. Due to the low thermal inertia of the microfurnace, a controlled heating or cooling rate as high as 200 °C/min is achieved. An automated furnace lift mechanism ensures the reproducible positioning of the sample (Willard et al., 1986; Gilson, 1970).

An automated temperature calibration programme is built into the system wherein the system is calibrated. The temperature of the furnace was calibrated with Ni and Fe (Curie point standards) along with a small horse shoe magnet placed around the microfurnace. A two point calibration is run to calibrate the TG PC-7 series analyzer. It takes care of the reaction kinetics and also detects the melting point of the compound, which is to be investigated.

### **Differential thermal analysis**

In differential thermal analysis (DTA) the temperature of a sample and a

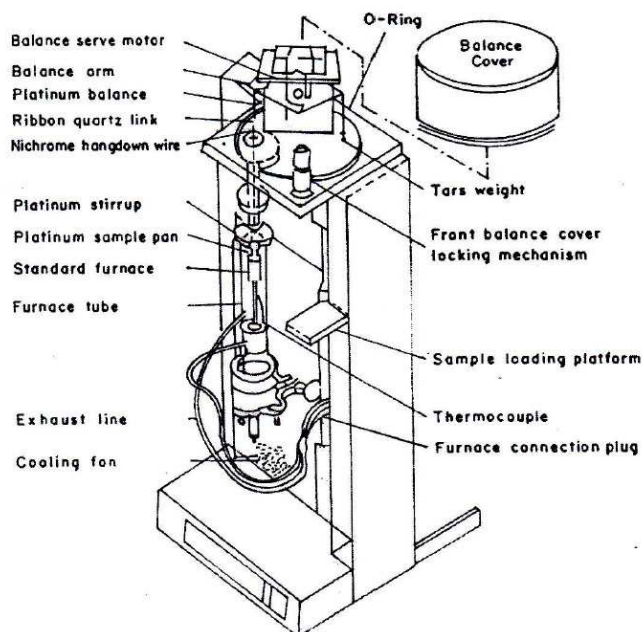


**Figure 2.11** Schematic diagram of TGA (Willard et al., 1986).

thermally inert reference material are measured as a function of temperature (usually sample temperature). Any transition which the sample undergoes will result in the liberation or absorption of the energy by the sample with corresponding deviation of its temperature from that of the reference (Willard et al., 1986).

### 2.6.5 Dielectric measurement

Impedance measurements are a basic means of evaluating electronic components and materials. Every material has a unique set of electrical characteristics that are dependent on its dielectric or insulation properties. Accurate measurements of these properties can provide valuable information to ensure an intended application or maintain a proper manufacturing process. And so what are these measurements and how are they made?

#### Dielectric constant

The dielectric constant measurement, also known as relative permittivity, is

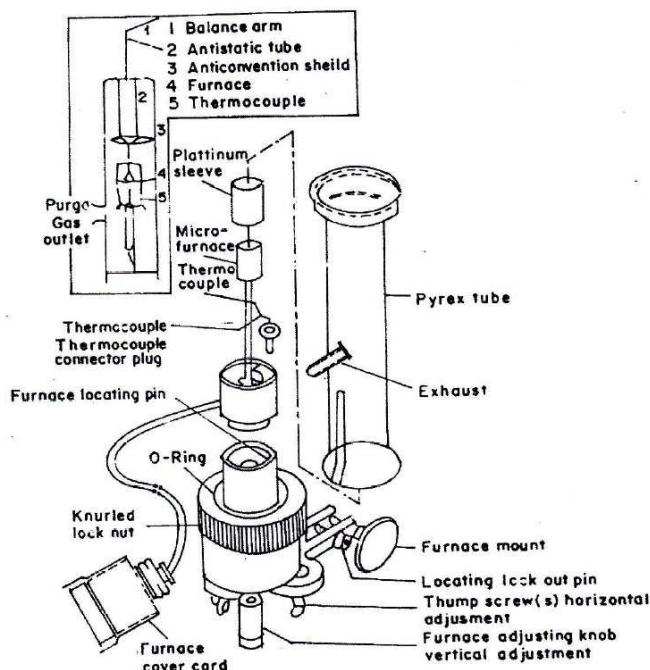


**Figure 2.12** Schematic diagram of ultra micro-furnace and sample holder (Willard et al., 1986).

one of the most popular methods of evaluating insulators such as rubber, plastics, and powders. It is used to determine the ability of an insulator to store electrical energy. The complex dielectric constant consists of a real part ( $\epsilon'$ ), which represents the storage capability and an imaginary part ( $D$ ), which represents the loss.

Dielectric constant measurements can be performed easier and faster than chemical or physical analysis techniques making them an excellent material analysis tool. The dielectric constant is defined as the ratio of the capacitance of the material to the capacitance of air, or  $\epsilon' = \frac{C_x}{C_o}$  where  $C_x$  is the capacitance with a dielectric material and  $C_o$  is the capacitance without material, or vacuum. The  $\epsilon'$  value of dry air is 1.00053, which for most measurement applications is usually close enough to the value of a vacuum, which is 1.0000. Thus if a material is to

be used for insulating purposes only, it would be better to have a lower dielectric constant, or as close to air as possible. To the contrary, if a material is to be used in electrical applications for storage of electrical charge, the higher the dielectric constant the better. More charge is stored when a dielectric is present than if no dielectric (air) is present. The dielectric material increases the storage capacity of the plate capacitor, hence the dielectric constant of any solid or liquid would be greater than 1.

#### Example of dielectric constants of common materials

|              |         |
|--------------|---------|
| Vacuum       | 1.0     |
| Air          | 1.00053 |
| Pure Teflon  | 2.047   |
| Fused Quartz | 3.78    |
| Water        | 78 .    |

#### **Dissipation factor**

Dissipation factor (D) is defined as the ratio of an insulating materials resistance to its capacitive reactance at a specified frequency. It measures the inefficiency or loss of the material, is always greater than 0, but usually much smaller than the dielectric constant. D measurements are an excellent means of quality control which can yield indication of contamination or deterioration. For example, if we wanted to check the purity of epoxy or some raw material for consistency in a production run why not just measure the D. Excessive moisture would increase the dissipation factor value telling us something has changed as compared to previously established values.

#### **How can these measurements be made?**

When making these measurements, connection of the material to the mea-

asuring instrument (an LCR Meter) is one of the major challenges faced, special fixtures are generally required depending on the material type. With copier toner, pvc compounds, and other powders the material can be compressed into a test slab or disk at a given thickness so it can be measured in a dielectric cell. In simplest terms a dielectric cell is a nothing more than a test fixture with two adjustable plates into which the sample is installed for evaluation of its electrical properties. The most common piece of test equipment for holding a variety of solid materials is the LD-3, a liquid tight, three terminal connection cell with electrode spacing adjustable by a precision micrometer. When connected to an automatic LCR meter, the capacitance (C) and loss (D) measurements can be read out directly yielding fast, reasonable results.

### **Quick, easy measurements of solid materials**

The International Electrotechnical Commission (IEC) and the American Society for Testing and Materials (ASTM) have developed published methods for the measurement of dielectric constant and dielectric loss. They are written for use by people highly skilled in testing electrical insulation and not easily understood by the less experienced on this subject. One method that is quick and easy, requires a minimum of calculations, but does sacrifice some accuracy, is the Contacting Electrode Method. The results would generally be within 10% if the sample is reasonably flat, thick and uniform.

Let's take a look at the process of what an actual measurement could consist of. First the sample is inserted in the cell and the electrodes closed with the micrometer until they just touch the sample lightly, Figure 2.13A. The micrometer spacing  $h_m$  is then recorded for this specimen. The capacitance value,  $C_{xm}$  and dissipation factor,  $D_{xm}$  are then measured with the LCR meter.

In this example:  $C_{xm} = 42.595 \text{ pF}$   $D_{xm} = 0.0536$   $h_m = 0.2875 \text{ cm}$ .

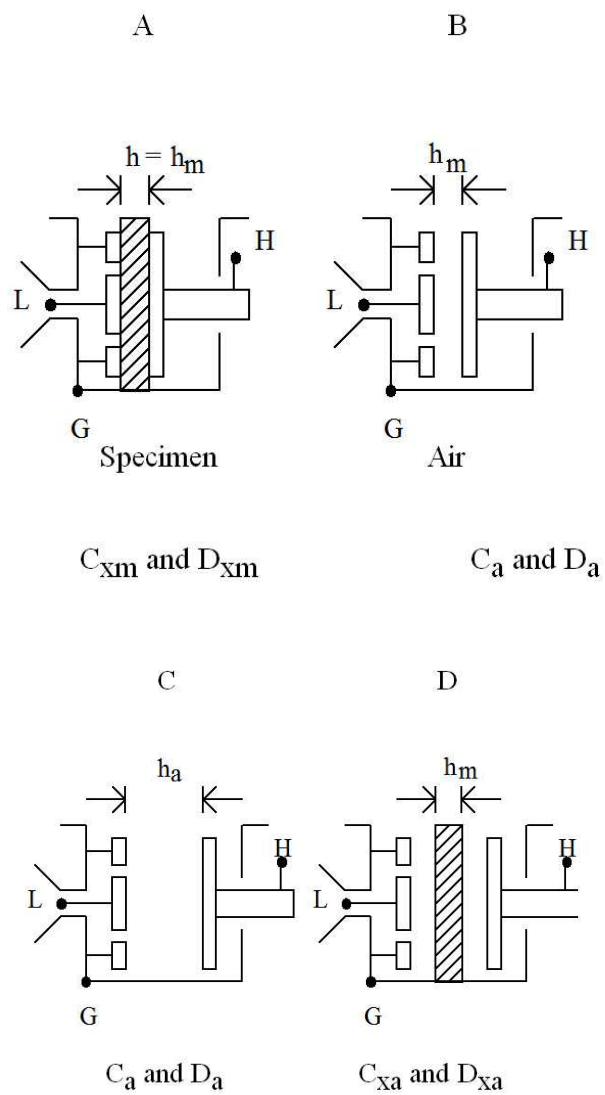


**Figure 2.13** Dielectric measurement ([www.tmworld/file/4402](http://www.tmworld/file/4402)).

The specimen is then removed from the cell, micrometer readjusted to  $h_m = 0.2875$  and the measurements repeated in air as  $C_a$  and  $D_a$ , Figure 2.13B.

$$C_a = 9.245 \text{ pF} \quad D_a = 0.0002 \quad h_m = 0.2875 \text{ cm.}$$

The dielectric constant of the specimen is (neglecting the small difference between  $C_a$  in air and  $C_0$  in a vacuum)  $\epsilon'_x = (1.00053) C_{xm}/C_a = 42.595/9.245 = 4.60$  and the dissipation factor is  $D_x = D_{xm} - D_a = 0.0534$ .

The factor 1.00053 in the formula for  $\epsilon'_x$  corrects for the dielectric constant of (dry) air. Subtracting  $D_a$  from  $D_{xm}$  removes any constant phase error in the instrument. Better accuracy can be obtained if the measured  $D_a$  is a significant percent of  $D_{xm}$  by adjusting the electrode spacing until the measured capacitance is approximately equal to  $C_{xm}$  and then measure  $D_a$ .

Note that both  $\epsilon_x$  and  $D_x$  will probably be somewhat low because there is always some air between the electrodes and the sample. This error is smallest for very flat samples, for thicker samples, and for those with low  $\epsilon'$  and  $D$  values.

Other methods for increased accuracy since a layer of air between specimen and electrodes can't be completely avoided a more accurate result is possible using another calculation and a specimen of known thickness. In this case the thickness of the sample is first measured at several different points and averaged to yield  $h_m$ , Figures 2.13C, D. The electrodes of the test cell are opened to 0.01 to 0.02 cm greater than  $h_m$  by setting the micrometer to a value of  $h_a$ . The capacitance and dissipation factor,  $C_a$  and  $D_a$ , are measured for  $h_a$ , with air as the dielectric. The specimen is then inserted between the electrodes, approximately in the center, and the new values,  $C_{xa}$  and  $D_{xa}$ , measured. The value for dielectric constant is then calculated from

$$\epsilon' = \frac{1}{1 - \frac{\Delta C}{C_{xa}} \frac{h_a}{h_m}}, \quad (2.19)$$

and  $D$  calculated from

$$D = D_{xa} + \left(\frac{h_a}{h_m} - 1\right)\varepsilon'(D_{xa} - D_a). \quad (2.20)$$

The accuracy of these results depends mainly upon the accuracy with which the two thicknesses (material and cell opening) can be measured. This is called the Air-Gap Method.

We can even take this one step further. When a specimen whose thickness is difficult to measure, because it is thin or not rigid, it can be measured without regard to its thickness. A measurement is first made with the cell and a fluid, usually air, then the specimen plus air (same as the air-gap method discussed earlier). Two more measurements are then made; the cell with a second fluid, and the specimen with this second fluid. This is called the Two-Fluid Method, which yields accurate results of dielectric constant and loss through a slightly more complex calculation. In this method the choice of fluid must be one that has known and stable dielectric properties, does not react with the test specimen and not too messy to deal with. Usually a silicon fluid base fits this requirement.

## Conclusion

LCR Meters as shown Figure 2.14 and specimen cells are readily available that make it easy to perform impedance measurements on materials. A measuring instrument with a wide programmable frequency range is important since the insulation properties can vary substantially with frequency. Accuracy of results can be enhanced by averaging several measurements and calculating results can be simplified through computer programs, all of which leads to better process control, increased efficiency and superior products.

([www.tmworld/file/4402-Jim Richards of QuadTech.doc?force=true](http://www.tmworld/file/4402-Jim%20Richards%20of%20QuadTech.doc?force=true))



Figure 2.14 LCR meter ([www.tmworld/file/4402](http://www.tmworld/file/4402)).

### 2.6.6 Piezoelectric measurement

A piezoelectric substance is one that produces an electric charge when a mechanical stress is applied (the substance is squeezed or stretched). Conversely, a mechanical deformation (the substance shrinks or expands) is produced when an electric field is applied. This effect is formed in crystals that have no center of symmetry. To explain this, we have to look at the individual molecules that make up the crystal. Each molecule has a polarization, one end is more negatively charged and the other end is positively charged, and is called a dipole. This is a result of the atoms that make up the molecule and the way the molecules are shaped. The polar axis is an imaginary line that runs through the center of both charges on the molecule. In a mono crystal the polar axes of all of the dipoles lie in one direction. The crystal is said to be symmetrical because if you were to cut

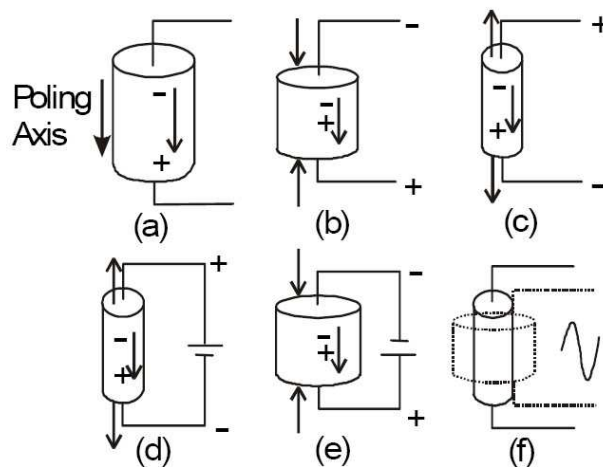


Figure 3: Example of Piezoelectric Effect

Figure 2.15 Example of the piezoelectric effect (www.aurelienr.com).

the crystal at any point, the resultant polar axes of the two pieces would lie in the same direction as the original. In a polycrystal, there are different regions within the material that have a different polar axis. It is asymmetrical because there is no point at which the crystal could be cut that would leave the two remaining pieces with the same resultant polar axis. The piezoelectric effect can now be observed in the crystal. Figure 2.15 (www.aurelienr.com/electronique/piezo/piezo.pdf) illustrates the piezoelectric effect. Figure 2.15(a) shows the piezoelectric material without a stress or charge. If the material is compressed, then a voltage of the same polarity as the poling voltage will appear between the electrodes (b). If stretched, a voltage of opposite polarity will appear (c). Conversely, if a voltage is applied the material will deform. A voltage with the opposite polarity as the poling voltage will cause the material to expand, (d), and a voltage with the same polarity will cause the material to compress (e). If an AC signal is applied then the material will vibrate at the same frequency as the signal (f).

### Using the piezoelectric effect

The piezoelectric crystal bends in different ways at different frequencies. This bending is called the vibration mode. The crystal can be made into various shapes to achieve different vibration modes. To realize small, cost effective, and high performance products, several modes have been developed to operate over several frequency ranges. These modes allow us to make products working in the low kHz range up to the MHz range.

([www.aurelienr.com/electronique/piezo/piezo.pdf](http://www.aurelienr.com/electronique/piezo/piezo.pdf))

### **2.6.7 UV-Vis spectrophotometry**

Spectrophotometers include promotion of electrons from the ground state to higher energy state. In the ground state the spins of the electrons in each molecular orbital are essentially paired. In the higher state, if the spins of the electrons are paired then it is called an excited singlet state. On the other hand, if the spins of the electrons in the excited state are parallel, it is called excited triplet state.

#### **Description of the instrument**

A spectrophotometer is a device which detects the percentage transmittance of light of certain intensity and frequency range is passed through the sample. Thus the instrument compares the intensity of the transmitted light with that of incident light. It consists of a source, focusing optics, standard sample cuvette, wavelength isolation device, and a detector with amplifier and readout system. Figure 2.16 shows the schematic representation of double beam UV-Vis spectrophotometer.

#### **Scanning double beam spectrophotometer**

Spectrophotometers of this type feature a continuous change in wavelength. One beam permanently accommodates a reference or blank, and the other the sample. An automatic comparison of transmittance of sample and reference is made

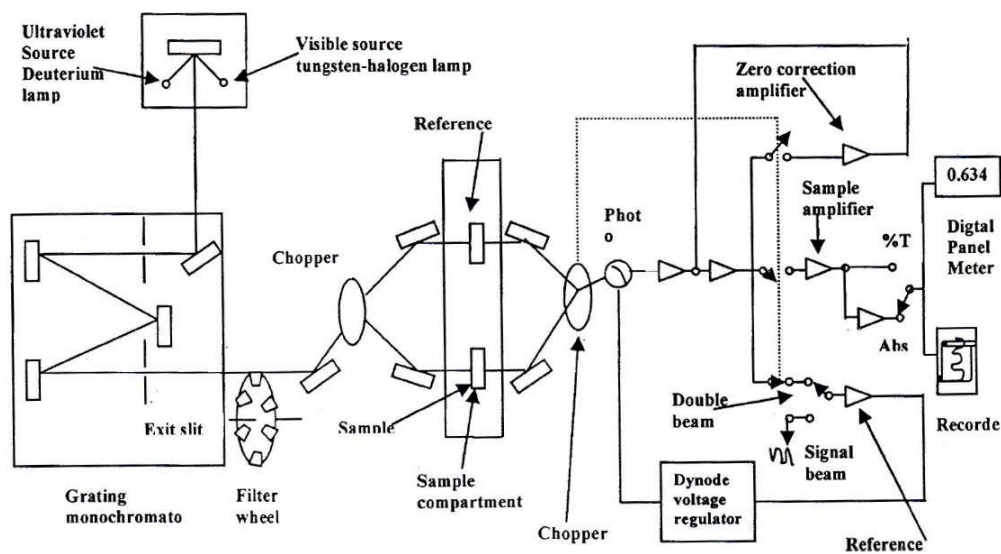


**Figure 2.16** UV-Vis-NIR spectrophotometer (Willard et al., 1986).

while scanning through the wavelength region. The ratio of sample to reference after conversion to absorbance values is plotted as a function of wavelength on a recorder.

In an optical arrangement light from either visible or ultraviolet source enters the grating monochromator. Broad band filters contained in a filter wheel are automatically indexed into position at a order from diffraction grating. The optical beam is then directed alternatively through the sample and reference cells by a system of rotating sector mirrors (choppers) and corner mirrors. Each beam, a pulse of light separated in time by a dark interval, is then directed onto a photomultiplier tube in a time sharing procedure. After amplification, the reference signal is used to provide a signal to dynode voltage regulator. The dynode voltage is varied to maintain a constant reference signal and keep all amplifiers within required operating limits. The sample signal is either processed through a logarithmic converter for absorbance measurements or is used directly for transmittance

measurements. The result is fed to recorder, meter or digital indicator (Willard, 1986).

### **2.6.8 Microhardness**

Hardness of a material is the resistance offered to indentation by a much harder body. It may be termed as a measure of the resistance against lattice destruction or the destruction or the resistance offered to permanent deformation or damage (Still, 1938). The term “Hardness” means in different ways. It is the resistance to penetration to a metallurgist, resistance to wear to a lubrication engineer, resistance to scratching to a mineralogist and resistance to cutting to a machinist. All these are related to the plastic flow stress of the material. The hardness properties are basically related to the crystal structure of the material. Microhardness study on the crystals brings out an understanding of the plasticity of the crystal (Desai and Rai, 1983).

Hardness is a technique, in which a crystal is subjected to a relatively high pressure within a localized area. By suitable choice of indenter material and relatively simple equipment construction, hardness tests can be easily carried out on all crystalline materials under various conditions of temperature and pressure. Deformation is local, so that a number of trials can be made on a single specimen of small dimensions and can be reproduced by maintaining the specimen indenter orientation relationship. Specimen of flat relatively smooth surface is required.

#### **Method of hardness test**

Hardness measurement can be carried out by various methods. They are classified as follows.

- Static indentation test
- Dynamic indentation test

- Scratch test
- Rebound test
- Abrasion test

The most popular and simplest form is the static indentation test wherein the specific. Geometry is pressed into the surface of a test specimen under a know load. The indenter may be ball or diamond cone or diamond pyramid. Upon removal of the indenter, a permanent impression is retained in the specimen. The hardness is calculated from the area or depth of indentation produced. The variables are the type of the indenter or load. The indenter is made up of a very hard material to prevent its deformation by the test piece so that it can cover materials over a wide range of hardness. For this reason either a hardened steel sphere or a diamond pyramid or cone is employed. A pyramid also has advantage that geometrically similar impressions are obtained at different loads. So naturally a pyramid indenter is preferred. In this static indentation test the indenter is pressed perpendicularly in the surface of the sample by means of an applied load. Then by measuring the cross sectional area or the depth of the indentation and knowing the applied load an empirical hardness number may be calculated. This procedure followed by Brinell, Meyer, Knoop and Rockwell test (Wyatt and Hughes, 1974; Tabor, 1951; Neil, 1967).

In the dynamic indentation test, a ball or a cone (or a number of small spheres) is allowed to fall from a definite height and the hardness number is obtained from the dimensions of the indentation and the energy of impact.

The scratch test can be classified into two types:

- Comparison test in which one material is said to be harder than another if the second material is scratched by the first.
- A scratch test with a diamond indenter on the surface at a steady rate

and under a definite load. The hardness number is expressed in terms of the width of depth of the groove formed.

In the rebound test an object of standard mass and dimensions is bounced from the test surface and the height of rebound is taken as the measure of hardness. In abrasion test, a specimen is loaded against a rotating disk and the rate of wear is taken as a measure of hardness.

### **Vickers test**

Among the various methods of hardness measurements discussed above, the most common and reliable method is the Vickers hardness test method. In this method, microindentation is made on the surface of a specimen with the help of diamond indenter (Figure 2.17). Smith and Sandland (1923) have proposed that a pyramid be substituted for a ball in order to provide geometrical similitude under different values of load. The Vickers pyramid indenter where opposite faces contain an angle ( $\alpha = 136^\circ$ ) is most widely accepted pyramid indenter. A pyramid is suited for hardness tests due to the following two reasons (Balta Calleja et al., 1980).

- The contact pressure for a pyramid indenter is independent of indent size.
- Pyramid indenters are less affected by elastic release than other indenters.

The base of the Vickers pyramid is square and the depth of indentation corresponds to  $1/7^{th}$  of the indentation diagonal. Hardness is generally defined as the ratio of the load applied to the surface area of the indentation. The Vickers hardness number  $H_v$  of Diamond Pyramid Number (DPN) is defined as

$$H_v = \frac{2P \sin \alpha/2}{d^2} \text{Kg/mm}^2, \quad (2.21)$$

where  $\alpha$  is the apex angle of the indenter ( $\alpha = 136^\circ$ ). The Vickers hardness number

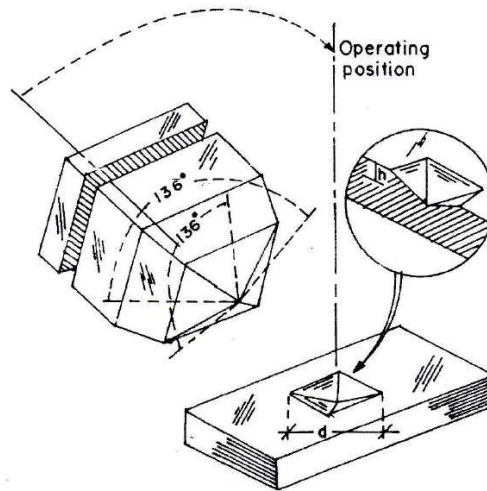


**Figure 2.17** Schematic diagram of Vickers diamond pyramid indenter and indentation produced (Balta Calleja et al., 1980).

is therefore calculated from the relation

$$H_v = \frac{1.8544P}{d^2} \text{Kg/mm}^2, \quad (2.22)$$

where  $P$  is the applied load in kg and  $d$  is the diagonal length of the indentation mark in mm. Hardness values are measured from the observed size of the impression remaining after a loaded indenter has penetrated and has been removed from the surface. Thus the observed hardness behavior in the final measurement of the residual impression is the summation of a number of effects involved in the materials response to the indentation pressure during loading.

## 2.6.9 Nonlinear optical measurement technique

### Second harmonic powder test

The basic configuration used for the study of second harmonic generation in powder is shown in Figure 2.18. It consists of a Q-switched laser whose beam

falls unfocused onto a thin section (0.2 mm) of powder of the material under study. After the fundamental beam is removed by a series of short wavelength passing filters, the second harmonic is detected by a photomultiplier and displayed on an oscilloscope. A reference beam is obtained by use of beam splitter placed ahead of the sample. This enables the intensity of the fundamental or second harmonics generated in a reference sample (Ducuin and Bloembergen, 1964) to be monitored by displaying both signals simultaneously on a dual-beam scope. The system also permitted the insertion of narrow pass filters at the second-harmonic wavelength between the shot filters and the photomultiplier to eliminate spurious signals. In order to improve the efficiency of second harmonic collection at the detector, a parabolic reflector was placed directly in front of the sample (i.e., between the laser and the sample) with a small access hole for the laser beam. Nd:YAG laser of 1064 nm was used. It was Q-switched by a rotating mirror at a rate of 400 Hz. Peak power in this case were 1 kW with pulsewidths of 200 nsec (Smith and Sandland, 1923).

### **Sample preparation and mounting**

Samples were prepared and mounted using several techniques. For qualitative results a thin layer (0.2 mm) of upgraded powder was placed on a microscope slide and held in place with transparent tape. For quantitative work, powders were graded by use of standard sieved to the desired range of particle sized (usually 75 - 150  $\mu\text{m}$ ) and loaded into a quartz cell of well known thickness (0.2 mm, 0.1 mm, etc.) with the aid of a vibrator to assure uniform packing. Particle sizes were checked by standard optical microscopy techniques. In the case of materials such as quartz, zinc oxide, and other materials having well known nonlinear coefficients and available in single-crystal form, powders were made from single crystals using a Spex vibrating ball mill, and then graded using standard sieves. A similar pro-

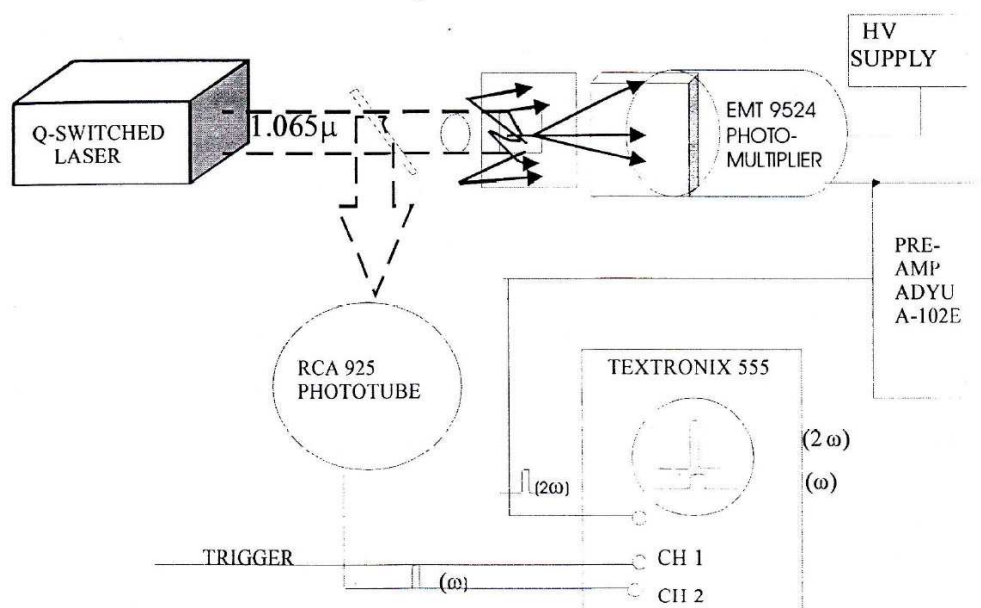


**Figure 2.18** Apparatus used for study of second harmonic generation in powders (Ducuin and Bloembergen, 1964).

cedure was followed in the case of minerals of polycrystalline or single-crystalline character (Kurt and Perry, 1968).

### Experimental results

In order to determine the essential features of second-harmonic generation in thin powder layers, a series of experiments were performed to measure the dependence of second-harmonic intensity on the following parameters, (1) angle between detector and direction of incident light beam ( $\theta$ ), (2) powder-layer thickness ( $L$ ), (3) average particle size ( $\hat{r}$ ), and (4) laser-beam diameter ( $D$ )

Within certain ranges of layer thickness and particle size it was found that a fairly simple and reproducible dependence on each of the above parameters could be obtained. The following discussion is limited basically to a domain in which  $\hat{r} \ll L \ll D$ . This ordering insures that the fundamental beam strikes large number particles of random orientation. Thereby performing a significant

statistical average. In addition a planar geometry is retained.

### Angular distribution

When the average particle size, layer thickness, and beam diameter satisfy the inequality as  $\hat{r} \ll L \ll D$ , it is found that the angular distribution of second-harmonic intensity for the powder in air is nearly cosinusoidal in  $\theta$  for both the forward and backward scattering directions. Thus, the sample considered as a source of second-harmonic radiation behaves like an isotropic planar radiator obeying Lambert's (cos) law (Born and Wolf, 1964):

$$I(\theta, \Phi) = I_0 \cos\theta, \quad (2.23)$$

where  $\theta$  and  $\Phi$  are spherical polar angles and the photometric intensity  $I_0$  (energy/sec/sr) is defined as

$$I_0 \equiv \int B dS \quad (2.24)$$

where  $B$  is the photometric brightness and  $dS$  is a surface element.

### Dependence of $I^{2\omega}$ on layer thickness $L$

The second-harmonic signal was found to vary linearly with layer thickness  $L$  for fixed particle size  $r$  after integrating over the  $4\pi$  solid angle. This implies that the second-harmonic intensity is proportional to the total number of particles present. A linear dependence on  $L$  was also found in the case of immersion of the powder in an index-matching liquid.

### Dependence of $I^{2\omega}$ on average particle size

The important features of the particle-size dependence are: (1) a peak in the intensity when the particle size is close to the average coherence  $I_c$ , (2) an approximately linear increase in intensity with increasing particle size  $\hat{r} \ll I_c$  and (3) an inversion relation between intensity and particle size (i.e.,  $I^{2\omega} \propto 1/\hat{r}$ ) for

$$\hat{r} \gg I_c$$

This technique allows only a rough estimate of nonlinear optical response. The powder sample is irradiated by a fundamental laser beam and the generated second harmonic light is detected by a photomultiplier tube. A reference sample with well known nonlinearity is also used to calibrate the second harmonic light.

## 2.7 References

- Alexandru, H.V., Antohe S. (2003). **Journal of Crystal Growth** 258: 149.
- Bairava Ganesh, R., Kannan, V., Sathyalakshmi V., Ramasamy, P. (2006). The Growth of L-glutamic acid hydrochloride crystal by Sankaranarayanan-Ramasamy (SR) method. **Materials Letters**. 61: 706.
- Balamurugan, N., Ramasamy, P. (2006). Investigation of the growth rate formular and bulk laser damage threshold KDP crystal growth from aqueous solution by the Sankaranarayanan-Ramasamy method. **Crystal Growth and Design**. 6: 1642.
- Balamurugan, N., Lenin, M., Ramasamy, P. (2007). Growth of Potassium acid phthalate crystals by Sankaranarayanan-Ramasamy (SR) method and its optical characterization. **Materials Letters**. 61: 1896.
- Balta Calleja, F.L., Rueda, D.R., Roster, R.S., Mead, W.T. (1980). **Journal Materials Science**. 15: 765.
- Bhagavannarayana, G. (1994). **Ph.D. Thesis**. University of Delhi. Delhi. India.
- Bhat, H.L. (1994). Growth and characterization of some novel crystals for nonlinear optical applications. **Bull Material Science**. 17: 1233.

- Bonse, U., Hart, M. (1965). **Applied Physics Letters**. 7: 238.
- Born, M., Wolf, E. (1964). **Principles of Optics**. The MacMillan Company. New York. p182.
- Boyd, R.W. (2003). **Nonlinear optics**. (2nd ed.). London. Academic press.
- Brice, J.C. (1986). **Crystal Growth Process**. John Wiley and Sons. New York. p109.
- Buckley, H.E. (1995). **Crystal Growth**. New York, John Wiley and Sons. Inc. London. Chapman Hall. Ltd. p44.
- Cheng L.T., Tam W., Stevenson S.H., Meredith G.R., Rikken G., Marder S.R. (1991). Experimental investigation of organic molecular nonlinear optical polarizabilities, 1. Methods and results of benzene and stilbene derivatives. **Journal Physics Chemistry**. 95: 10631.
- Chernov, A.A. (1984). **Modern crystallography**. Crystal Growth Ed., Springer Verlag. Bierline. Vol. 3.
- Claude, A. (2006). **Ph.D. Thesis**. Anna University. Chennai. India.
- Desai, C.C., Rai, J.L. **Bull Materials Science**. 5: 453.
- Ducuing, J., Bloembergen, N. (1964). **Physicals Review**. 133: 1493.
- Gilman, J.J. (1963). **The Art and Science of Growing Crystal**. John Wiley and Sons. Inc. New York.
- Gilson, T.R., Hendra, P.J. (1970). **Laser Raman Spectroscopy**. Wiley Interscience, London.
- [http://serc.carleton.edu/research\\_education/gochemsheets/techniques/SXD.html](http://serc.carleton.edu/research_education/gochemsheets/techniques/SXD.html)

- Hugh G., Gallagher, Ranko M., Vrcelj, John N., Sherwood. (2003). **Journal of Crystal Growth** 250: 486.
- Kavitha, N., Arivanandan, M., Ramanoorthy, K., Ragavenderan, K., Sankaranarayanan, K. (2004). Microbial inhibition, growth of Li<sup>+</sup>-doped Lap single crystals and their characterization **Optical Matter**. Vol. 26: 275.
- Krishan Lal, Bhagavannarayana, G. (1989). **Journal of Applied Crystals**. 22: 209.
- Kurtz, S.K., Perry, T.T. (1968). **Journal of Applied Physics**. 39: 3798.
- Lalama S.J., Garito A.F. (1997). Origin of the nonlinear second order optical susceptibilities of organic system. **Physical Review A**. 20: 1179.
- Laudise, R.A., Ueda, R., Mullin, J.B. (1975). Crystal Growth and Characterization. **Proceedings of ISSCG2**. Spring School, Japan, Amsterdam : North - Holland Pub. Co. p255.
- Lenin, M. (2008). **Ph.D. Thesis**. Anna University. Chennai. India.
- Lenin, M., Balamurugan, N., Ramsamy P. (2007). Growth of Sulphamic acid single crystals by Sankaranarayanan-Ramasamy (SR) method **Crystals Growth Research and Technology**. 42: 39.
- Nalwa, H.S., Miyata, S. (1997). Nonlinear Optics of Organic Molecules and Polymers. **CRC Press**. Boca Raton.
- Neil, H.O. (1923). **Hardness Measurement of Metals and Alloys**. Chapman and Hall, London.

- Sankaranarayanan K. (2005). Growth of large size  $\langle 110 \rangle$  benzophenone crystal using uniaxially solution-crystallization method of Sankaranarayanan-Ramsamy (SR). **Journal of Crystal Growth**. 284: 203.
- Sankaranarayanan, K., Ramsamy, P. (2005). Unidirectional seeded single crystal growth from solution of benzophenone. **Journal of Crystal Growth**. 280: 467.
- Sankaranarayanan, K., Ramsamy, P. (2006). Unidirectional crystallization of large diameter benzophenone single crystal from solution at ambient temperature. **Journal of Crystal Growth**. 292: 445.
- Santhanaraghavan, P., Ramasamy, P. (2001). **Crystal growth process and method**. India, KRU publications.
- Senthil Pandian M., Ramasamy, P. (2009). Unidirectional growth of  $\langle 001 \rangle$  tetraglycine barium chloride (TGBC) single crystal by Sankaranarayanan-Ramasamy method. **Journal of Crystal Growth**. 311(3): 944.
- Senthil Pandian, M., Urit Charoen-In, Ramasamy, P., Prapun Manyum, Lenin, M., Balamurugan, N. (2010). Unidirectional growth of sulphamic acid single crystal and its quality analysis using etching, microhardness, HRXRD, UV-visible and Thermogravimetric-Differential thermal characterizations. **Journal of Crystal Growth**. 312(3): 397.
- Sethuraman, K., Ramesh Babu, R., Gopalakrishnan G., Ramasamy, P. (2006). Unidirectional growth of  $\langle 110 \rangle$  ammonium dihydrogen orthophosphate single crystal by Sankaranarayanan-Ramasamy method. **Journal of Crystal Growth**. 294: 349.
- Smith, R.L., Sandland, G. (1923). **Proc. Inst. Mech. Engrs.** 1: 623.

Stillwel, C.W. (1938). **Crystal Chemistry**. McGraw Hill, New York.

Stringfellow, G.B. (1979). In *Crystal Growth: A Tutorial Approach*, W. Bardsley, D.T.J. Hurle and J.B. Mullin, North - Holland: Amsterdam.

Tabor, D. (1951). **The Hardness of Metals**. Clarendon Press.

Willard, H.H., Merritt, L.L., Dean, JR. J.A., Settle, JR. F.A. (1986). *Instrumental Methods of Analysis*, Wadsworth Pub. Co.

[www.aurelienr.com/electronique/piezo/piezo.pdf](http://www.aurelienr.com/electronique/piezo/piezo.pdf)

[www.tmworld/file/4402-Jim Richards of QuadTech.doc?force=true](http://www.tmworld/file/4402-Jim%20Richards%20of%20QuadTech.doc?force=true)

Wyatt, O.H., Hughes, D.D. (1974). **Metals, Ceramics and Polymers**. Cambridge University Press, Cambridge.

# CHAPTER III

## UNIDIRECTIONAL GROWTH OF SULPHAMIC ACID SINGLE CRYSTAL AND ITS QUALITY ANALYSIS USING ETCHING, MICROHARDNESS, HRXRD, UV-VISIBLE AND TG-DTA CHARACTERIZATIONS

### 3.1 Abstract

A uniaxial sulphamic acid single crystal having dimensions of 35 mm diameter and 150 mm length was grown. Employing slow evaporation technique sulphamic acid crystals of size  $10 \times 10 \times 5 \text{ mm}^3$  were grown. Etching, microhardness, high resolution X-ray diffraction, laser damage threshold, UV-Visible, Thermogravimetric and differential thermal analysis were made on conventional and Sankaranarayanan-Ramasamy method grown sulphamic acid crystals. Etching behaviour of the (100) plane of conventional and Sankaranarayanan-Ramasamy method grown sulphamic acid crystals was investigated with different etchants. Vicker's microhardness test on the (100) plane confirmed the mechanical stability of the conventional and Sankaranarayanan-Ramasamy method grown sulphamic acid crystals. High resolution X-ray diffraction results show that the crystalline perfection of sulphamic acid single crystals grown by Sankaranarayanan-Ramasamy method is extremely good compared to the conventional slow evaporation method grown sulphamic acid crystal. Thermogravimetric and differential

thermal analysis was carried out to determine the thermal properties of the grown crystal.

### 3.2 Introduction

Sulphamic acid ( $\text{H}_2\text{NSO}_3\text{H}$ ) is the monoamide of sulfuric acid and is formed as orthorhombic crystal. It is highly stable and it can be kept for years without any change in properties. It is a strong inorganic acid, while mixing it with water it exhibits zwitterionic form (Kanda and King, 1951). Sulphamic acid finds application in MSF (Multi stage flash evaporation) desalination plants for cleaning demisters, heat exchangers and cooling water systems. Japanese industrial standard has established this reagent as a standard substance for titrimetric analysis. The conventional solution grown crystals have different facets, growth bands, growth sectors and growth sector boundaries (Bhat, 1985). But from application point of view, specific orientation with bulk size, good crystalline perfection, good mechanical and optical quality of crystal are needed. The most significant features of the dislocation structure are a tendency for certain dislocation types to nucleate in pairs and at growth sector boundaries (Alexandru and Antohe, 2003). The boundaries between growth sectors are more strained than the extended growth sectors due to mismatch of the lattices on either side of the boundary as a result of preferential incorporation of impurities. But in SR method the multi-faceted growth is avoided, so the growth sector boundaries are absent and hence the dislocations of the above causes are avoided. The enhancement of crystalline perfection, laser damage threshold, microhardness and optical transparency of the SR grown benzophenone, TGS, KDP, benzimidazole, KAP crystals have been already reported (Sankaranarayanan and Ramasamy, 2006; Balamurugan and Ramasamy, 2006; Justin Raj et al., 2008; Senthil Pandian et al., 2008; Sankaranarayanan,

2005; Vijayan et al., 2007 ). SR method (Sankaranarayanan and Ramasamy 2006; Balamurugan and Ramasamy 2006; Lenin, et al. 2007) facilitates growth of bulk size single crystals along a desired orientation needed for device application. Sulphamic acid (SA) crystals of length 60 mm were already grown by SR method and the results of XRD, FTIR, UV transmission and dielectric studies of these crystals were reported in the earlier paper (Lenin et al., 2007). In this paper we report the growth of SA crystal of length 150 mm using SR method. The conventional and SR grown SA crystals were subjected to etching, Vicker's micro-hardness, HRXRD, UV-Vis analysis, Thermo gravimetric and differential thermal analysis to reveal the dislocations and etch pit density, mechanical strength, perfection, optical quality and thermal stability. Several samples were used and the results were reproducible.

### 3.3 Crystal growth

According to the solubility data (26.4 g/100 ml at 30 °C) the saturation solution of sulphamic acid was prepared at room temperature and stirred well to yield a homogeneous mixture of solution using Merck (GR- grade) chemical reagents dissolved in Millipore water of resistivity 18.2 MΩ cm. The sulphamic acid saturation solution was then poured into a beaker and dried in dust free atmosphere with perforated covering. After five days transparent single crystals were obtained by spontaneous nucleation from the mother solution. The process of re-crystallization was carried out to purify the SA crystal for SEST and SR methods of crystal growth. It is essential to increase the purity to a reputable level before proceeding further. The crystals were allowed to grow further to get well developed maximum dimension of about  $10 \times 10 \times 5 \text{ mm}^3$  (Figure 3.1). The major faces (100), (011), (0 $\bar{1}$ 1) (01 $\bar{1}$ ) and (0 $\bar{1}\bar{1}$ ) were observed in the conventional

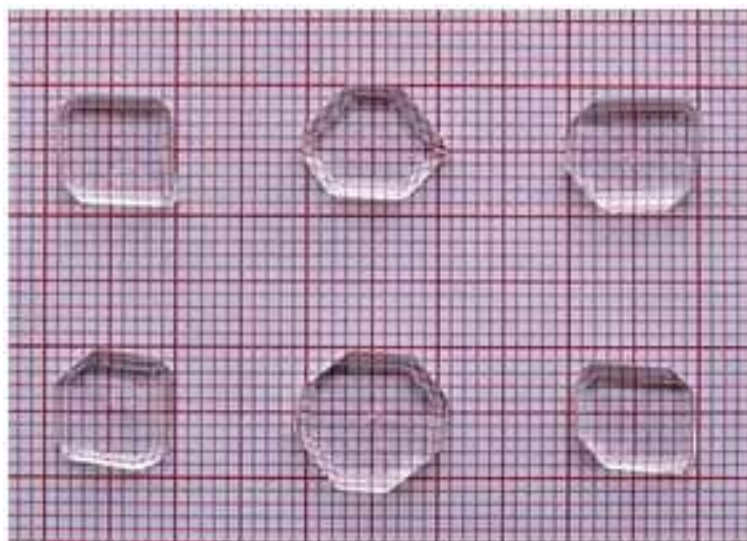


**Figure 3.1** Conventional method grown SA crystals.

method grown SA crystals. In the present study (100) plane of the SA crystal was selected to impose the orientation in the growing crystal. The saturated solution of SA was prepared and transferred into a (100) seed crystal mounted glass ampoule. Once the system attains equilibrium, the growth was initiated with a suitable temperature provided by the ring heater at the top of the solution. Top of the growth ampoule was maintained at 40 °C for solvent evaporation. The temperature around the growth region is maintained at 33 °C with  $\pm 0.01$  °C accuracy for the growing crystals. After one week, the seed crystal mounted at the bottom starts to grow. Under this condition the highly transparent crystal was seen and the growth system was kept constant for a long period for attaining continuous growth which at the end has yielded SA crystal of length 150 mm and diameter 35 mm within 50 days (Figure 3.2(a, b)). The average growth rate was nearly 3 mm/day.



**Figure 3.2** (a) As grown and (b) Cut and polished SR grown Sulphamic acid crystal.

## 3.4 Results and discussions

### 3.4.1 Chemical etching analysis

Etching property is used as the most convenient method for the visualization of defects. Etching studies were made on the (100) plane of both crystals grown by conventional and SR method. In the present work water and methanol were used as etchants. Etching of the conventional grown SA crystal with water for 5 s produces oval shaped with well defined etch pits (Figure 3.3(a)). The etch pit density (EPD) was  $1.1 \times 10^3 \text{ cm}^{-2}$ . On successive etching for 15 s and 25 s the oval etch pits enlarge in size, but retaining their geometrical shape and do not disappear, suggesting that the etch pits are due to dislocations. Figure 3.3(b) shows the etch pits of SA crystal grown by SR method after 5 s etching with water. In this case the number of etch pits was less and the EPD was  $1.6 \times 10^{-2}$ . In an etched surface shallow (S) and deep (D) etch pits are observed. Grain boundaries are observed in conventional method grown SA crystals. Similar observations were reported on (100) faces of NaCl crystals (Sangwal and Zaniewska, 1984). On increasing the etching time there was no change of shape, but the size of the oval pits increased. When SA crystals grown by conventional and SR methods were etched

for 20 s using methanol as etchant diamond shaped pits were observed (Figures 3.3(c, d)). The shape of the etch pit varies with the different etchants, because the morphology of etch pits is connected with the nature of chemical complexes present in solution (Sangwal and Zaniewska, 1984).

The number of etch pits in the conventional slow evaporation technique (SEST) grown crystals is larger than the SR method grown crystals. In utilizing single crystals for devices it is necessary to grow single crystals containing a reduced dislocation density (Sunagawa, 2007). The generation of dislocations is strongly correlated with the formation of inclusions in the crystals (Kishnan RaoK and Surender, 2001). A variety of reasons such as variation in supersaturation during the growth, non-uniform growth rates etc are responsible for the formation of inclusions. Liquid inclusions getting trapped parallel to the interfaces are due to drastic changes in growth condition (Kishnan RaoK and Surender, 2001). In crystal growth, such defects may arise from all kinds of inclusions (inclusions of mother solution, impurity particles, solute precipitates). Inclusions generating growth dislocations also arise from growth face instabilities induced by fluctuations of growth conditions. Large inclusions usually emit bundles of many dislocations (Maiwa et al., 1989). In SR method as there are no such growth fluctuations or non-uniform growth rates the dislocations of the above causes are avoided. The low EPD in SR grown TGS, KAP crystals has been already reported (Senthil Pandian, 2008).

### **3.4.2 Mechanical strength analysis**

Microhardness indentations were made on the well developed conventional and SR method grown (100) plane of SA crystals using Leitz-Wetzlar hardness tester fitted with a diamond pyramidal indenter and the indentation time was

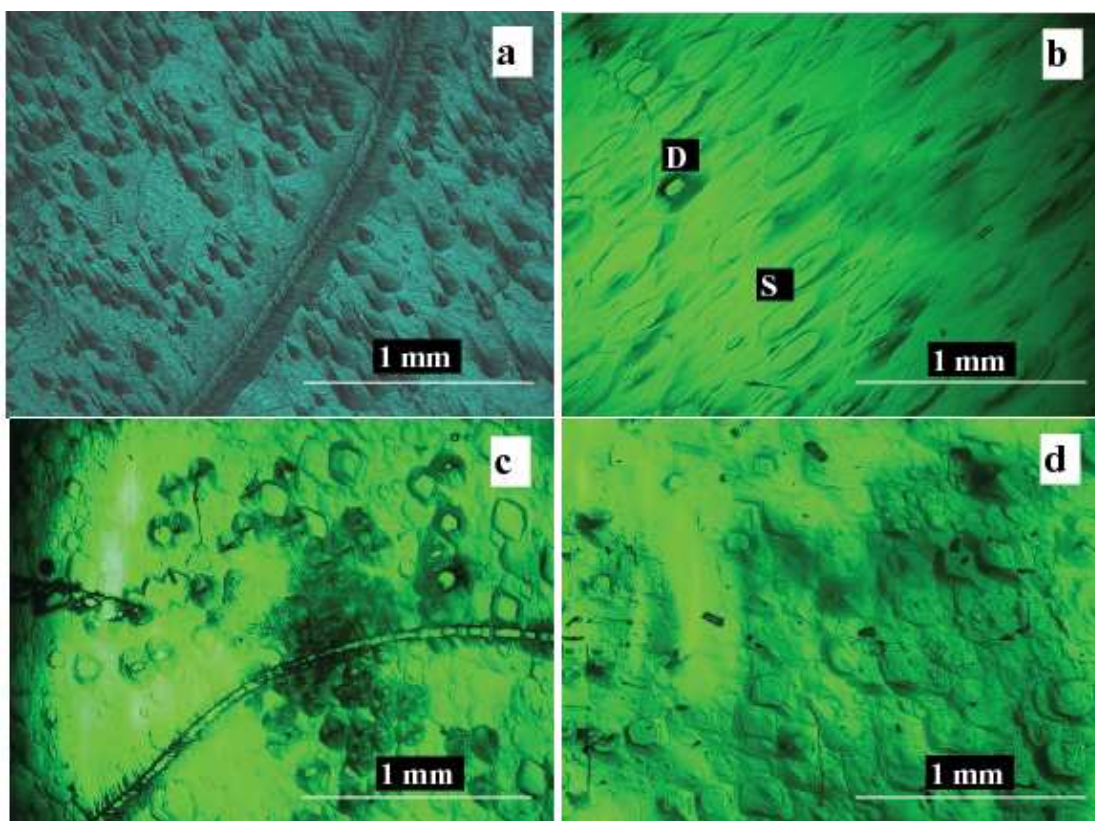


**Figure 3.3** Etch pattern produced on the (100) plane of (a) conventional and (b) SR grown SA crystals by water after etching for 5 sec. Surface of (c) conventional and (d) SR grown SA crystals by methanol after etching for 20 sec.

kept at 10 s. A diamond indenter is pressed into the surface of the SA crystal under the influence of a known load (10 - 100 g) and the size of the resulting indentation is measured. Owing to the observed micro cracks at the corners of the impressions made on the crystals, the maximum indenter load applied was 100 g. This may be due to the release of internal stresses generated locally by indentation (Ushasree et al., 1998) and further measurements are not possible. Hardness value is calculated from the expression:

$$H_V = 1.854P/d^2 \quad \text{kg/mm}^2 \quad (3.1)$$

where  $P$  is the applied load in g and  $d$  is the diagonal length in mm. The micro-hardness value was taken as the average of several impressions made. A steep rise and fall in hardness number was observed in the range of 10-100 g and having maximum  $H_V$  at 65 g (Figure 3.4). The major contribution to hardness is attributed to the high stress required for homogenous nucleation of dislocation in the dislocation free region indented. Hence higher hardness value for SR grown SA crystal indicates greater stress required to form dislocation which confirms greater crystalline perfection. The highest values of hardness were found to be 101.5 kg/mm<sup>2</sup> for (100) plane of SR grown SA crystal and 97.3 kg/mm<sup>2</sup> for SEST grown crystal at the load of 70 g. The load variation can be interpreted by using Meyer's law  $P = ad^n$ . Meyer's index ( $n$ ) has been estimated from the plot of log  $P$  vs log  $d$ . From careful observations on various materials Onitsch (Onitsch, 1947) and Hanneman pointed out that  $n$  lies between 1 and 1.6 for moderately hard materials and it is more than 1.6 for soft materials. The value of  $n$  obtained for (100) plane of SR grown SA crystal was 1.9 and conventional grown SA crystal was 2.2. Low work hardening coefficient shows less dislocation (Jerome Das and Gopinathan, 1992) in

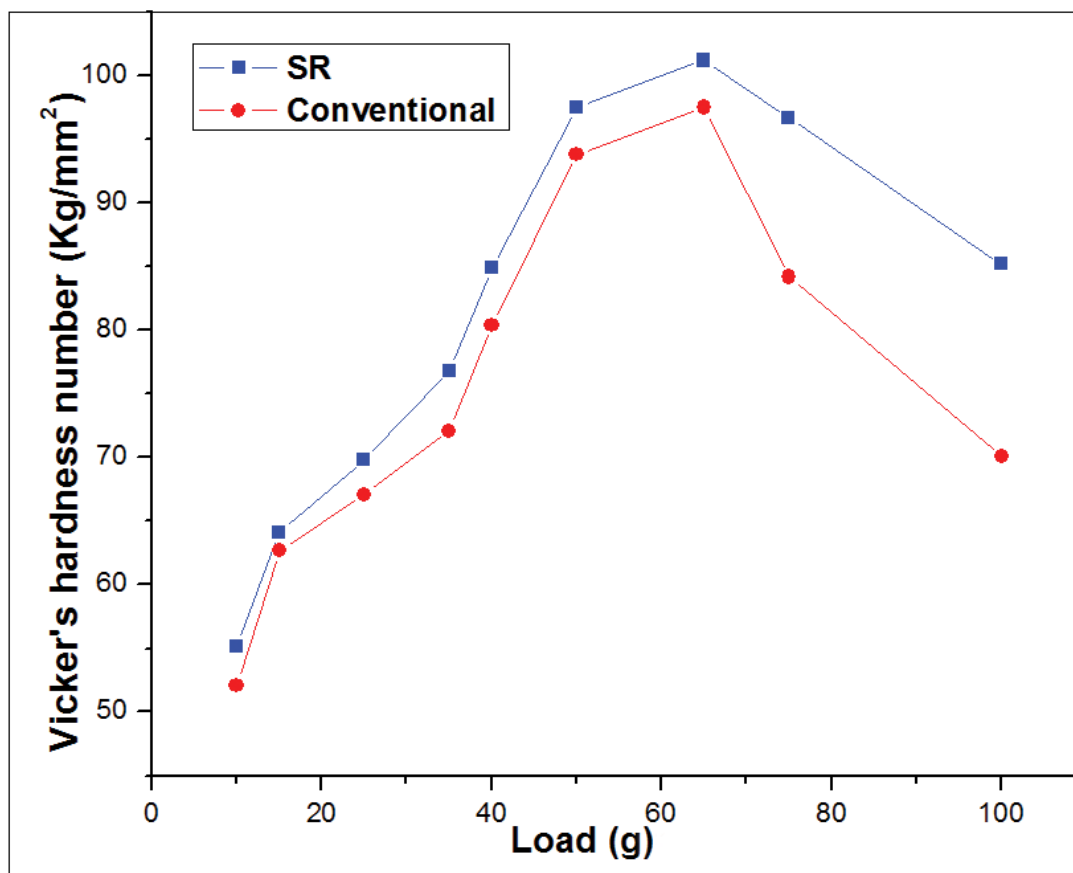


**Figure 3.4** Vicker's microhardness analysis of SA.

the SR method grown SA crystal. Lesser hardness for conventional solution grown crystals may be due to entrapment of solvent during growth (Vijayan, 2006).

### 3.4.3 High resolution X-ray diffraction analysis

The crystalline perfection of the conventional slow evaporation and SR method grown SA single crystals was evaluated by HRXRD using a multicrystal X-ray diffractometer developed at National Physics Laboratory (NPL). The well-collimated and monochromated  $\text{MoK}\alpha_1$  beam obtained from the three monochromator Si crystals set in dispersive (+, -, -) configuration has been used as the exploring X-ray beam. The specimen crystal is aligned in the (+, -, -, +) con-

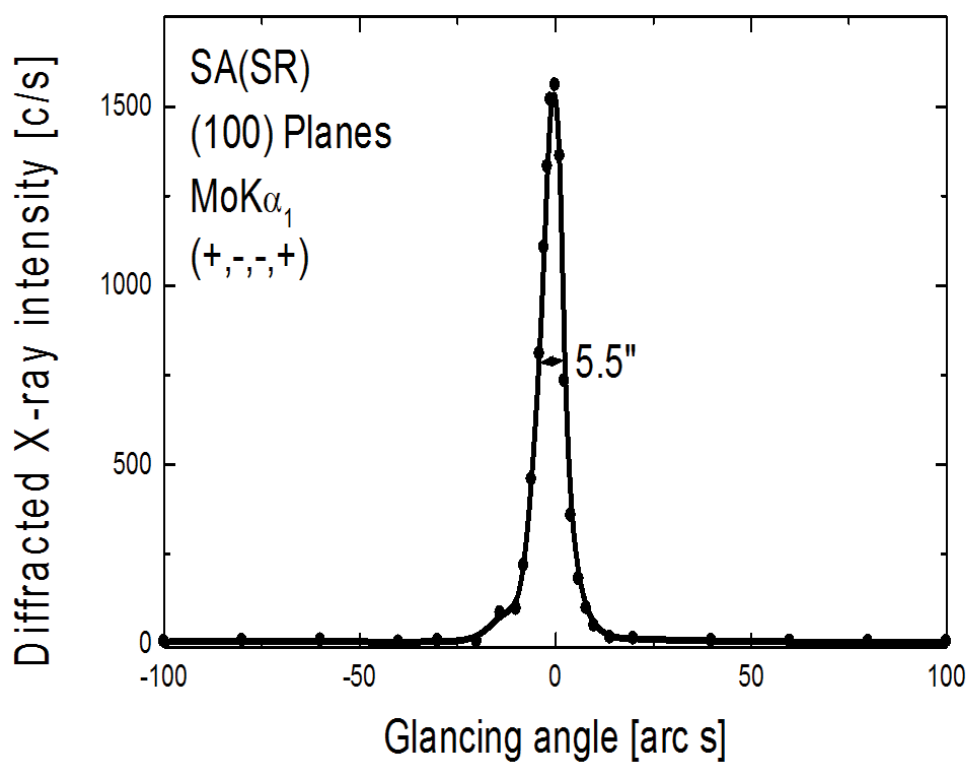
figuration. Due to dispersive configuration, though the lattice constant of the monochromator crystals and the specimen are different, the unwanted dispersion broadening in the diffraction curve (DC) of the specimen crystal is insignificant. The specimen can be rotated about the vertical axis, which is perpendicular to the plane of diffraction, with minimum angular interval of 0.4 arc s. The DC was recorded by the so-called  $\omega$  scan wherein the detector was kept at the same angular position  $2\theta_B$  with wide opening for its slit. Before recording the diffraction curve in order to remove the non-crystallized solute atoms which remained on the surface of the sulphamic acid crystal and also to ensure the surface planarity, the specimen was first lapped and chemically etched in a non preferential etchant of water and acetone mixture in 1:2 volume ratio.

Figure 3.5 shows the high-resolution DC recorded for SR-grown SA single crystal using (100) diffracting planes in symmetrical Bragg geometry by employing the multicrystal X-ray diffractometer described above with  $\text{MoK}\alpha_1$  radiation. The curve is extremely sharp having full width at half maximum (FWHM) of 5.5 arc s as expected for a nearly perfect crystal from the plane wave dynamical theory of X-ray diffraction (Batterman and Cole, 1964). Absence of additional peaks and the very sharp DC shows that the crystalline perfection of the SA crystal is extremely good without having any internal structural grain boundaries and mosaic nature. Figure 3.6 shows the high-resolution DC recorded for a typical SEST-grown SA single crystal specimen using (100) diffracting planes. The solid line (convoluted curve) is well fitted with the experimental points represented by the filled circles. On deconvolution of the diffraction curve, it is clear that the curve contains two additional peaks, which are 13 and 18 arc s away from the main peak. These two additional peaks correspond to two internal structural very low angle (tilt angle  $\leq 1$  arc min) boundaries (Bhagavannarayana et al.,

2005) whose tilt angles (misorientation angle between the two crystalline regions on both sides of the structural grain boundary) are 13 and 18 arc s from their adjoining regions. The impurities could be the solvent molecules entrapped in the crystalline matrix during growth, which is common in solution growth. The segregation of impurities or the entrapment of solvent molecules at the boundaries could be responsible for the observed very low angle boundaries and these low angle boundaries are observed in the many conventional slow evaporation solution grown crystals (Batterman and Cole, 1964; Srinivasan, 2006; Krishnakumar and Nagalakshmi, 2007; Ramesh Babu et al., 2006). The FWHM of the main peak and the low angle boundaries are respectively 15, 12 and 50 arc s. Though the specimen contains very low angle boundaries, the relatively low angular spread of around 3 arc min of the diffraction curve and the low FWHM values show that the crystalline perfection is reasonably good.

#### **3.4.4 Optical studies**

The UV-Vis NIR spectrum was recorded using Perkin-Elmer Lambda 35 spectrophotometer in the range of 200 - 1100 nm with slit width 2 nm. An optically polished SR method grown SA crystal plate of 2 mm was used. Similarly in the conventional grown crystal a plate of 2 mm thickness in (100) plane was selected for this study. The SR and conventional method grown SA single crystals have transmittance of 67%, 63% respectively in the wavelength range 220 - 1100 nm. The transmittance of SR grown SA crystals is 4% higher than the transmittance of the conventional slow evaporation method grown SA crystal. The improvement in the percentage of transmission by 4% may be attributed to a reduced scattering from crystal's point and line defects. The recorded spectrum is shown in Figure 3.7. The enhancement of optical transparency of SR method grown TGS, KAP



**Figure 3.5** HRXRD curve of SR grown sulphamic acid crystal.

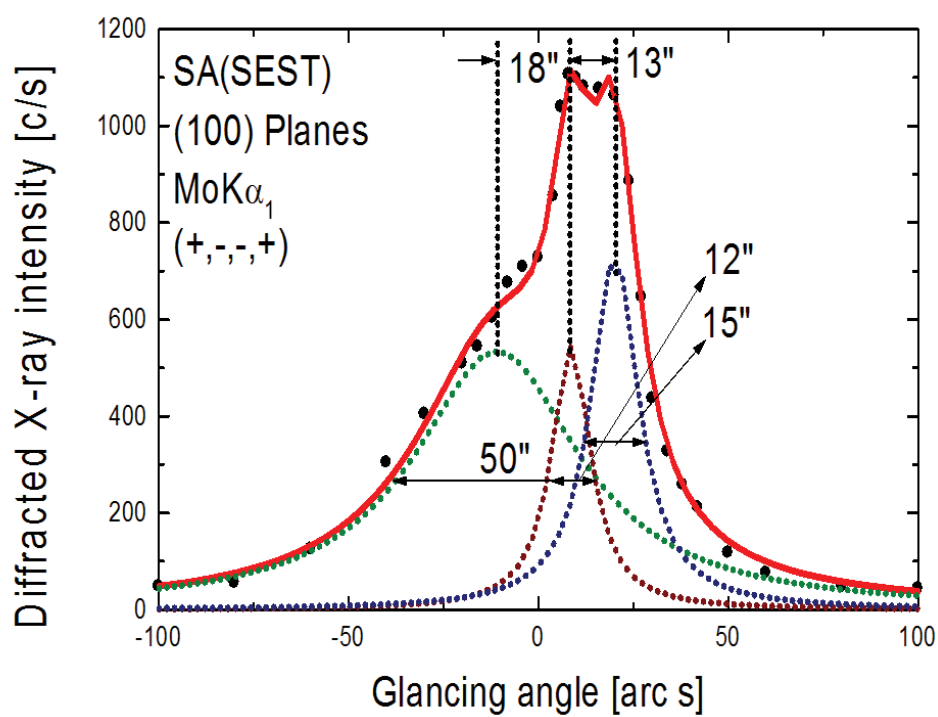
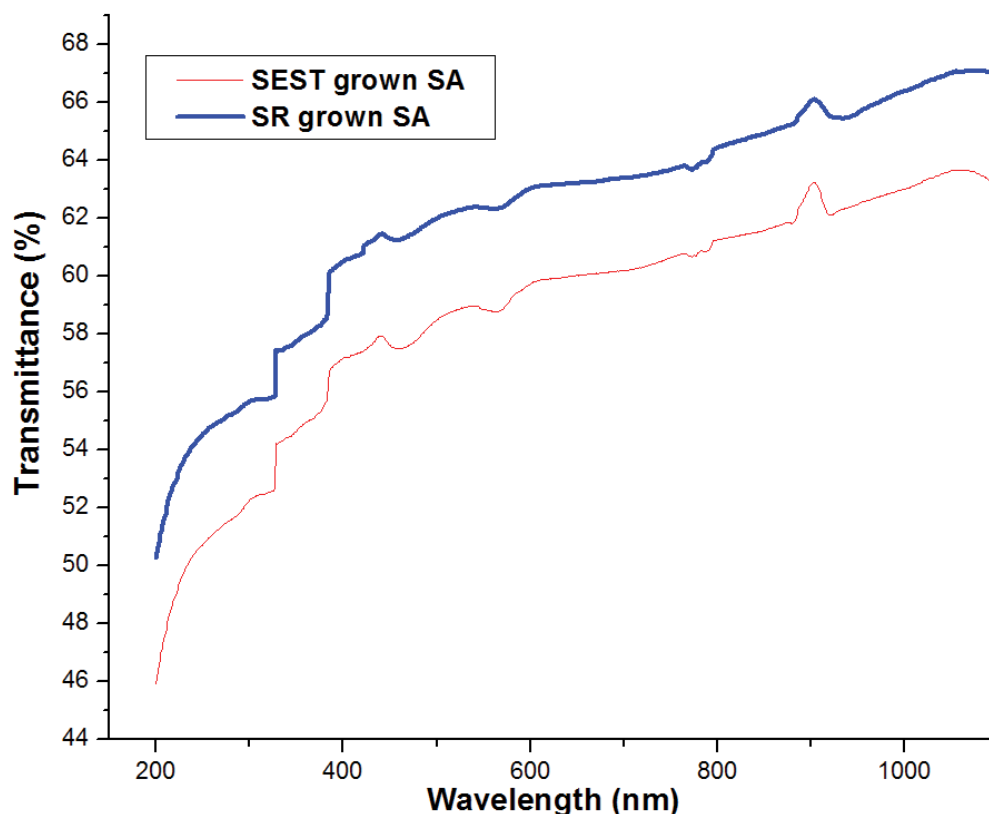


Figure 3.6 HRXRD curve of conventional grown sulphamic acid crystal.



**Figure 3.7** UV-Vis NIR analysis of SA.

and KDP crystals has been already reported (Justin Raj, 2008; Senthil Pandian et al., 2008).

### **3.4.5 Thermo gravimetric-Differential thermal analysis**

TG-DTA of SR method grown SA crystal was carried out between 35 °C to 700 °C in nitrogen atmosphere using STA 409 PC analyzer at a heating rate 10 °C per minute. Weight loss between 219 °C to 482 °C is due to decomposition of sample (Figure 3.8). A decomposition product of SA is nitrogen oxide and sulfur dioxide (Material safety data sheet (MSDS)-Sigma aldirch chemical co, Acros organics, Q-max solutions inc, Miracle sealants company, Wego chemical and mineral corporation, Barloworld scientific, Danlin industries corporation, Advanced

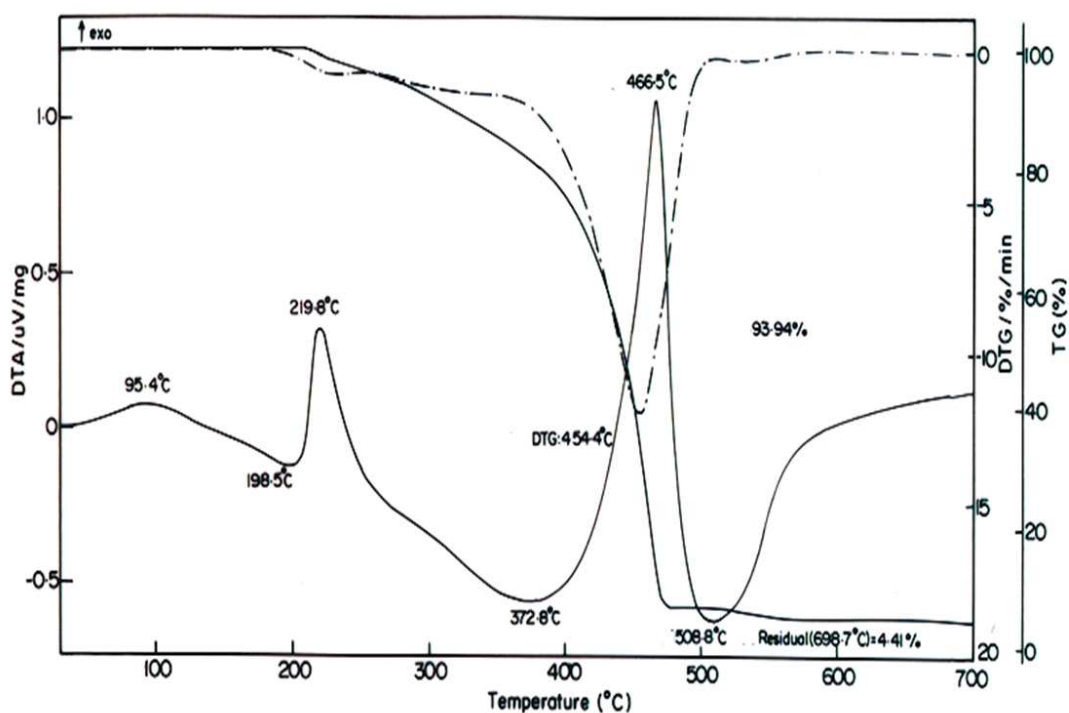


**Figure 3.8** TG-DTA analysis of SA.

chemical technology inc, Clear tech industries inc, Chem one Ltd, Lab chem inc). SA may liberate one molecule of nitrogen oxide (NO) and one molecule of sulphur dioxide (SO<sub>2</sub>) when heated from 219 °C to 482 °C. In this stage of decomposition the theoretical weight loss is 97% and experimental loss of weight is 96%, which is very close to theoretical value. Hence we can conclude that SA crystal is suitable for any application upto 219 °C

### 3.5 Conclusions

(100) directed sulphamic acid single crystal with 150 mm in length and 35 mm in diameter has been grown by Sankaranarayanan-Ramasamy method. Etch pit density is less in Sankaranarayanan-Ramasamy method grown crystal compared to conventional method grown crystal. The Vicker's hardness value of

Sankaranarayanan-Ramasamy method grown sulphamic acid crystal is higher than that of the conventional slow evaporation method grown crystal. Full width at half maximum value of Sankaranarayanan-Ramasamy method grown sulphamic acid crystal, which is 5.5 arc s, shows that the crystalline perfection is extremely good. Full width at half maximum of conventional method grown sulphamic acid crystal contains two additional peaks, which are 13 and 18 arc sec away from the main peak and these two additional peaks correspond to two internal structural very low angle boundaries. The sulphamic acid crystals grown by Sankaranarayanan-Ramasamy method have 4% higher transmittance than conventional method grown crystal. Sulphamic acid crystal decomposed at 219 °C. Investigations showed that Sankaranarayanan-Ramasamy method grown sulphamic acid crystal has better perfection than conventional method grown sulphamic acid crystal.

### 3.6 Acknowledgements

The authors thank Dr.G. Bhagavannarayana, Materials Characterization Division, NPL, New Delhi, for HRXRD measurement. The authors are grateful to Prof.K. Kishan Rao, Department of Physics, Kakatiya University, Warangal, for providing the microhardness test facilities and Department of Mechanical Engineering, SSN College of Engineering, for the help in etching studies.

### 3.7 References

- Alexandru, H.V., Antohe, S. (2003). Prismatic faces of KDP crystal, kinetic and mechanism of growth from solutions. **Journal of Crystal Growth**. 258(1-2): 149.
- Balamurugan, N., Ramasamy, P. (2006) **Crystal Growth and Design**. 6: 1642.

- Batterman, B.W., Cole, H. (1964). Dynamical diffraction of x rays by perfect crystals **Reviews of Modern Physics**. 36(3): 681.
- Bhagavannarayana, G., Ananthamurthy, R.V., Budakoti, G.C., Kumar, B. and Bartwal, K.S. (2005). A study of the effect of annealing on Fe-doped LiNbO<sub>3</sub> by HRXRD, XRT and FT-IR. **Journal of Applied Crystallography**. 38(5): 768.
- Bhat, H.L. (1985). X-ray topographic assessment of dislocations in crystals grown from solution. **Progress In Crystal Growth And Characterization**. 11(2): 57.
- Jerome Das, S., Gopinathan, R. (1992). **Crystal Research and Technology**. 27: k17.
- Justin Raj, C., Krishnan, S., Dinakaran, S., Uthrakumar, R. and Jerome Das, S. (2008). Growth and optical absorption studies on potassium dihydrogen phosphate single crystals. **Crystal Research and Technology** 43(3): 245.
- Kanda, F.A., King, A.J. (1951). The crystal structure of sulfamic acid. **Journal of the American Chemical Society**. 73(5): 2315.
- Kishnan RaoK., Surender, V. (2001). Surface studies on as-grown (111) faces of sodium bromate crystals. **Bulletin of Materials Science**. 24(6): 665.
- Krishnakumar, V., Nagalakshmi, R. (2007). Crystal growth and characterization of K[CS(NH<sub>2</sub>)<sub>2</sub>]<sub>4</sub>Br-A semiorganic non-linear optical crystal. **Spectrochimica Acta - Part A: Molecular and Biomolecular Spectroscopy**. 68(3): 443.

- Lenin, M., Balamurugan, N. and Ramasamy P. (2007). Growth and characterization of sulphamic acid single crystals grown by Sankaranarayanan-Ramasamy (SR) method. **Crystal Research and Technology**. 42(1): 39.
- Maiwa, K., Tsukamoto, K., Sunagawa, I., Chuan-zhen Ge and Nai-ben Ming. (1989). Observation of screw and mixed dislocations in barium nitrate crystals by means of birefringence and x-ray topography. **Journal of Crystal Growth**. 98(4): 590.
- Onitsch, E.M. (1947). **Mikroskopie** 2: 131.
- Ramesh Babu, R., Sethuraman, K., Vijayan, N., Bhagavannarayana, G., Gopalakrishnan R. and Ramasamy, P. (2006). Etching and dielectric studies on L-lysine monohydrochloride dihydrate single crystal. **Crystal Research and Technology**. 41(9): 906.
- Sangwal, K., Zaniewska, G. (1984). Influence of impurities on the etching of NaCl crystals. **Journal of Materials Science** 19(4): 1131.
- Sankaranarayanan, K. (2005). Growth of large size  $\langle 110 \rangle$  benzophenone crystal using uniaxially solution-crystallization method of Sankaranarayanan-Ramasamy (SR). **Journal of Crystal Growth**. 284(1-2): 203.
- Sankaranarayanan, K., Ramasamy, P. (2006). Unidirectional crystallization of large diameter benzophenone single crystal from solution at ambient temperature. **Journal of Crystal Growth** 292(2): 445.
- Senthil Pandian, M., Balamurugan, N., Bhagavannarayana, G. and Ramasamy P. (2008). Characterization of  $\langle 010 \rangle$  directed KAP single crystals grown

by Sankaranarayanan-Ramasamy (SR) method. **Journal of Crystal Growth**. 310(18): 4143.

Senthil Pandian, M., Balamurugan, N., Ganesh, V., Rajashekar, P.V., Kishan Rao K. and Ramasamy, P. (2008). Growth of TGS single crystal by conventional and SR method and its analysis on the basis of mechanical, thermal, optical and etching studies. **Materials Letters**. 62(23): 3830.

Srinivasan, P., Kanagasekaran, T., Gopalakrishnan, R., Bhagavannarayana G. and Ramasamy, P. (2006). Studies on the growth and characterization of L-asparaginium picrate (LASP) - A novel nonlinear optical crystal. **Crystal Growth and Design**. 6(7): 1663.

Sunagawa, I. (2007). Crystal growth, morphology and perfection, Cambridge University Press, Cambridge,

Vijayan, N., Bhagavannarayana, G., Ramesh Babu R., Gopalakrishnan, R., Maurya, K.K. and Ramasamy, P. (2006). A comparative study on solution- and Bridgman-grown single crystals of benzimidazole by high-resolution X-ray diffractometry, fourier transform infrared, microhardness, laser damage threshold, and second-harmonic generation measurements. **Crystal Growth and Design**. 6(6): 1542.

Vijayan, N., Nagarajan K., Alex Slawin M. Z., Shashidharan Nair C.K. and Bhagavannarayana, G. (2007). Growth of benzimidazole single crystal by sankaranarayanan-ramasamy method and its characterization by high-resolution X-ray diffraction, thermogravimetric/ differential thermal analysis, and birefringence studies. **Crystal Growth and Design** 7(2): 445.

Ushasree, P.M., Jayavel, R., Subramanian C. and Ramasamy, P. (1998). Growth and micromorphology of as-grown ZTS single crystals and the etching studies. **Bulletin of Electrochemistry**. 14(11): 407.

# CHAPTER IV

## COMPARATIVE STUDY ON L-ALANINIUM MALEATE SINGLE CRYSTAL GROWN BY SANKARANARAYANAN-RAMASAMY METHOD AND CONVENTIONAL SLOW EVAPORATION SOLUTION TECHNIQUE

### 4.1 Abstract

Single crystals of L-alaninium maleate (LAM) were successfully grown by Sankaranarayanan-Ramasamy (SR) method and conventional slow evaporation solution technique (SEST) which have the sizes of 32 mm in length, 18 mm in diameter and  $18 \times 13 \times 2 \text{ mm}^3$  respectively. The grown LAM crystals have been subjected to single crystal X-ray diffraction, high resolution X-ray diffraction (HRXRD), chemical etching, dielectric constant, dielectric loss, Thermo gravimetric-differential thermal analysis, UV-Vis NIR and Vickers microhardness analysis and the results were compared. Single crystal X-ray diffraction confirmed the lattice parameters of the grown LAM crystals. The HRXRD analysis indicated that the crystalline perfection of the SR method grown LAM crystals is quite good without having any internal structural grain boundaries. Chemical etching studies represent the distribution of structural defects in LAM crystal and etch pit density of conventional and SR methods grown LAM crystals was calculated. The dielectric constant and loss measurement was made as function of temperature in the

range of 40 - 140 °C. From thermo gravimetric-differential thermal analysis of the grown crystal the thermal stability was found to be upto 158°C. The range and percentage of optical transmission are represented by recording UV-vis analysis. Mechanical strength of the grown LAM crystals was analyzed by Vickers micro-hardness test and the hardness of SR method grown LAM crystal is higher than the hardness of the crystal grown by conventional method.

## 4.2 Introduction

L-alaninium maleate (LAM) is an organic non-hygroscopic material. It has been grown by conventional slow evaporation solution technique. It belongs to orthorhombic system and the lattice parameters are  $a = 5.5873$  (11) Å,  $b = 7.3864$  (17) Å,  $c = 23.688$  (3) Å and the space group is  $P2_12_12_1$  (Alagar et al., 2001). There are a few papers reported about the growth of LAM in conventional method including its characterization (Natarajan et al., 2006; Martin Britto Dhas et al. 2007; Vasantha and Dhanuskodi, 2004). However the conventional SEST grown crystals have a small size, different morphology, with many faces and poor transparency. For devices we need a large size, defect-free, mechanically and optically good quality single crystals. The crystal with specific orientation can be grown from solution by SR (Sankaranarayanan and Ramasamy, 2005) method. This method can be used to grow single crystals along a selected crystal direction, which is very important for the preparation of functional crystals. For example, as the conversion efficiency of SHG is always highest along the phase-match direction for nonlinear optical crystals, the unidirectional crystal growth method is most suitable for the crystal growth along that direction. In addition, the unidirectional solution crystallization usually occurs at around room temperature; much lower thermal stress is expected in these crystals over those grown at high tem-

peratures (Jingran Su et al., 2009). From this point of view, we have attempted to grow unidirectional, bulk, good quality single crystals of LAM from its aqueous solution by SR method.

In the present investigation, bulk single crystals of LAM were grown by conventional SEST and SR methods. The grown crystals were subjected to various studies in order to determine their properties and the results are compared with one another.

## 4.3 Experiments

### 4.3.1 Conventional method

LAM was synthesized using L-alanine and maleic acid from Merck (GR grade) in the stoichiometric ratio 1:1 with Millipore water of resistivity 18.2 M $\Omega$  cm. The reactants were thoroughly dissolved in Millipore water and stirred well for about 2 hours using a temperature controlled magnetic stirrer to yield a homogeneous mixture of solution. The single crystals of LAM have been grown from saturated solution by conventional SEST at room temperature. After seven days, small crystals with rectangular shape were observed in the beaker. LAM crystals were purified by recrystallization process in Millipore water three times to eliminate any impurities and good transparent crystals were collected for studies and SR-seed crystal. It is essential to increase the purity to a reputable level before proceeding further. LAM crystal (Figure 4.1(a)) was successfully grown with the dimension of 18  $\times$  13  $\times$  2 mm<sup>3</sup>. No microbial contamination is observed in the growth solution of LAM even when solutions are kept for a long time.

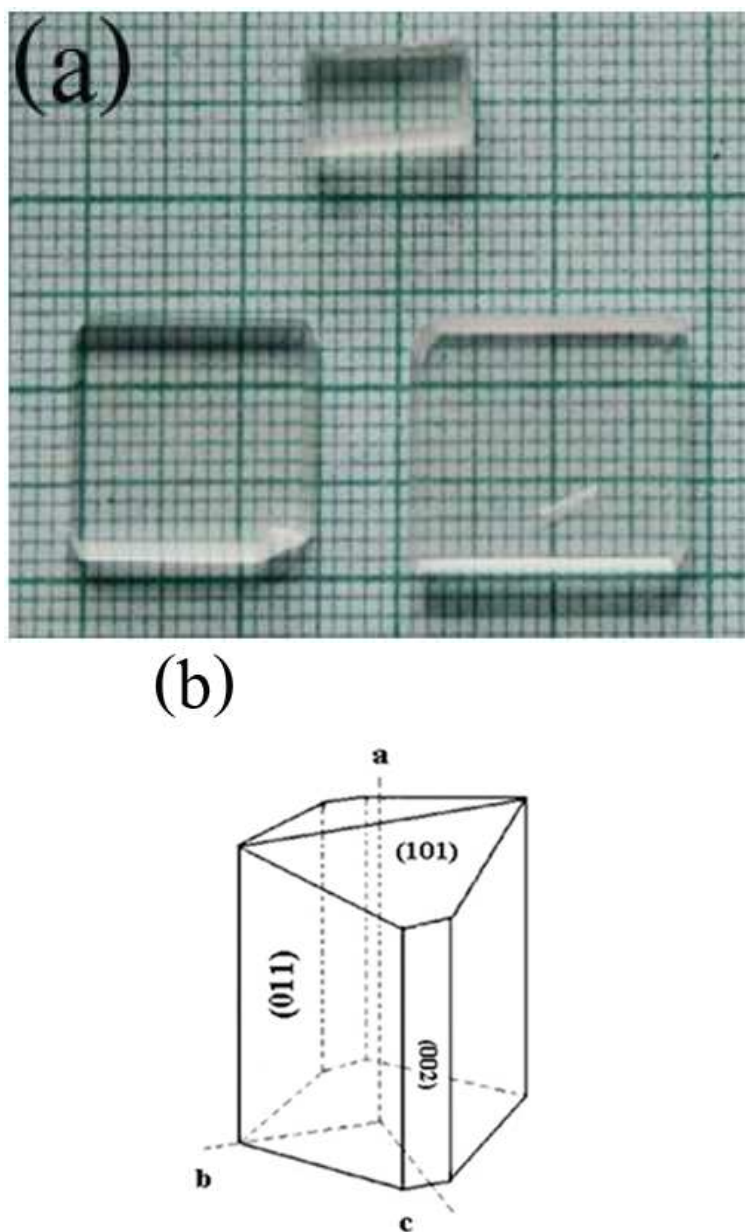


**Figure 4.1** (a) Conventional method grown LAM crystal and (b) Morphology of LAM crystal.

### 4.3.2 SR method

According to the solubility data [52.04 g/100 ml at 30 °C], saturated solution of LAM was prepared at room temperature. Growth of LAM crystals were carried out by conventional SEST as well as SR methods. The good transparent LAM seed crystals were allowed to grow further to get well developed maximum size by conventional SEST and a well faceted crystal was chosen for SR method. The morphology of the LAM crystal in Figure 4.1(b) has been already reported (Natarajan et al., 2006). There are 8 prominent faces on the crystal. The major faces (011), (002) and (101) were observed in the conventional grown LAM crystals. Based on the morphology of the LAM crystal, the (011) face was selected in the present study to impose the unidirectional growth in the crystal. Carefully cut and polished portion of LAM crystal along (011) face was fixed in the bottom of the growth ampoule. The saturation solution of LAM was prepared and fed into a glass ampoule. The SR method experimental set-up was already reported (Sankaranarayanan and Ramasamy, 2005, 2006). Once the system attains equilibrium, the growth was initiated with a suitable temperature provided by the ring heater at the top of the solution. Top of the growth ampoule was maintained at 38 °C for solvent evaporation. The temperature around the growth region is maintained at 34 °C for the growing crystals. After one week, the seed crystal mounted at the bottom starts to grow. Under this condition the highly transparent crystal was monitored and the growth system was kept constant for a long period for attaining continuous growth which at the end has yielded LAM crystal of 32 mm in length and 18 mm in diameter within 30 days (Figure 4.2(a)). The average growth rate was about 1 mm/day. Figure 4.2(b) shows the single crystalline (011) ingots fabricated from LAM crystals (Figure 4.2(a)) grown by employing SR method.

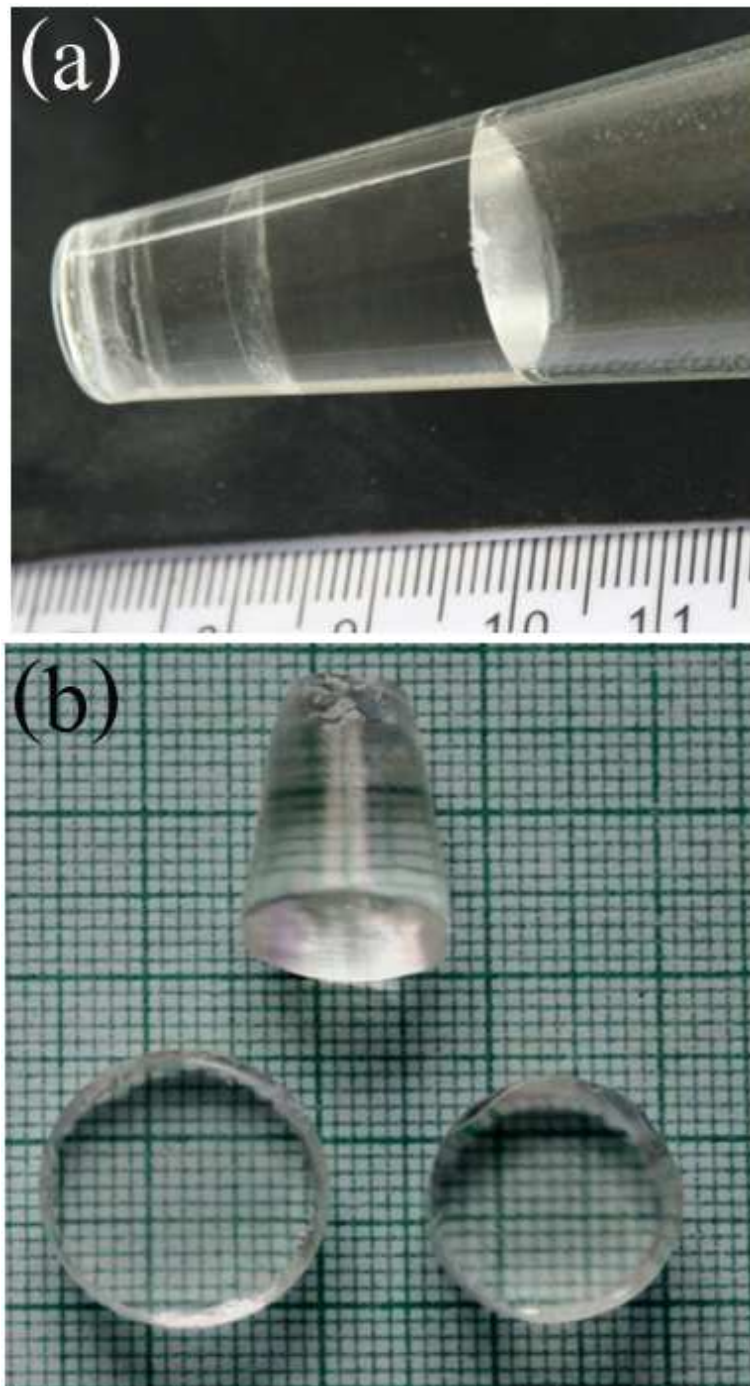


**Figure 4.2** (a) SR-grown LAM crystal, (b) Cut and polished LAM crystals with various diameters.

## 4.4 Results and discussions

### 4.4.1 Single crystal X-ray diffraction

The grown LAM crystals were subjected to single crystal X-ray diffraction studies using Enraf nonius (AD4-MV3) single crystal X-ray diffractometer to determine the cell parameters. From the single crystal X-ray diffraction analysis, the crystal belongs to orthorhombic system and the lattice parameters are  $a = 5.593(1) \text{ \AA}$   $b = 7.384(4) \text{ \AA}$  and  $c = 23.715(4) \text{ \AA}$  and the space group is  $P2_12_12_1$  which are in very good agreement with the reported values (Alagar, 2001).

### 4.4.2 High resolution X-ray diffraction

Figure 4.3(a) shows the high resolution X-ray diffraction curve (HRXRD) recorded for a typical SEST grown LAM single crystal specimen using (005) diffracting planes in symmetrical Bragg geometry by employing the multocrystal X-ray diffractometer with  $\text{MoK}\alpha_1$  radiation. On deconvolution of the diffraction curve, it is clear that the curve contains an additional peak, which is 10 arc s away from the main peak. This additional peak depicts an internal structural very low angle (tilt angle,  $\alpha < 1 \text{ arc min}$ ) boundary (Bhagavannarayana et al., 2005) whose tilt angle [misorientation angle,  $\alpha$  between the two crystalline regions on both sides of the structural grain boundary] is 10 arc s from its adjoining region. The full width at half maximum (FWHM) for both main peak and the very low angle boundary is 9 arc s. Though the specimen contains a very low angle boundary, the relatively low angular spread of around 10 arc s of the diffraction curve and the low FWHM values show that the crystalline perfection is reasonably good. The effect of such very low angle boundaries may not be very significant in many device applications, but for applications like phase matching, it is better to know

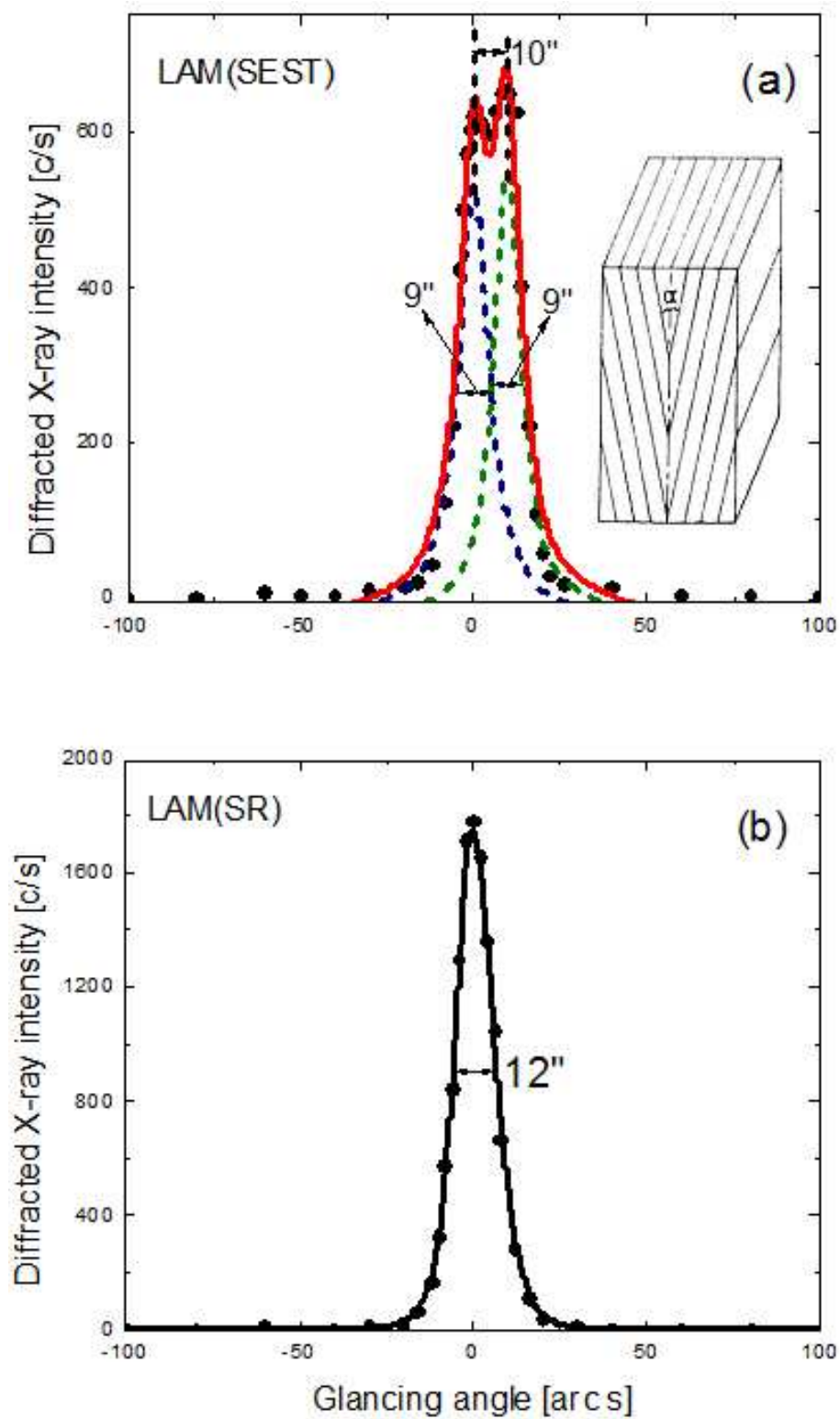


**Figure 4.3** High-resolution X-ray diffraction curves recorded for (005) diffracting planes of LAM crystals grown by (a) conventional and (b) SR methods.

these minute details regarding crystalline perfection. Thermal fluctuations, the segregation of impurities or entrapment of solvent molecules during the growth process could be responsible for the observed very low angle boundary (Senthil Pandian et al., 2010). It may be mentioned here that such low angle boundaries could be detected with well resolved peaks in the diffraction curve only because of the high-resolution of the multicrystal X-ray diffractometer used in the present studies.

Figure 4.3(b) shows the diffraction curve (DC) recorded for the SR method grown LAM crystal recorded under identical conditions as that of Figure 4.3(a). As seen in the figure the DC contains a single peak without any satellite peaks as observed in Figure 4.3(a). This clearly indicates that the SR method grown crystal does not contain any internal structural grain boundaries. The FWHM of the curve is 12 arc s which is very close to that expected from the plane wave theory of dynamical X-ray diffraction (Batterman and Cole, 1964), for an ideally perfect crystal. However, the scattered intensity along the wings of the DC indicates that the crystal contains point defects. Such defects are very common to observe in almost all real crystals including nature gifted crystals and are many times unavoidable due to thermo dynamical conditions. More details may be obtained from the study of high-resolution diffuse X-ray scattering measurements (Krishan Lal and Bhagavannarayana, 1989), which is not the main focus of the present investigation. It is worth mentioning here that the observed scattering due to point defects is of short range order. Because the strain due to such minute defects was limited to the defect core, the long range order could not be expected. On comparison of curves in Figures 4.3(a) and (b) one can conclude that the SR method grown crystals are not only having good size but also they have good crystalline perfection.

### 4.4.3 Chemical etching analysis

The chemical etching studies were carried out on the grown single crystals of LAM to study the symmetry of the crystal face from the shape of etch pits and the distribution of structural defects in the grown crystals. The (011) face of conventional SEST and SR methods grown LAM crystals were subjected to etching with water. The surface of conventional SEST grown LAM single crystal was dipped for 10 s in the water etchant for etching. The etched samples were dried using tissue paper and the etch patterns were observed using an optical microscope (Magnus MLX). Figure 4(a) represents etch pit patterns produced on the (011) face of the conventional SEST grown LAM crystal. Etch pits of pyramidal shape were observed and the etch pit density (EPD) was  $29.3 \times 10^3 \text{ cm}^{-2}$ . The etch pits did not disappear upon continuous etching, suggesting that the pits were due to dislocations. Figure 4(b) represents the etch pits observed for SR method grown LAM on the (011) face and EPD was  $13.7 \times 10^3 \text{ cm}^{-2}$ . In SR method grown LAM crystal the size of the etch pit is large compared to conventional method grown LAM. Such observations were reported on  $\langle 100 \rangle$  directed DGZC,  $\langle 001 \rangle$  directed TGS,  $\langle 101 \rangle$  and  $\langle 100 \rangle$  directed KDP single crystals (Senthil Pandian and Ramasamy, 2010; Senthil Pandian et al., 2008; Balamurugan et al., 2008; Balamurugan and Ramasamy, 2008). The possible reasons for large size etch pits in SR crystal may be due to the crystalline perfection. When the crystal was etched in an etchant the etch pit occurred more quickly in the less impurity content region. In utilizing single crystals for any applications it is essential to grow single crystals containing a reduced dislocation density (Senthil Pandian and Ramasamy, 2010). The most significant features of the dislocation structure were a tendency for certain dislocation types to nucleate in pairs and at growth sector boundaries. Among the numerous processes, which are influenced by crystallographic defects,

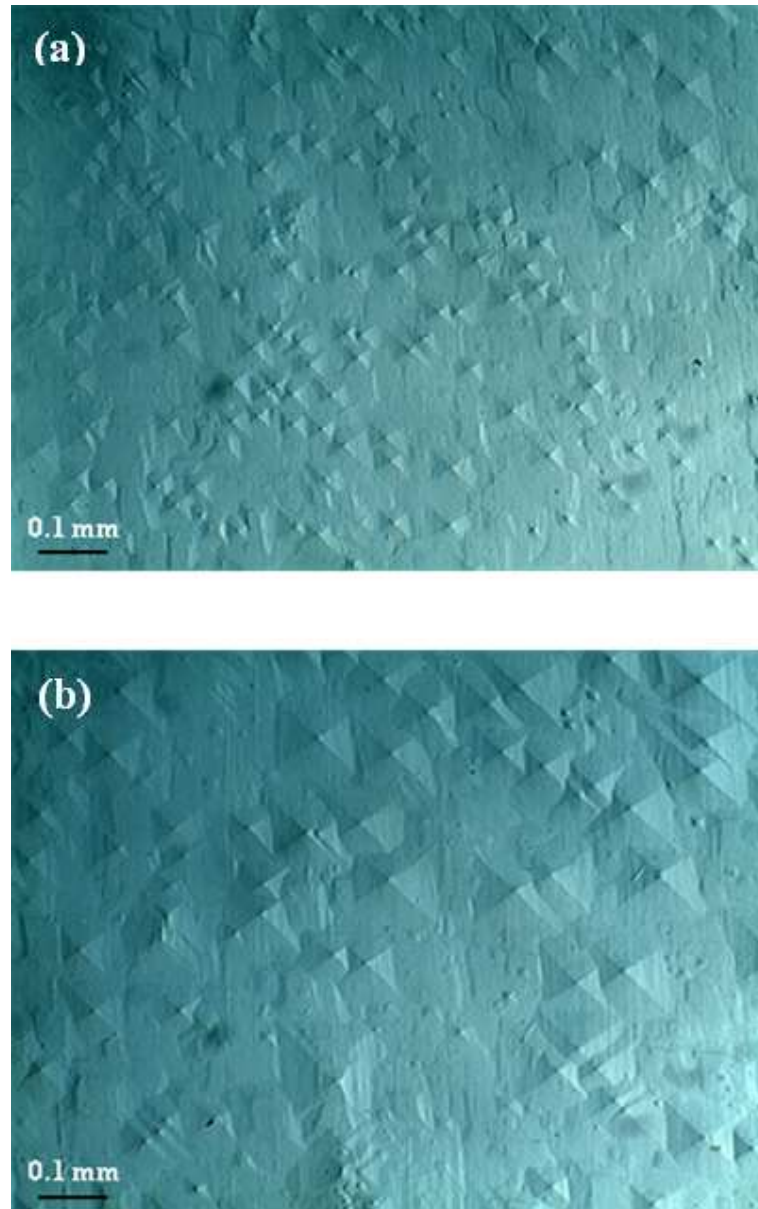


**Figure 4.4** Etching study on (011) face of LAM crystals grown by (a) conventional and (b) SR methods.

there can be few situations in which the interconnections are as close as in the case of crystal growth. Crystallization both influences, and is influenced by, the defect structure of a crystal. Some of the dislocation pairs formed at isolated nucleation points originate at growth sector boundaries (Ester et al., 1999). In SR method, the faceted growth is avoided so that the growth sectors will be reduced. Hence the dislocations which are associated with growth sector boundaries are absent in SR method grown crystal. This is the reason for low dislocation density in SR method grown crystal. Decrease in etch pits is associated with more systematic packing of the atoms/molecules, the strains formed during growth could be less though the growth rate is more in SR method (Senthil Pandian et al., 2008). The possible reasons for lower EPD of SR method grown crystals were reported (Senthil Pandian et al., 2008). Less number of EPD in SR method grown LAM shows that the quality of the crystals grown by SR method is better than conventional method grown crystals. The enhancement of crystalline quality of the unidirectional method grown DGZC, TGS, KAP and KDP crystals has been already reported (Senthil Pandian and Ramasamy, 2010; 2009; Senthil Pandian et al., 2008).

#### 4.4.4 Dielectric measurements

The cut and polished single crystal ( $9 \times 9 \times 2 \text{ mm}^3$ ) of LAM was used for dielectric studies. The sample was electroded on either side with graphite coating to make it behave like a parallel plate capacitor. Using the LCR meter, the capacitance and dielectric loss ( $\tan \delta$ ) of the samples prepared from these crystals were measured at the frequency of 100 Hz, 1 kHz, 10 kHz, 100 kHz and 1 MHz at various temperatures. The dielectric permittivity of the crystal was calculated using the relation  $\epsilon'_r = C_{crys}/C_{air}$ , where  $C_{crys}$  is the capacitance of the

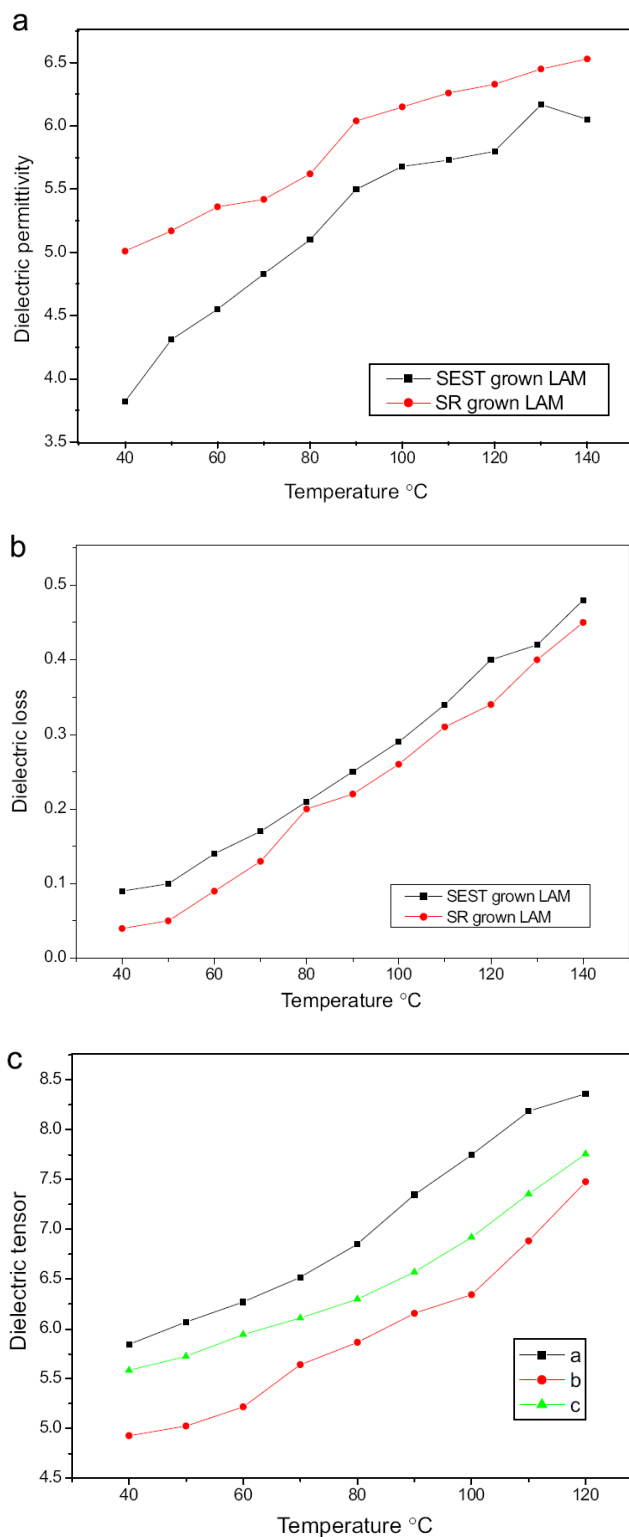


**Figure 4.5** (a) Dielectric permittivity, (b) dielectric loss curve of LAM crystals and (c) dielectric tensor long a-,b-and c-directions as a function of temperature at 1 kHz frequency.

crystal and  $C_{air}$  is the capacitance of the same dimension of air. Dielectric properties are correlated with the electro-optic property of the crystals (Boomadevi and Dhanasekaran, 2004). The magnitude of dielectric permittivity depends on the degree of polarization charge displacement in the crystals. Figures 4.5(a), (b) and (c) show the dielectric permittivity ( $\epsilon_r$ ), the dielectric loss of the crystal and the dielectric tensor along a-, b- and c-direction for 1 kHz frequency with various temperatures respectively. From the Figures 4.5(a) and (b), it is found that the values of dielectric permittivity and dielectric loss increase with the increase in temperature. The dielectric permittivity has a higher value (SR-6.5, SEST-6) in the higher temperature region (140 °C) and it then decreases (SR-5, SEST-3.8) with the applied lower temperature (40 °C). The dielectric permittivity of materials is due to the contribution of electronic, ionic, dipolar and space charge polarizations which depend on the frequencies. At low frequencies, all these polarizations are active (Meena and Mahadevan, 2008; Dharmaprasanth and Mohan Rao, 1989). In order to get the reproducibility the above experiment was repeated several times and the same results were obtained. The reproducibility was observed clearly. Dielectric loss obtained in the present study for SR method grown LAM crystal and conventional method grown LAM crystal is shown in Figure 4.5(b). In SEST grown LAM crystal, the dielectric loss has a high value of  $0.48 \pm 0.01$  at 140 °C and decreases to  $0.09 \pm 0.01$  at 40 °C. But in SR method grown LAM crystal the dielectric loss has a high value of  $0.45 \pm 0.01$  at 140 °C and decreases to  $0.04 \pm 0.01$  at 40 °C. The low value of dielectric loss indicates that the SR method grown LAM crystal contains less defects. The obtained values are in good agreement with the reported values (Rajesh, 2009; Ramesh Babu, 2006; Diem, 1968). The present study, in effect, shows that high dielectric permittivity and low dielectric loss is obtained for the crystal grown by SR method compared to the crystal grown by

conventional method. These results clearly indicate that the crystal grown by SR method has higher quality than the crystal grown by conventional method. These reports concur well with the reported values (Balamurugan, 2008). The dielectric permittivity of a crystalline material is a second rank tensor. For an orthorhombic system there are three independent components. The dielectric properties of a crystal may be characterized by the magnitudes and directions of three principal dielectric permittivities. Apart from the measurement on the (011) plane the SR-grown LAM crystal was cut along the (100), (010) and (001) planes with the thickness of 1 mm and then polished. The dielectric measurement was performed on these planes. Anisotropy in the dielectric behavior was observed while measuring for individual planes. The dielectric tensor for LAM single crystal was determined as a function of temperature at 1 kHz frequency along a-, b- and c directions. The dielectric tensor values vary with orientations in the range of 5.85 - 8.36 (a-direction), 4.93 - 7.48 (b-direction) and 5.59 - 7.76 (c-direction). The variations of these values are provided in Figure 4.5(c). As seen that  $\epsilon_{xx}$  (along a-direction)  $>$   $\epsilon_{zz}$  (along c-direction)  $>$   $\epsilon_{yy}$  (along b-direction). The LAM crystal shows dielectric anisotropies and the dielectric values increase as the temperature increases. The space charge polarization is generally active at low frequencies and high temperature.

#### 4.4.5 Thermo gravimetric and differential thermal analysis

Thermal analysis was performed using NETZSCH-STA 409 instrument in nitrogen atmosphere. The resulting TG-DTA trace is shown in Figure 4.6. There is no weight loss between 100 and 150 °C. This indicates that there is no inclusion of water in the crystal lattice, which was used as the solvent for crystallization. The TG curve reveals that the major weight loss (around 95%) starts at 165 °C.

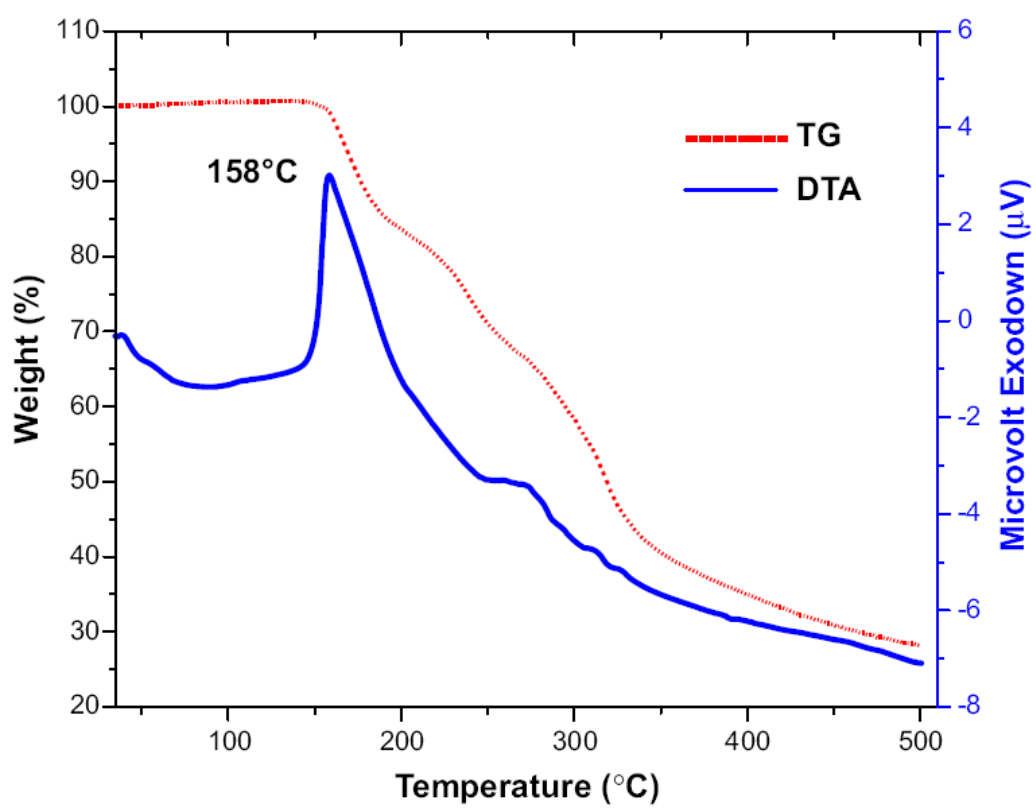


Figure 4.6 TG-DTA measurement of LAM.

**Table 4.1** Comparative thermal stability of organic NLO materials.

| Organic NLO materials            | Decomposition point (°C) | Reference                  |
|----------------------------------|--------------------------|----------------------------|
| L-alaninium maleate              | 158                      | (Present work)             |
| L-arginine maleate               | 93                       | Tapati Mallik et al., 2005 |
| L-histidine acetate              | 124                      | Madhavan et al., 2007      |
| L-arginine bis(trifluoroacetate) | 115                      | Zhihua Sun et al., 2009    |

The nature of weight loss indicates the decomposition point of the material. In the DTA spectrum an irreversible exothermic peak observed around 158 °C can be attributed to the decomposing point of the sample. Hence, this compound has a good thermal stability up to 158 °C and we can conclude that LAM crystal is suitable for any application upto 158 °C and it has a good thermal stability, compared to other organic NLO crystals such as L-arginine maleate (Tapati Mallik, 2005), L-histidine acetate (Madhavan, 2007), L-arginine bis(trifluoroacetate) (Zhihua Sun, 2009). Table 4.1 shows the comparative thermal stability between the present work and some organic NLO materials.

#### 4.4.6 UV-Vis NIR analysis

Optical window width is an important characteristic. Hence, it is necessary that the transmission of electromagnetic waves of the UV-Vis spectroscopy range is measured. Good transparent crystals grown by conventional SEST (Figure 4.1(a)) and SR method (Figure 4.2(b)) were carefully prepared with the same thickness of 2 mm for comparative study. UV-Vis NIR spectrum was recorded with Perkin-Elmer Lambda 35 spectrophotometer in the range of 200 - 1100 nm

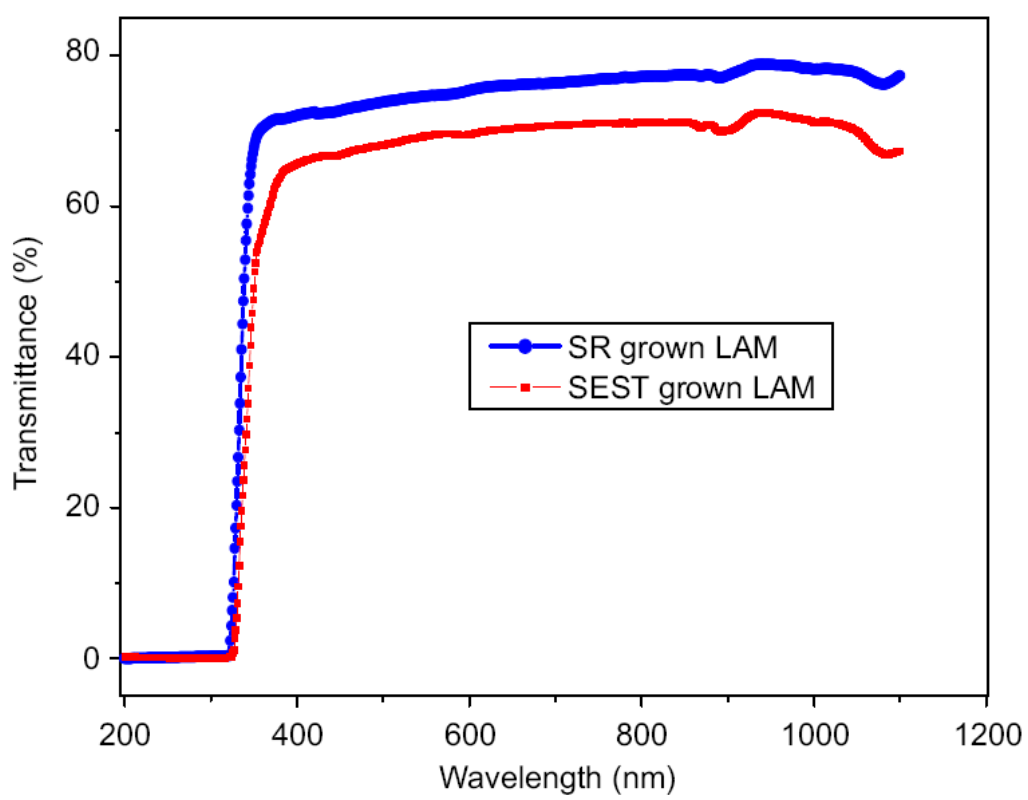


**Figure 4.7** UV-Visible analysis of LAM.

covering entire near ultraviolet, visible and higher energy part of near IR regions to find the transmission range to know the suitability for optical application. The recorded optical transmission spectra are shown in Figure 4.7. It is observed that the crystals have good transmission in the entire visible and IR region. The lower UV cut off wavelength is at 320 nm. The transmittance of SR method grown LAM crystal is 79% which is 7% higher than the transmittance of the conventional SEST grown LAM crystal. In order to confirm the reproducibility, the transmittance studies were repeated several times using different parts of the grown crystals and the same results were observed. The absence of absorption of light in the visible region is an intrinsic property of all amino acids (Ambujam, 2006). Absence of absorption in the region between 320 and 1100 nm shows that this crystal could be used for optical window applications. The improvement in the percentage of transmission by 7% may be attributed to the reduction of scattering from crystal's point and line defects. The improvement of optical transparency of SR method grown sulphamic acid, DGZC, KAP, TGS, KDP and ADP crystals has been already reported (Senthil Pandian, 2010; 2008).

#### 4.4.7 Vickers microhardness test

The crystals were subjected to Vickers microhardness tests using a Shimadzu (Model SMV2) hardness tester. A diamond indenter was pressed into the surface of (011) planes of LAM crystals under the influence of a known load (10 - 100 g) and the size of the resulting indentation was measured. The indentation time was 10 s for all the trials. The Vickers hardness number was calculated using the expression

$$H_v = 1.854(P/d^2) \quad kg/mm^2, \quad (4.1)$$

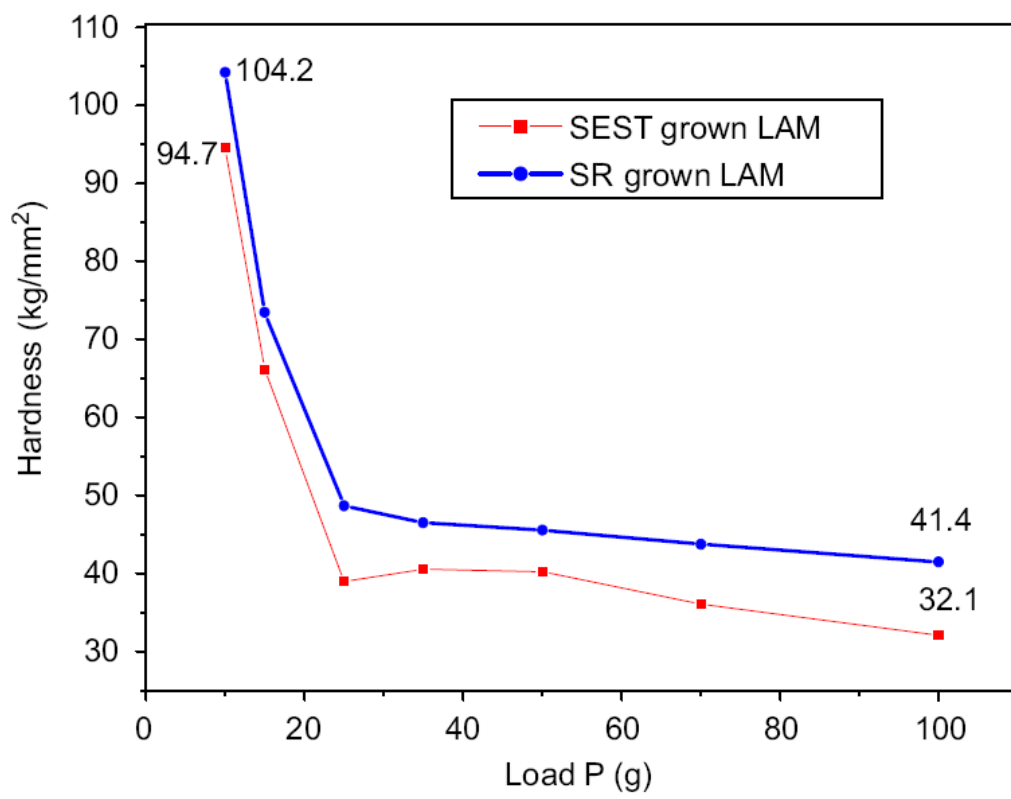


**Figure 4.8** Vickers microhardness analysis of LAM.

where  $H_v$  is the Vickers hardness number in  $\text{kg}/\text{mm}^2$ ,  $P$  is the applied load in g and  $d$  is the average diagonal length of the indentation in mm. A steep rise and fall in hardness number was observed in the range of 10 to 100 g. The  $H_v$  values were plotted as a function of applied load and it is shown in Figure 4.8. The microhardness values reduced very rapidly from 104 to  $50 \text{ kg}/\text{mm}^2$  when increasing the load from 10 to 25 g for the LAM crystal grown by the SR method. Similar result was observed for the SEST grown LAM crystals in which they reduce from 94 to  $40 \text{ kg}/\text{mm}^2$ . However, the  $H_v$  values change only slightly after that when increasing the load up to 100 g. For an indentation load of 100 g, cracks were initiated on the SEST and SR methods grown LAM crystal's surface, around the indenter. This again confirms that the mechanical property of the SR method grown LAM single crystal is also better than the crystal grown by conventional method. Hardness is the resistance offered by a solid to the movement of dislocation. Due to the application of mechanical stress by the indenter, dislocations are generated locally at the region of the indentation. Higher hardness value for the SR method grown crystal indicates that greater stress is required to produce dislocations thus confirming greater crystalline perfection. LAM single crystal grown by the SR method has a good mechanical hardness, when it compared to other organic NLO crystals such as DAST, DBCH, 2A-5CB and benzophenone (Haja Hameed, 2006; Udaya Lakshmi, 2005; Gulam Mohamed, 2007; Arivanandhan, 2008). The mechanical strength of the SR grown LAM crystal reveals that the crystal has higher hardness. An increase in the mechanical strength will have significant effect on fabrication and processing such as ease in polishing and less wastage due to cracking/breakage while polishing (Rajesh, 2009). The high mechanical hardness contributes to attractiveness of the present compound in practical applications.

Table 4.2 shows the comparative study results on the FWHM of HRXRD,

**Table 4.2** Comparative results of HRXRD, EPD dielectric loss, UV-transmittance and hardness on LAM crystals grown by SEST and SR methods.

| The characterization of LAM Crystal | SR method                       | SEST method                     |
|-------------------------------------|---------------------------------|---------------------------------|
| HRXRD, FWHM                         | Single peak,<br>12 arc sec      | Double peak<br>9 arc sec        |
| Chemical etching, EPD               | $13.7 \times 10^{-3}$           | $29.3 \times 10^{-3}$           |
| Dielectric loss                     | $0.45 \pm 0.01$ at 140 °C       | $0.48 \pm 0.01$ at 140 °C       |
|                                     | $0.04 \pm 0.01$ at 40 °C        | $0.09 \pm 0.01$ at 40 °C        |
| UV-vis, optical transmittance       | 79%                             | 72%                             |
| Microhardness                       | 41.4 kg/mm <sup>2</sup> at 100g | 32.1 kg/mm <sup>2</sup> at 100g |

etch pit density (EPD), dielectric loss, UV-transmittance and mechanical hardness on conventional SEST and SR method grown LAM crystals. Thus, single peak and low FWHM 12 arc s, low etch pit density ( $13.7 \times 10^3 \text{ cm}^{-2}$ ), good optical transmittance (79%), low dielectric loss ( $0.04 \pm 0.01$  at 40 °C), and high mechanical strength (41.4 kg/mm<sup>2</sup> at 100 g) of the SR method grown LAM indicates that the crystal is suitable for various applications.

## 4.5 Conclusions

An 18 mm diameter and 32 mm length LAM crystal of orientation (011) was successfully grown by Sankaranarayanan-Ramasamy method. The cell parameter was confirmed and it agrees with the reported values. Our HRXRD analysis shows that the crystal grown by the SR method has good crystalline perfection compared to the crystal grown by conventional method. Etching study reveals that the EPD of the SR method grown LAM crystal is less compared to the conventional

method grown crystal. Dielectric study showed that the higher dielectric constant and lower value of dielectric loss are due to less defects present in the SR method grown LAM crystal. The crystals have good thermal stability up to 158 °C. The transmittance of the SR method grown LAM crystal is 7% higher than that of the conventional SEST grown crystal. Vickers microhardness measurement shows that the crystals grown by the SR method have a higher hardness than these grown by the conventional method. HRXRD, chemical etching, dielectric constant, dielectric loss, optical transmittance and mechanical strength studies show that SR method is a capable method to grow crystals of good crystalline perfection with high optical quality and good mechanical stability.

#### 4.6 Acknowledgements

The authors are thankful to Dr. G. Bhagavannarayana, Head of Material Characterization Division, National Physical Laboratory, New Delhi, for the HRXRD study, Dr. C.K. Mahadevan, Physics Research Centre, S.T. Hindu College, Nagercoil, for the dielectric measurement and Department of Mechanical Engineering, SSN College of Engineering, for etching studies. The authors are also very much thankful to Prof. K. Kishan Rao, Department of Physics, Kakatiya University, Warangal, for microhardness measurement.

#### 4.7 References

- Alagar, M., Krishnakumar, R.V., Subha Nandhini, M. and Natarajan, S. (2001). L-alaninium maleate. **Acta Crystallographica Section E** 57: o855.
- Ambujam, K., Selvakumar, S., Prem Anand, D., Mohamed, G. and Sahayaraj, P. (2006). Crystal growth, optical, mechanical and electrical properties of

organic NLO material  $\gamma$ -glycine. **Crystal Research and Technology**. 41(7): 671.

Arivanandhan, M., Sankaranarayanan, K. and Ramasamy, P. (2008). Growth of longest  $\langle 100 \rangle$  oriented benzophenone single crystal from solution at ambient temperature. **Journal of Crystal Growth**. 310(7-9): 1493.

Balamurugan, S., Bhagavannarayana, G. and Ramasamy, P. (2008). Growth of unidirectional potassium dihydrogen orthophosphate single crystal by SR method and its characterization. **Materials Letters**. 62(24): 3963.

Balamurugan, S., Ramasamy, P. (2008). Bulk growth of (101) KDP crystal by Sankaranarayanan-Ramasamy method and its characterization. **Materials Chemistry and Physics**. 112(1): 1.

Batterman, B.W., Cole, H. (1964). Dynamical diffraction of x rays by perfect crystals. **Reviews of Modern Physics**. 36(3): 681.

Bhagavannarayana, G., Ananthamurthy, R.V., Budakoti, G.C., Kumar, B. and Bartwal, K.S. (2005). A study of the effect of annealing on Fe-doped  $\text{LiNbO}_3$  by HRXRD, XRT and FT-IR. **Journal of Applied Crystallography**. 38(5): 768.

Boomadevi, S., Dhanasekaran, R. (2004). Synthesis, crystal growth and characterization of L-pyrrolidone-2-carboxylic acid (L-PCA) crystals. **Journal of Crystal Growth**. 261(1): 70.

Dharmaprakash, S.M., Mohan Rao, P. (1989). Dielectric properties of hydrated barium oxalate and barium cadmium oxalate crystals. **Journal of Materials Science Letters**. 8(10): 1167.

- Diem, M., Polavarapu, P.L., Oboodi, M. and Nafie, L.A. (1968). **J. Am. Chem. Soc.** 104: 1387.
- Ester, G. R., Price, R. and Halfpenny, J.P. (1999). Relationship between crystal growth and defect structure: a study of potassium hydrogen phthalate using X-ray topography and atomic force microscopy. **Journal of Physics D: Applied Physics.** 32(10 A): A128.
- Gulam Mohamed, M., Rajarajan, K., Mani, G., Vimalan, M., Prabha, K., Madhavan, J. and Sagayaraj, P. (2007). Growth and characterization of 2-amino-5-chlorobenzophenone (2A-5CB) single crystals. **Journal of Crystal Growth.** 300(2): 409.
- Haja Hameed, A.S., Rohani, S., Yu, W.C., Tai, C.Y. and Lan, C.W. (2006). Surface defects and mechanical hardness of rapidly grown DAST crystals. **Journal of Crystal Growth.** 297(1): 146.
- Jingran Su, Youting Song, Daofan Zhang and Xinan Chang. (2009). **Powder diffraction** 24: 234.
- Krishan Lal, Bhagavannarayana, G. (1989). A high-resolution diffuse X-ray scattering study of defects in dislocation-free silicon crystals grown by the float-zone method and comparison with Czochralski-grown crystals. **Journal of Applied Crystallography.** 22(3): 209.
- Natarajan, S., Martin Britto Dhas, S.A. and Ramachandran, E. (2006). Growth, thermal, spectroscopic, and optical studies of L-alaninium maleate, a new organic nonlinear optical material. **Crystal Growth and Design.** 6(1): 137.
- Madhavan, J., Aruna, S., Anuradha, A., Premanand, D., Vetha Potheher, I.,

- Thamizharasan, K. and Sagayaraj, P. (2007). Growth and characterization of a new nonlinear optical l-histidine acetate single crystals. **Optical Materials.** 29(9): 1211.
- Martin Britto Dhas, S.A., Ramachandran, E., Raji, P., Ramachandran, K. and Natarajan, S. (2007). Photoacoustic studies on the thermal properties of the NLO compound: L-alaninium maleate **Crystal Research and Technology.** 42(6): 601.
- Meena, M., Mahadevan, C.K. (2008). Growth and electrical characterization of L-arginine added KDP and ADP single crystals. **Crystal Research and Technology** 43(2): 166.
- Rajesh, P., Ramasamy, P. (2009). Growth of dl-malic acid-doped ammonium dihydrogen phosphate crystal and its characterization. **Journal of Crystal Growth.** 311(13): 3491.
- Ramesh Babu, R., Vijayan, N., Gopalakrishnan, R. and Ramasamy, P. (2006) Growth and characterization of L-lysine monohydrochloride dihydrate (L-LMHCl) single crystal. **Crystal Research and Technology.** 41(4): 405.
- Sankaranarayanan , K., Ramasamy , P. (2005). Unidirectional seeded single crystal growth from solution of benzophenone. **Journal of Crystal Growth.** 280(3-4): 467.
- Sankaranarayanan , K., Ramasamy , P. (2006). Unidirectional crystallization of large diameter benzophenone single crystal from solution at ambient temperature **Journal of Crystal Growth.** 292(2): 445.

- Senthil Pandian, M., Balamurugan, N., Bhagavannarayana, G. and Ramasamy, P. (2008). Characterization of  $\langle 010 \rangle$  directed KAP single crystals grown by Sankaranarayanan-Ramasamy (SR) method. **Journal of Crystal Growth**. 310(18): 4143.
- Senthil Pandian, M., Balamurugan, N., Ganesh, V., Raja Shekar, P.V., Kishan Rao, K. and Ramasamy, P. (2008). Growth of TGS single crystal by conventional and SR method and its analysis on the basis of mechanical, thermal, optical and etching studies. **Materials Letters**. 62(23): 3830.
- Senthil Pandian, M., Ramasamy, P. (2009). Unidirectional growth of  $\langle 001 \rangle$  tetraglycine barium chloride (TGBC) single crystal by Sankaranarayanan-Ramasamy method **Journal of Crystal Growth**. 311(3): 944.
- Senthil Pandian, M., Ramasamy, P. (2010). Conventional slow evaporation and Sankaranarayanan-Ramasamy (SR) method grown diglycine zinc chloride (DGZC) single crystal and its comparative study. **Journal of Crystal Growth**. 312(3): 413.
- Senthil Pandian, M., Urit Charoen-In, Ramasamy, P., Prapun Manyum, Lenin, M. and Balamurugan, N. (2010). Unidirectional growth of sulphamic acid single crystal and its quality analysis using etching, microhardness, HRXRD, UV-visible and Thermogravimetric-Differential thermal characterizations. **Journal of Crystal Growth**. 312(3): 397.
- Tapati Mallik, Tanusree Kar, Cryst. (2005). Synthesis, growth and characterization of a new nonlinear optical crystal: L-arginine maleate dihydrate. **Crystal Research and Technology**. 40(8): 778.
- Udaya Lakshmi, K., Ramamurthi, K. (2005). Growth and characterization of 2,6

- Dibenzylidenecyclohexanone single crystal. **Crystal Research and Technology.** 40(12): 1165.

Vasanth, K., Dhanuskodi, S. (2004). The structural, thermal and optical characterizations of a new nonlinear optical material. **Journal of Crystal Growth.** 263(1-4): 466.

Zhihua Sun, Guanghui Zhang, Xinqiang Wang, Zeliang Gao, Xiufeng Cheng, Shaojun Zhang and Dong Xu. (2009). **Crystal Growth and Design.** 9: 3251.

# CHAPTER V

## UNIDIRECTIONAL GROWTH OF ORGANIC NONLINEAR OPTICAL L-ARGININE MALEATE DIHYDRATE SINGLE CRYSTAL BY SANKARANARAYANAN-RAMASAMY METHOD AND ITS CHARACTERIZATION

### 5.1 Abstract

Unidirectional organic nonlinear optical L-arginine maleate dihydrate (LAMD) single crystal has been successfully grown by Sankaranarayanan-Ramasamy (SR) method. The SR as-grown crystal was transparent and the size was 65 mm in length and 15 mm in diameter. The grown LAMD crystals have been subjected to single crystal X-ray diffraction, high resolution X-ray diffraction (HRXRD), piezoelectric, dielectrics, UV-Vis NIR, Vickers microhardness, second harmonic generation (SHG) efficiency study and the results were discussed. The lattice parameters of the grown LAMD crystal were confirmed by single crystal X-ray diffraction and the morphology was investigated in conventional grown LAMD crystal. Crystalline perfection was observed from HRXRD analysis. Piezoelectric charge coefficients of the grown crystal have been determined. The dielectric constant and loss measurements was made as a function of temperature in the range between 40 and 140 °C. The improved transparency of the grown crystal was investigated by recording UV-Vis analysis. Microhardness measurements revealed

that the mechanical strength of the SR-grown LAMD crystal was higher than that of the conventional method grown crystal. SHG measurements indicate that the SHG efficiency of the grown LAMD crystal at a fundamental wavelength of 1064 nm was roughly 1.4 times that of KDP.

## 5.2 Introduction

Nonlinear optical (NLO) materials have attracted much attention because of their wide applications in high-speed information processing, laser frequency conversion, optical data storage, signal communications and optical modulating (Dmitriev et al., 1999; Burland et al., 1994). Organic materials are expected to have relatively strong nonlinear optical (NLO) properties due to the presence of delocalized  $\pi$ -electrons conjugate system, connecting donor and acceptor groups, responsible for enhancing their asymmetric polarizabilities (Balasubramanian et al., 2008). This expectation explains extensive search for better NLO materials because of high flexibility in terms of molecular structure, high optical damage threshold, low cost and short response time to optical excitations among organic crystals (Boomadevi et al., 2004). L-Arginine is one of the essential amino acids widely distributed in biological substances. It forms a number of salts with organic and inorganic acids showing non-linear optical properties. L-Arginine maleate dihydrate (LAMD,  $C_6H_{14}N_4O_2 \cdot C_4H_4O_4 \cdot 2H_2O$ ) is one of these L-arginine salts which is a complex of strongly basic amino acid. It is also a nonlinear optical material with second harmonic generation efficiency 1.4 times that of KDP (Kalaiselvi et al., 2005). LAMD crystals are grown from solution by solvent evaporation. The crystal belongs to the triclinic system with space group P1. The growth of high-quality single crystals remains a challenging task for crystal growers. Growth of defect free transparent bulk single crystals along a particular axis is very important

for the preparation of functional crystals. For example the conversion efficiency of SHG is always highest along the phase matching direction for nonlinear optical crystals. From this point of view, the Sankaranarayanan-Ramasamy (SR) method is a capable method to grow bulk single crystal along a specific orientation (Balamurugan et al., 2009; Rajesh and Ramasamy, 2009; Senthil et al., 2009; Senthil Pandian and Ramasamy, 2009; Senthil Pandian et al., 2008; Senthil Pandian et al., 2010). The unidirectional crystal growth method is most suitable for the crystal growth along particular direction. In addition, the unidirectional solution crystallization usually occurs at around room temperature; much lower thermal stress is expected in these crystals over those grown at high temperatures (Jingran Su et al., 2009).

In the present investigation, bulk single crystals of LAMD were grown by SR method. Identical samples were subjected to single crystal X-ray diffraction, HRXRD, dielectric measurement, piezoelectric measurement, UV-Vis NIR analysis, Vickers microhardness measurement and SHG conversion efficiency in order to determine their properties and the results are discussed.

## **5.3 Experimental procedures**

### **5.3.1 Synthesis and crystal growth**

LAMD was synthesized by dissolving the equimolar quantities of L- arginine and maleic acid in Millpore water of resistivity 18.2 M $\Omega$  cm at room temperature. The synthesized LAMD was purified by repeated crystallization process several times before growth. The recrystallization was carried out to minimize the impurities of the raw materials, which in turn enhances the optical quality of the grown crystals. The saturated solution was prepared in accordance with the solu-

bility data (Tapati Mallik and Tanusree Kar, 2005). LAMD crystals were grown by slow evaporation solution technique (SEST). After 20 days of growth, a transparent crystal with the dimension  $10 \times 8 \times 3 \text{ mm}^3$  was successfully harvested. The SEST-grown LAMD crystal is shown in Figure 5.1(a). The morphology of the SEST-grown crystal is as seen in Figure 5.1(b), there are 6 prominent faces on the crystal. The major faces are (001), ( $\bar{1}10$ ), ( $\bar{2}\bar{1}0$ ) and ( $0\bar{1}4$ ). Based on the morphology, (001) face was selected to impose the orientation of the grown crystal. Cut and polished portion of LAMD crystal along (001) face was fixed at the bottom of the ampoule. Slightly under saturated LAMD solution was prepared and slowly poured in to the ampoule. The top portion of the ampoule was covered by a plastic sheet with a hole at the center to limit the evaporation. Then, the whole ampoule was kept in the double container using water medium to prevent the fluctuations in temperature. A detailed discussion of the particular experimental set-up is given in reference (Sankaranarayanan and Ramasamy, 2005). Once the system attains equilibrium, the growth was initiated with a suitable temperature provided by the ring heater at the top of the solution. Top of the growth ampoule was maintained at  $38 \text{ }^\circ\text{C}$  for solvent evaporation. The temperature around the growth region is maintained at  $34 \text{ }^\circ\text{C}$  for the growing crystals. The experimental conditions were closely monitored and found that the LAMD seed crystal started to grow after 10 days. In a time span of 40 days, a good quality single crystal of LAMD was harvested from the ampoule. The SR-grown LAMD crystal was carefully separated by cutting the wall of the ampoule which is shown in the Figure 5.2(a). The average growth rate was about  $2 \text{ mm/day}$ . In order to characterize the crystal, disc-shape specimen required for various measurements were cut by the crystal cutter perpendicular to the crystal portion as shown in the Figure 5.2(b).

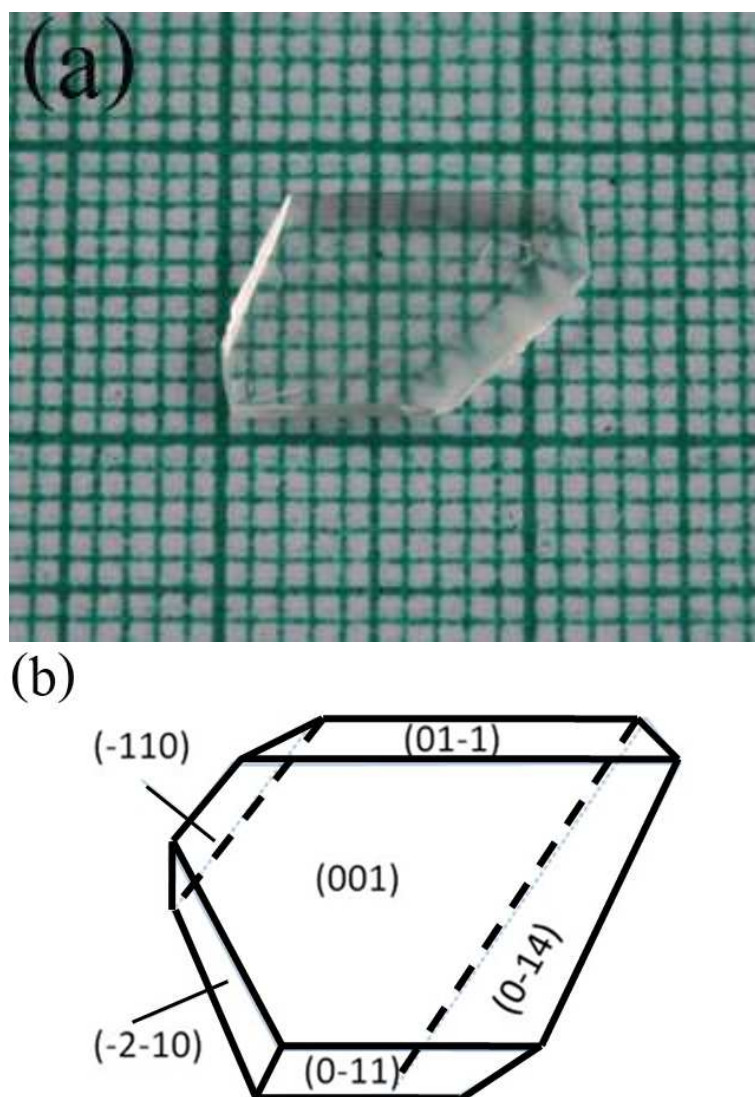


**Figure 5.1** (a) Conventional method grown LAMD crystal and (b) Morphology of LAMD crystal.

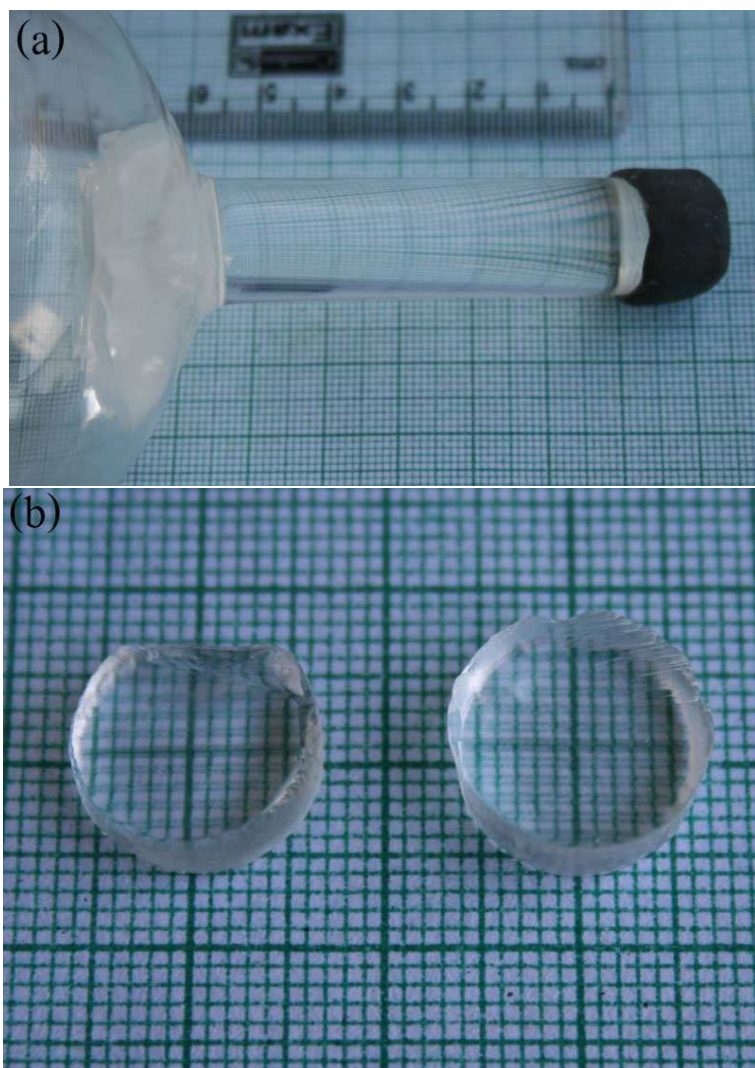


**Figure 5.2** (a) SR-grown LAMD crystal, (b) Cut and polished SR-grown LAMD crystals.

## 5.4 Characterization

Identical samples were prepared by using the same orientation LAMD grown by SR and SEST methods and subjected to various studies. Lattice parameter of the grown single crystal was obtained using Enraf nonius (AD4-MV3). Morphology of the grown crystal was identified by the single crystal X-ray diffraction studies (Bruker Kappa APEXII). The crystalline perfection of the as-grown single crystal of LAMD was characterized by HRXRD by employing a multocrystal X-ray diffractometer developed at NPL (Lal and Bhagavannarayana, 1989). The piezoelectric studies were made using piezometer system. A precision force generator applied a calibrated force (0.25N) which generated a charge on the piezoelectric material under test. The dielectric constant and dielectric loss analysis were measured using Agilent 4284-A LCR meter. The error in the measurement is  $\pm 1.5\%$ . UV-Vis transmittance spectrum was recorded using Perkin-Elmer Lambda 35 UV-Vis spectrophotometer in the range of 200 - 1100 nm. The mechanical strength of the grown crystal was made on the prominent (001) plane using a Shimadzu (Model HVM2) tester fitted with a diamond pyramidal indenter. The indentations were made on the crystal for different loads and the diagonal lengths of the indentation marks were measured at 5 s for all cases. The SHG conversion efficiency was tested using the method of Kurtz and Perry (Kurtz and Perry, 1968).

## 5.5 Results and discussions

### 5.5.1 Single crystal X-ray diffraction

From the single-crystal XRD measurement, it is found that the grown single crystal belongs to the triclinic system and has a noncentrosymmetric nature with the space group P1. The determined lattice parameters are  $a = 5.259 (3)\text{\AA}$ ,  $b =$

8.041 (2)Å,  $c = 9.791$  (3)Å and  $\alpha = 106.27$  (3)°,  $\beta = 97.24$  (3)°,  $\gamma = 101.69$  (3)° and Volume = 381.8 (3)Å<sup>3</sup>. The observed values are consistent with the reported literature value (Mallik, 2005).

## 5.5.2 Crystalline perfection

To reveal the crystalline perfection of the specimen crystals, high-resolution diffraction curves (DC) were recorded with the multicrystal X-ray diffractometer. The specimen crystal is aligned in the (+, -, -, +) configuration. Before recording the diffraction curve, the specimen surface was prepared by lapping and polishing and then it was chemically etched by a nonpreferential chemical etchant mixed with water and acetone in 1:2 ratio. Figure 5.3(a) shows the high-resolution diffraction curve (DC) recorded for a typical SEST-grown LAMD single crystal specimen using (100) diffracting planes in symmetrical Bragg geometry by employing the multicrystal X-ray diffractometer with MoK $\alpha_1$  radiation. The solid line (convoluted curve) is well fitted with the experimental points represented by the filled circles. On deconvolution of the diffraction curve, it is clear that the curve contains two additional peaks, which are 24 and 18 arc s away from the main peak (at zero glancing angle). These two additional peaks correspond to two internal structural very low angle boundaries (tilt angle  $\leq 1$  arc min) (Bhagavannarayana, 2005) whose tilt angles (Tilt angle may be defined as the misorientation angle between the two crystalline regions on both sides of the structural grain boundary) are 25 and 30 arc s from their adjoining regions. The full width at half maximum (FWHM) of the main peak and the very low angle boundaries are respectively 25, 20 and 30 arc s. Figure 5.3(b) shows the DC for the SR-grown specimen crystal recorded under identical conditions as that of curve Figure 5.3(a). This DC also is not a single peak but consists of one additional peak which is 30 arc s away

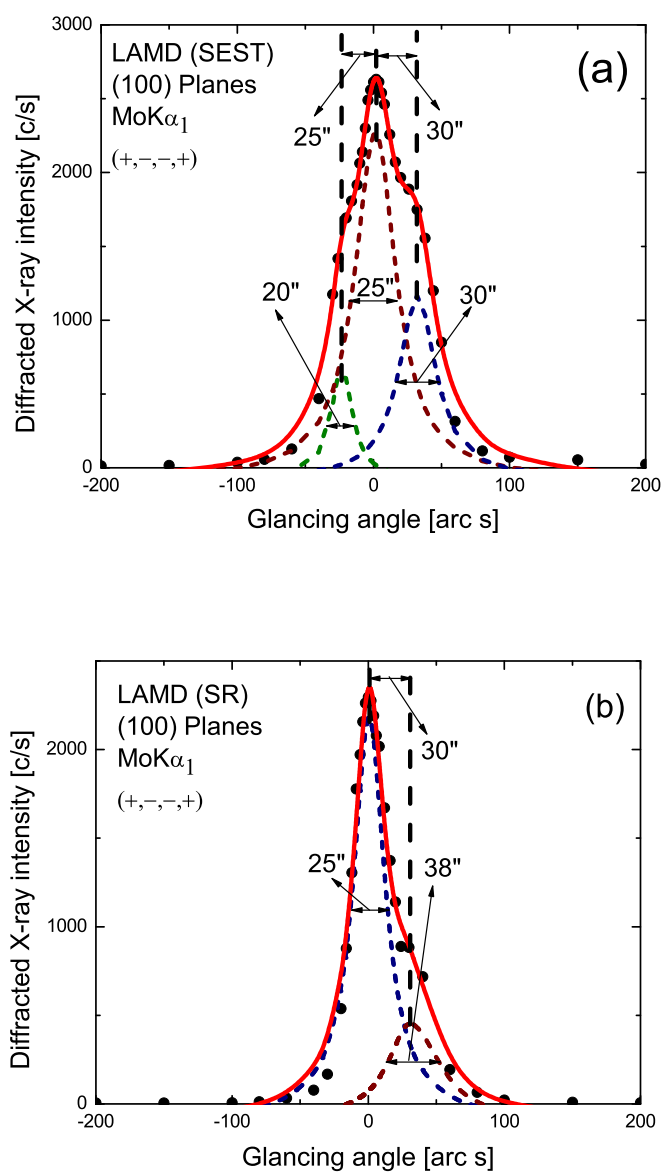


**Figure 5.3** High-resolution X-ray diffraction curves recorded for (100) diffracting planes of LAMD crystals grown by (a) conventional and (b) SR methods.

from the main peak showing that the specimen contains a very low angle internal structural grain boundary. The FWHM values of the main and satellite peaks are respectively 25 and 38 arc s. Though the specimen contains a very low angle boundary, the relatively low angular spread of around 200 arc s of the diffraction curve and the low FWHM values show that the crystalline perfection is reasonably good. The effect of such very low angle boundaries may not be very significant in many device applications, but for applications like phase matching, it is better to know these minute details regarding crystalline perfection. When we compare the DCs of SEST- and SR-grown LAMD specimens, it is clear that the crystalline perfection of SR-grown crystal is much better.

### 5.5.3 Piezoelectric measurement

A piezoelectric substance is one that produces an electric charge when a mechanical stress is applied. The piezoelectric property is related to the polarity of the material (Ge Wenwei et al., 2008). The obtained piezoelectric coefficient measurement was carried out for the grown crystals without poling the crystal. From oscilloscope the output was obtained directly. The piezoelectric coefficient ( $d_{33}$ ) was measured in units of  $\text{pCN}^{-1}$ . The obtained  $d_{33}$  value increased from  $0.64 \text{ pCN}^{-1}$  for SEST-grown LAMD crystal to  $0.80 \text{ pCN}^{-1}$  for SR method grown LAMD crystal. Higher crystalline perfection may be the reason for the higher piezoelectric values of the SR method grown LAMD crystals.

### 5.5.4 Dielectric studies

Dielectric properties are related with the electric field distribution within solid materials. Study of dielectric properties provides with quality information of materials (Hiremath, 2003). The cut and polished single crystal ( $9 \times 9 \times 2 \text{ mm}^3$ )

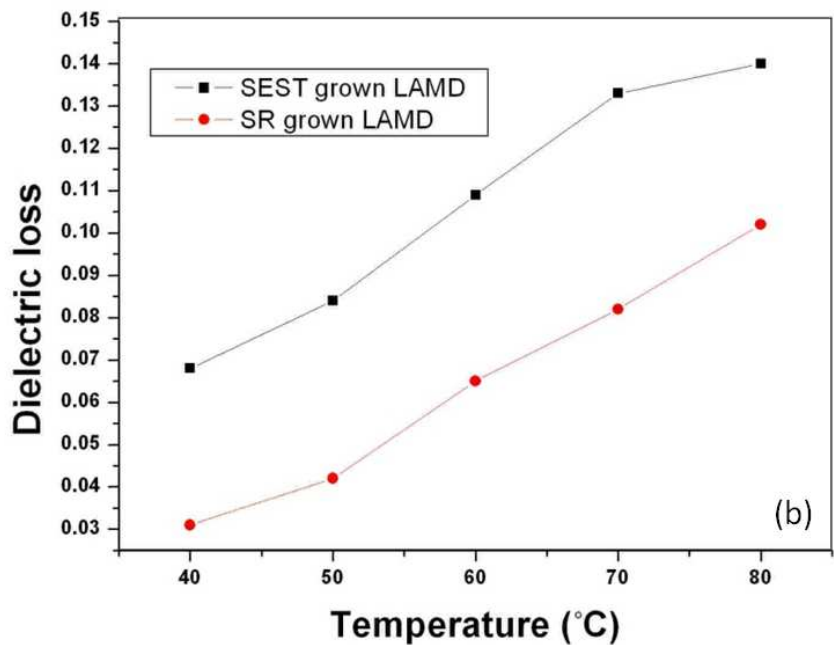
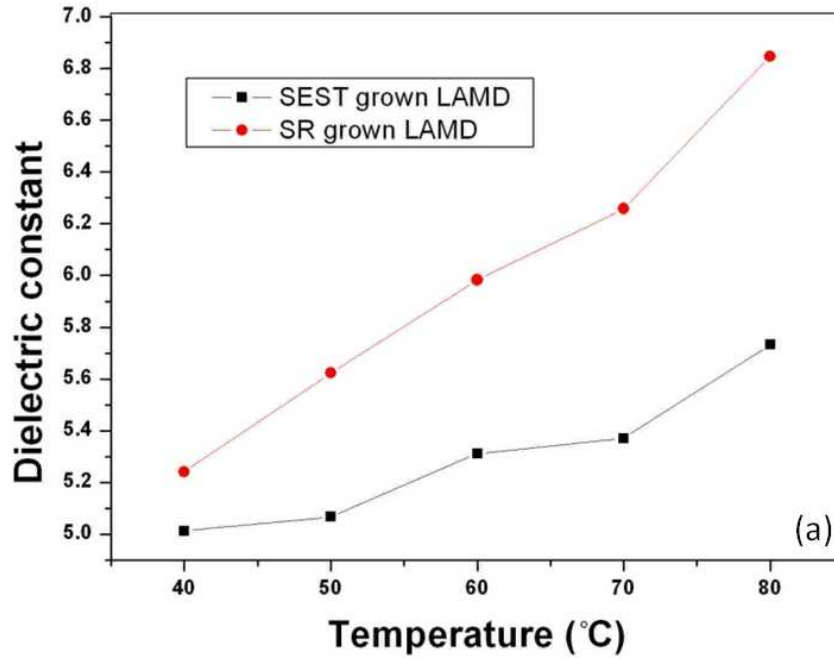


**Figure 5.4** (a) Dielectric constant and (b) Dielectric loss curve as function of temperature at 1 kHz frequency of LAMD.

of LAMD was used for dielectric studies. The sample was electroded on either side with graphite coating to make it behave like a parallel plate capacitor. The capacitance and dielectric loss ( $\tan\delta$ ) of the samples prepared from these crystals were measured as a function of temperature at a frequency of 1 kHz. The dielectric constant of the crystal was calculated using the relation  $\epsilon'_r = C_{crys}/C_{air}$ , where  $C_{crys}$  is the capacitance of the crystal and  $C_{air}$  is the capacitance of the same dimension of air. Figure 5.4(a) shows the variation in dielectric constant with the temperature at 1 kHz. As seen in the figure, the dielectric constants are slightly increased by the temperature variation without distinct anomaly or dispersion. The SR-grown LAMD crystal has a dielectric constant value higher than the dielectric constant of SEST-grown crystal. The dielectric constant of materials is due to the contribution of electronic, ionic, dipolar and space charge polarizations which depend on the frequencies. At low frequencies, all these polarizations are active (Rajesh, 2009; Ramesh Babu, 2006). The space charge polarization is generally active at low frequencies and high temperature. Variation of dielectric loss with frequency at different temperature is given in Figure 5.4(b), which reveals that the dielectric loss becomes large with increasing temperature. The lower value of dielectric loss in the SR-grown LAMD crystal indicates that the crystal is with lesser defects which is of vital importance for NLO materials in their application.

### 5.5.5 Transmittance

A good optical transmittance is very desirable in an NLO crystal since the absorptions, if any, in an NLO material near the fundamental or the second harmonic of a Nd:YAG laser, 1064 and 532 nm respectively, will lead to loss of conversion efficiency of SHG. Also the UV range from 200 to 400 nm is very important for the realization of SHG output in this range using diode laser. In

order to find the transmission range to know the suitability for optical application, cut and polished good transparent SR method grown crystal (Figure 5.2(b)) with thickness of 8 mm was used at face (001) for this study. The transmission spectra of LAMD crystal along (001) plane is shown in Figure 5.5. It is observed that the crystals have good transmission in the entire visible and IR region. The lower UV cut off wavelength is at 320 nm. The transmittance of SR method as grown LAMD crystal of the thickness 8 mm is  $\sim 80\%$ . The improvement in the percentage of transmission may be attributed to the reduction of scattering from point and line defects of the crystal. In order to confirm the reproducibility, the transmittance studies were repeated several times using different parts of the grown crystals and the same results were observed. The percentage of transmission for 8 mm thick SR method grown crystal is 80% where as 2 mm thick SEST crystal had only 45% transmission (Kalaiselvi, 2008; Tapati Mallik, 2005; Mallik, 2005). Transmittance in the region between 320 and 1100 nm shows that this crystal could be used for optical window applications.

### 5.5.6 Microhardness study

The microhardness testing is the simplest characterization technique that can be best employed to study the mechanical properties of material, such as fracture behavior, yield strength, brittleness index and temperature of cracking (Lawn, 1975). For each load several trials of indentations were carried out. The Vickers microhardness ( $H_v$ ) of the crystal was evaluated using the relation  $H_v = 1.8544 (P/d^2) \text{ kg/mm}^2$ , where P is the indenter load in g and d is the mean diagonal length of the impression in mm. The measurement was performed on the (001) plane of the SR and SEST grown LAMD crystals. Improvement in the hardness behavior has been observed while measuring for individual planes. The

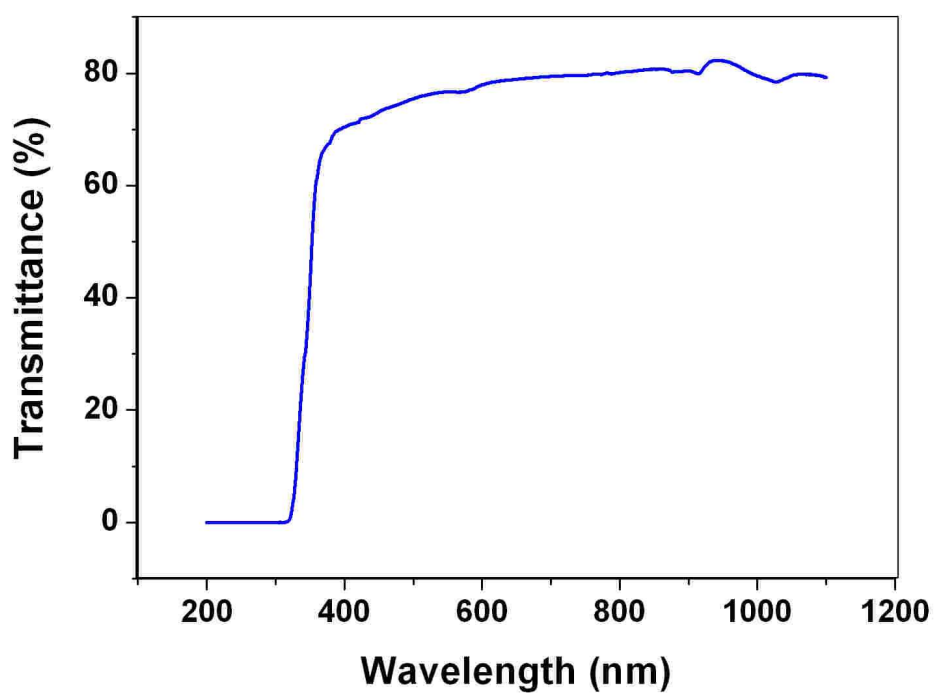


Figure 5.5 UV-Visible analysis of LAMD.

microhardness values vary with the method to grow crystals in the range (SEST) 12.4 - 32.2 and (SR) 15.2 - 36.7 kg/mm<sup>2</sup>. The microhardness for single crystal of LAMD was determined as a function of load and variations of these values are provided in the Figure 5.6. Due to the application of mechanical stress by the indenter, dislocations are generated locally at the region of indentation. Hence larger hardness value for SR method growth LAMD crystal indicates greater stress required to form dislocation thus confirming greater crystalline perfection. The mechanical strength of SR grown LAMD crystal reveals that the crystal has a good hardness and it is useful for any applications. An increase in the mechanical strength will have significant effect on fabrication and processing such as ease in polishing and less wastage due to cracking/breakage while polishing (Senthil Pandian, 2010). The high mechanical hardness contributes to attractiveness of the present compound in practical applications.

### 5.5.7 SHG study

The SHG efficiency of LAMD is measured by using the Kurtz-Perry powder technique. A fundamental wave with a pulse width of 8 ns, repetition frequency of 10 Hz, a beam diameter of 1 mm, energy of the laser pulse around 300 mJ and a wave length of 1064 nm radiated from Nd:YAG laser source was focused on the samples by a lens with focal length of 120 mm. The grown single crystal of LAMD was powdered with a uniform particle size and densely filled into the quartz cell. A sample of potassium dihydrogen phosphate (KDP), also powdered to the identical size as the experimental sample was used as a reference material in the SHG measurement. The transmitted fundamental wave was absorbed by a CuSO<sub>4</sub> solution and the second harmonic signal was detected by a photomultiplier tube and displayed on a storage oscilloscope. The generation of the second harmonics

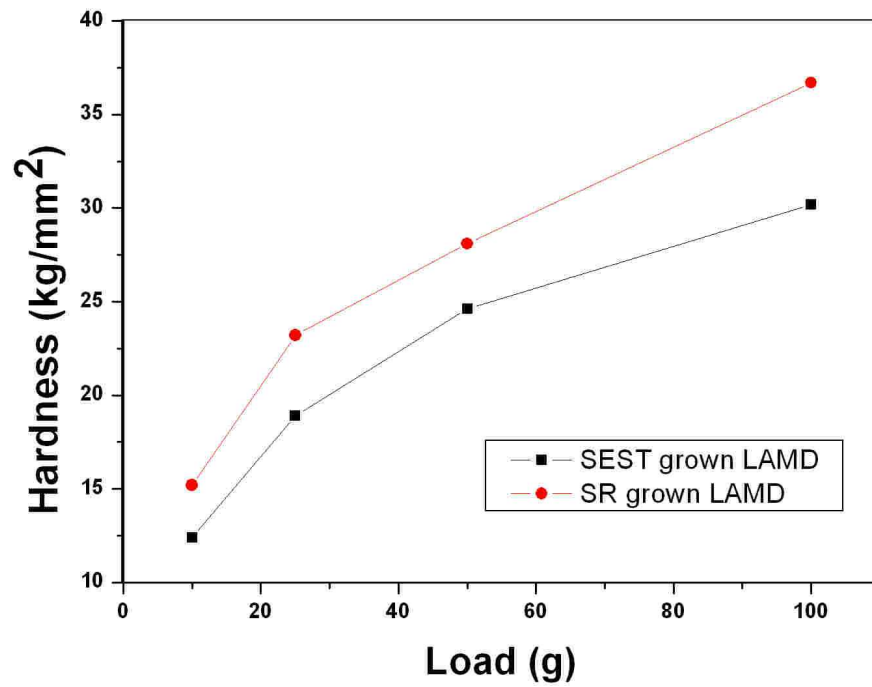


Figure 5.6 Vickers microhardness analysis of LAMD.

was confirmed by green radiation of 532 nm in both the conventional and SR method grown LAMD samples. The SHG conversion efficiency of both crystals grown from the SR method and SEST is found to be nearly 1.4 times greater than that of KDP crystal.

## 5.6 Conclusions

A 65 mm length and 15 mm diameter unidirectional LAMD single crystal has been successfully grown by Sankaranarayanan-Ramasamy method. X-ray single-crystal diffraction confirms the lattice parameter of the LAMD grown crystal. Morphology investigation reveals face appearing on the SEST-grown LAMD crystal. The SR method grown crystal contains a very low angle boundary and the low full width at half of maximum values show that the crystalline perfection is reasonably good. Dielectric study showed that the higher dielectric constant and lower value of dielectric loss are due to less defects present in the SR method grown LAMD crystal. The SR method grown LAMD crystal shows higher piezoelectric charge coefficient because of having better crystalline quality. Optical transmittance indicates that the transmission region of the SR-grown LAMD crystal is from 320 - 1100 nm which is sufficient for its SHG efficiency and the transmittance is more than 80% with the UV cutoff at 320 nm. Vickers microhardness measurement reveals that the crystals grown by the SR method have a higher hardness than those by the conventional method. The SHG conversion efficiency of both crystal samples is approximately 1.4 times greater than that of standard KDP. The study will be useful to grow unidirectional large size single crystal with higher crystalline perfection, higher hardness and good optical quality for SHG applications.

## 5.7 Acknowledgements

The authors are thankful to Dr. G. Bhagavannarayana, Head of Material Characterization Division, National Physical Laboratory, New Delhi, for the HRXRD study, Dr. C.K. Mahadevan, Physics Research Centre, S.T. Hindu College, Nagercoil, for the dielectric measurement and Dr. Binay Kumar, Department of Physics and Astrophysics, University of Delhi, India for piezoelectric studies. The authors are also very much thankful to Prof. K. Kishan Rao, Department of Physics, Kakatiya University, Warangal, for microhardness measurement.

## 5.8 References

- Balasubramanian, D., Sharkar, R., Siva Sankar, V., Murugakoopthan, P., Arulmozhihelvan P. and Jayavel, R. (2008). Growth and characterization of semiorganic nonlinear optical rubidium bis-dl-malato borate single crystals Mater. **Materials Chemistry and Physics**. 107(1): 57.
- Balamurugan, S., Ramasamy, P., Sharma, S.K., Yutthapong Inkong and Prapun Manyum. (2009). Investigation of SR method grown  $\langle 001 \rangle$  directed KDP single crystal and its characterization by high-resolution X-ray diffractometry (HRXRD), laser damage threshold, dielectric, thermal analysis, optical and hardness studies. **Materials Chemistry and Physics**. 117(2-3): 465.
- Bhagavannarayana, G., Ananthamurthy, R.V., Budakoti, G.C., Kumar, B. and Bartwal, K.S. (2005). A study of the effect of annealing on Fe-doped  $\text{LiNbO}_3$  by HRXRD, XRT and FT-IR. **Journal of Applied Crystallography**. 38(5): 768.

- Boomadevi, S., Mittal, H. and Dhansekaram, R. (2004). Synthesis, crystal growth and characterization of 3-methyl 4-nitropyridine 1-oxide (POM) single crystals. **Journal of Crystal Growth**. 261(1): 55.
- Burland, D.M., Miller, R.D. and Walsh, C. A. (1994). Second-order nonlinearity in poled-polymer systems. **Chemical Reviews**. 94(1): 31.
- Dmitriev, V.G., Gurzadyan, G.G. and Nicogosyan, D.N. (1999). **Handbook of Nonlinear Optical Crystals**. Spriger-Verlag; New York.
- Ge Wenwei, et al. (2008) Growth and characterization of  $\text{NaO.5BiO.5TiO}_3\text{-BaTiO}_3$  lead-free piezoelectric crystal by the TSSG method. **Journal of Alloys and Compounds**. 456(1-2): 503.
- Hiremath, V.A., Venkataraman, A. (2003). Dielectric, electrical and infrared studies of  $\text{Fe-Fe}_2\text{O}_3$  prepared by combustion method. **Bulletin of Materials Science**. 26(4): 391.
- Jingran Su, Youting Song, Daofan Zhang and Xinan Chang. (2009). **Powder diffraction**. 24: 234.
- Kalaiselvi, D., Mohan Kumar, R. and Jayavel, R. (2008). Growth and characterization of nonlinear optical l-arginine maleate dihydrate single crystals. **Materials Letters**. 62(4-5): 755.
- Kurtz, S.K., Perry, T.T. (1968). A powder technique for the evaluation of nonlinear optical materials. **Journal of Applied Physics**. 39(8): 3798.
- Lal K., Bhagavannarayana, G. (1989). A high-resolution diffuse X-ray scattering study of defects in dislocation-free silicon crystals grown by the float-zone method and comparison with Czochralski-grown crystals. **Journal of Applied Crystallography**. 22(3): 209.

- Lawn, B.R., Fuller, E.R. (1975). Equilibrium penny-like cracks in indentation fracture. **Journal of Materials Science**. 10(12): 2016.
- Mallik T., Kar T., Bocelli, G. and Musatti, A. (2005). Synthesis, crystal structure and solubility of  $C_6H_{14}N_4O_2 \cdot C_4H_4O_4 \cdot 2H_2O$ . **Science and Technology of Advanced Materials**. 6(5): 508.
- Rajesh, P., Ramasamy, P. (2009). Growth of dl-malic acid-doped ammonium dihydrogen phosphate crystal and its characterization. **Journal of Crystal Growth**. 311(13): 3491.
- Ramesh Babu, R., Vijayan, N., Gopalakrishnan R. and Ramasamy, P. (2006). Growth and characterization of L-lysine monohydrochloride dihydrate (L-LMHCl) single crystal **Crystal Research and Technology**. 41(4): 405.
- Sankaranarayanan, K., Ramasamy, P. (2005). Unidirectional seeded single crystal growth from solution of benzophenone. **Journal of Crystal Growth**. 280(3-4): 467.
- Senthil, A., Ramesh Babu, R., Balamurugan, N. and Ramasamy, P. (2009). Unidirectional growth of largest L-LMHCl dihydrate crystal by SR method. **Journal of Crystal Growth**. 311(3): 544.
- Senthil Pandian, M., Balamurugan, N., Bhagavannarayana, G. and Ramasamy, P. (2008). Characterization of  $\langle 010 \rangle$  directed KAP single crystals grown by Sankaranarayanan-Ramasamy (SR) method. **Journal of Crystal Growth**. 310(18): 4143.
- Senthil Pandian M., Ramasamy, P. (2009). Unidirectional growth of  $\langle 001 \rangle$  tetra

glycine barium chloride (TGBC) single crystal by Sankaranarayanan-Ramasamy method. **Journal of Crystal Growth.** 311(3): 944.

Senthil Pandian, M., Ramasamy, P. (2010). Conventional slow evaporation and Sankaranarayanan-Ramasamy (SR) method grown diglycine zinc chloride (DGZC) single crystal and its comparative study. **Journal of Crystal Growth.** 312(3): 413.

Senthil Pandian, M., Urit Charoen-In, Ramasamy, P., Prapun Manyum, Lenin, M. and Balamurugan, N. (2010). Unidirectional growth of sulphamic acid single crystal and its quality analysis using etching, microhardness, HRXRD, UV-visible and Thermogravimetric-Differential thermal characterizations. **Journal of Crystal Growth.** 312(3): 397.

Tapati Mallik, Tanusree Kar, (2005). Synthesis, growth and characterization of a new nonlinear optical crystal: L-arginine maleate dihydrate. **Crystal Research and Technology.** 40(8): 778.

**CHAPTER VI**

**GROWTH OF DICHLORO BIS(L-PROLINE)**

**ZINC(II) SINGLE CRYSTAL BY**

**SANKARANARAYANAN-RAMASAMY**

**METHOD AND ITS CHARACTERIZATION**

**6.1 Abstract**

Single-crystalline dichlorobis(L-proline)zinc(II) (LPZ) was successfully grown by Sankaranarayanan-Ramasamy (SR) method. The dimension of the grown crystal is  $70 \times 20 \times 10 \text{ mm}^3$ . The lattice parameters of the grown LPZ crystal were confirmed by single crystal X-ray diffraction. Excellent crystalline perfection without having any low angle internal structural grain boundaries was observed from high-resolution X-ray diffraction (HRXRD) analysis. Etch pit density of the grown LPZ crystal was calculated and the distribution of structural defect was observed in chemical etching studies. Piezoelectric charge coefficient of the grown crystal was higher than the conventional method grown LPZ. The dielectric constant and loss measurement was made as function of temperature in the range between 40 and 140 °C. The low dielectric loss was observed for the SR method grown crystal. The improved transparency of the grown LPZ crystal is investigated by recording UV-Vis analysis. Microhardness measurements reveal the mechanical strength of the grown crystal. Second harmonic generation (SHG) measurement indicates that the SHG efficiency of the grown LPZ crystal at a

fundamental wavelength of 1064 nm is roughly equal to that of KDP.

## 6.2 Introduction

The growth of high-quality single crystals remains a challenging endeavor of materials science. Crystals of large size and structural perfection are required for fundamental research and practical implementation in photonic and optoelectronic technology. Semi-organic nonlinear optical (NLO) crystals have attracted attention because they have been proposed as a new approach for materials with fascinating NLO properties which have the combined properties of both inorganic and organic crystals like high damage threshold, wide transparency range, less deliquescence and high non-linear coefficients which make them suitable for device fabrication (Jiang, 1999). The complex of amino acid and inorganic salts represents an important class of semi-organic crystals, which have a wide range of electronic characteristics, mechanical hardness and thermal stability. Proline is an abundant amino acid in collagen and is exceptional among the amino acids. Because it is the only one in which the amine group is part of a pyrrolidine ring, making it rigid and directional in biological systems (Myung, 2005). A series of semi-organic compounds for example L-proline cadmium chloride monohydrate (Kandasamy, 2007) and L-proline lithium chloride monohydrate (Uma Devi, 2009) crystals have been reported with good SHG efficiency. A new semi-organic, dichlorobis(L-proline)zinc(II) (LPZ)  $((C_5H_9NO_2)_2ZnCl_2)$  crystal belongs to orthorhombic system. The lattice parameters are  $a = 6.631(5) \text{ \AA}$ ,  $b = 13.502(6) \text{ \AA}$ ,  $c = 16.230 \text{ \AA}$ ,  $V = 1453.0 \text{ \AA}^3$ ,  $\alpha = \beta = \gamma = 90^\circ$  and the space group is  $P2_12_12_1$  (Anandha Babu, 2009). The crystals have been grown by the conventional slow evaporation solution technique (SEST) and several studies have been reported (Anandha Babu, 2009; Lydia Caroline, 2009). The Sankaranarayanan-Ramasamy

method (Sankaranarayanan and Ramasamy, 2005) attracted the researchers due to the growth of defect free transparent bulk single crystals along a particular axis, which is very important for the preparation of functional crystals. For example, as the conversion efficiency of SHG is always highest along the phase matching direction for nonlinear optical crystals, the unidirectional crystal growth method is most suitable for the crystal growth along that direction. In addition, the unidirectional solution crystallization usually occurs at around room temperature; much lower thermal stress is expected in these crystals over those grown at high temperatures (Jingran Su, 2009). The SR method was successfully used to grow unidirectional large size single crystal of several substances like KDP, ADP, L-LMHCl, TGBC, KAP and sulphamic acid (Balamurugan, 2009; Rajesh, 2009; Senthil 2009; Senthil Pandian, 2010; 2009; 2008). From this point of view, we have attempted to grow large size, good quality single crystals of LPZ from its aqueous solution by the SR method.

In the present investigation, bulk single crystals of LPZ were grown by conventional SEST and SR methods. Identical samples prepared with similar orientation were subjected to HRXRD, etching study, dielectric measurement, piezoelectric measurement, UV-Vis NIR analysis, Vickers microhardness measurement and SHG conversion efficiency in order to determine their properties and the results are discussed.

## **6.3 Experiment**

### **6.3.1 Crystal growth**

The starting materials, L-proline and zinc chloride (Merck Analytical Reagents) were taken in the stoichiometric ratio of 2:1. The calculated amount

of material was dissolved in Millipore water of resistivity 18.2 M $\Omega$  cm at room temperature. Single crystals of LPZ were grown from saturated solution by the conventional SEST at 34 °C using constant temperature bath (CTB). After 15 days, small crystals with needle shape were observed in the beaker. It is essential to increase the purity to a reputable level before proceeding further. The LPZ crystals were recrystallized several times to minimize impurities. Good quality transparent crystals were collected as seeds to get large size crystals. According to the solubility data (Anandha Babu, 2009), the saturated solution of LPZ was prepared at 34 °C and it was kept in the CTB. A seed crystal was inserted into a saturated solution in the beaker using nylon thread. After one week the growth was observed and the crystal was allowed to grow further to get well developed maximum size. After 30 days of growth, a good quality crystal with the dimension of 26  $\times$  8  $\times$  4 mm<sup>3</sup> was successfully harvested. Figure 6.1(a) shows a crystal grown by conventional seed hanging technique. The grown crystal was used as a seed for SR method and also to compare the crystalline quality with the SR method grown crystal. The morphology of the LPZ crystal is given in Figure 6.1(b). There are 12 prominent faces on the crystal. The major faces (010), (013), (001) and (102) were observed in the conventional SEST grown LPZ crystals. Based on the morphology of the LPZ crystal, the fast growth rate  $\langle 100 \rangle$  direction was selected in the present study to improve the size and quality of the crystal. Cut and polished portion of LPZ crystal along  $\langle 100 \rangle$  direction was fixed at the bottom of the ampoule. The saturation solution of LPZ was prepared and fed into an ampoule. A detailed discussion of the particular experiment setup is given in reference (Sankaranarayanan, 2005). Once the system attains equilibrium, the growth was initiated with a suitable temperature provided by the ring heater at the top of the solution. Top of the growth ampoule was maintained at 38 °C for

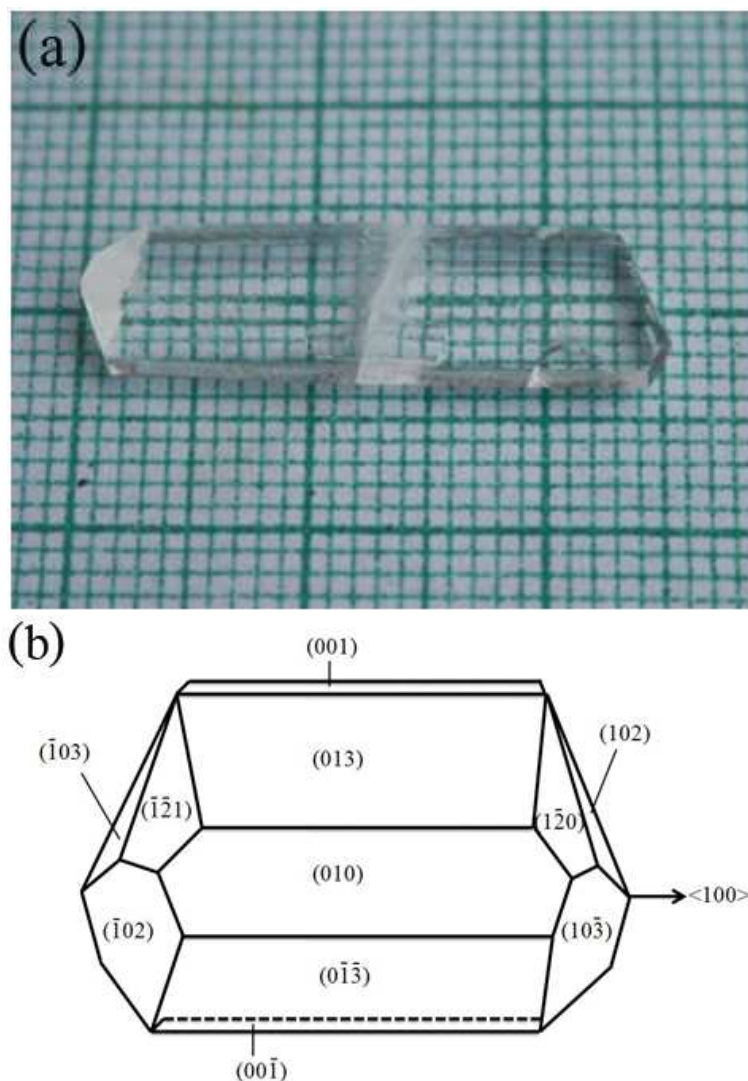


**Figure 6.1** (a) Conventional grown LPZ crystal and (b) Morphology of LPZ crystal.

solvent evaporation. The temperature around the growth region is maintained at 34 °C for the growing crystals. After five days, the seed crystal mounted at the bottom started to grow. Under this condition the highly transparent crystal was monitored and the growth system was kept constant for a long period for attaining continuous growth which has yielded LPZ crystal of 70 mm length and 20 mm diameter within 35 days. The SR-method grown LPZ crystal is shown in the Figure 6.2. The average growth rate was about 2 mm/day.



**Figure 6.2** SR-grown LPZ crystal.

### 6.3.2 Characterization

The single crystal XRD data of the LPZ crystal was obtained using Enraf nonius (AD4-MV3) single crystal X-ray diffractometer. Morphology of the grown crystals was identified by the single crystal X-ray diffraction studies (Brukerkappa APEXII). To reveal the crystalline perfection of the grown single crystal, a multocrystal X-ray diffractometer (MCD) designed and developed at NPL (Lal and Bhagavannarayana, 1989), has been used to record high-resolution diffraction curves (DCs). The specimen crystal was aligned in the (+, -, -, +) configuration. In chemical etching, etch patterns were observed using an optical microscope (Magnus MLX). In the present case the (010) face of conventional SEST and SR methods grown LPZ crystals were subjected to etching with water. The surface of conventional SEST grown LPZ single crystal was dipped for 10 s in the water etchant for etching. The etched samples were dried using tissue paper and the etch patterns were observed. The dielectric constant and dielectric loss were measured using Agilent 4284-A LCR meter. The error in the measurement is  $\pm 1.5\%$ . The

cut and polished single crystal ( $8 \times 8 \times 2 \text{ mm}^3$ ) of LPZ was used for dielectric studies. The sample was electroded on either side with graphite coating to make it behave like a parallel plate capacitor. The capacitance and dielectric loss ( $\tan \delta$ ) of the samples prepared from these crystals were measured at the frequencies of 100 Hz, 1 kHz, 10 kHz, 100 kHz and 1 MHz at various temperatures. The dielectric constant of the crystal was calculated using the relation  $\epsilon'_r = C_{crys}/C_{air}$ , where  $C_{crys}$  is the capacitance of the crystal and  $C_{air}$  is the capacitance of the same dimension of air. The piezoelectric studies were made using piezometer system. A precision force generator applied a calibrated force (0.25 N) which generated a charge on the piezoelectric material under test. UV-Vis transmittance spectrum was recorded using Perkin-Elmer Lambda 35 UV-Vis spectrophotometer in the range 200-1100 nm covering the entire near-ultraviolet, visible and higher energy part of near-infrared region. Good transparent SR method as grown crystal (Figure 6.2) with thickness of 10 mm without any polishing, also conventional SEST as grown crystal (Figure 6.1(a)) with thickness of 4 mm and 1 mm polished SEST grown crystal were used at face (010) for this study. The hardness measurements were made on the prominent (010) plane of the crystal using the Shimadzu (Model HMV2) tester fitted with a diamond pyramidal indenter. The indentations were made on the crystal for different loads and the diagonal lengths of the indentation marks were measured at 5 s for all cases. The Vickers microhardness ( $H_v$ ) was calculated using the equation  $H_v = 1.8544 P/d^2$  ( $\text{kg}/\text{mm}^2$ ). For each load several trials of indentations were carried out. The SHG conversion efficiency was tested using the method of Kurtz and Perry. A fundamental wave with a pulse width of 8 ns, repetition frequency of 10 Hz, a beam diameter of 1 mm, energy of the laser pulse around 300 mJ and a wave length of 1064 nm radiated from Nd:YAG laser source was focused on the samples by a lens with focal length of 120 mm.

The grown single crystal of LPZ was powdered with a uniform particle size and densely filled into the quartz cell. A sample of potassium dihydrogen phosphate (KDP), also powdered to the identical size as the experimental sample was used as a reference material in the SHG measurement. The transmitted fundamental wave was absorbed by a  $\text{CuSO}_4$  solution and the second harmonic signal was detected by a photomultiplier tube and displayed on a storage oscilloscope.

## 6.4 Results and discussions

### 6.4.1 Singly crystal X-ray diffraction

From the single crystal X-ray diffraction analysis, it was observed that the crystal belongs to orthorhombic system with space group  $P2_12_12_1$ . The calculated lattice parameter values are  $a = 6.602$  (2) Å,  $b = 13.536$  (4) Å,  $c = 16.253$  (3) Å and Volume = 1452.4 (6) Å<sup>3</sup>. The observed values are consistent with the reported literature (Anandha Babu, 2009; Lydia Caroline, 2009).

### 6.4.2 High resolution X-ray diffraction

The physical properties of the single crystal may change when the defects are created during growth. Also, the quality of the crystal highly depends on the method and material used for the growth. The defects like impurity and dislocation are normally formed during growth from solution. Therefore, the defect analysis of crystal is important for device fabrication. Figure 6.3(a) shows the high-resolution diffraction curve (DC) recorded for a typical SEST grown LPZ single crystal using (024) diffracting planes in symmetrical Bragg geometry by employing the multocrystal X-ray diffractometer with  $\text{MoK}\alpha_1$  radiation. As seen in the figure, the DC contains a single peak and indicates that the specimen is free

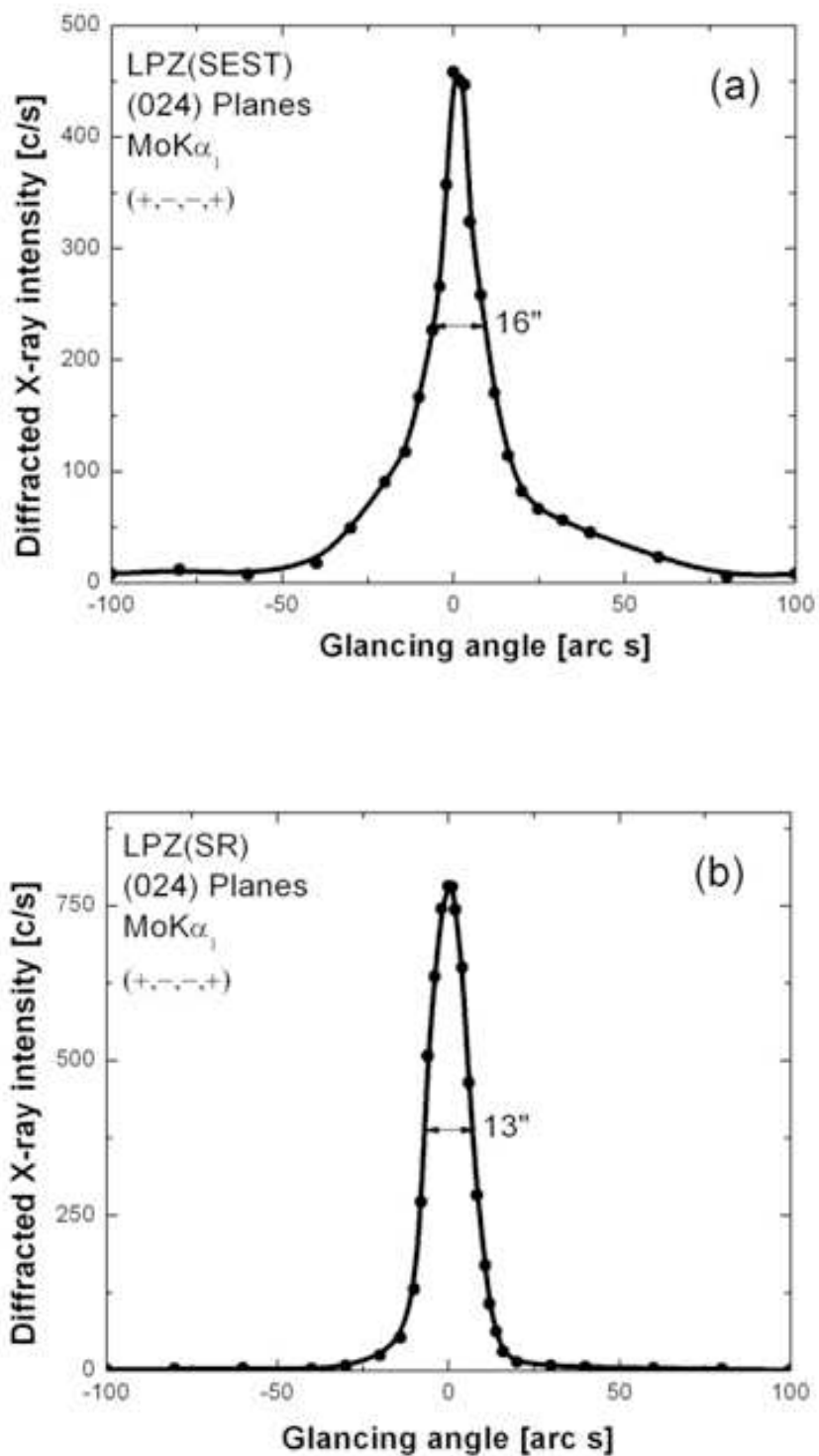


**Figure 6.3** High-resolution X-ray diffraction curves recorded for (024) diffracting planes: (a) SEST and (b) SR-grown single crystals of LPZ.

from structural grain boundaries. The full width at half maximum (FWHM) of the curve is 16 arc s which is somewhat more than that expected from the plane wave theory of dynamical X-ray diffraction (Batterman and Cole, 1964), for an ideally perfect crystal but close to that expected for nearly perfect real life crystals. This much broadness with good scattered intensity along the wings of the DC indicates that the crystal contains both vacancy and interstitial type of defects. Such defects are very commonly observed in almost all real crystals including naturally occurring crystals and are many times unavoidable due to thermodynamical conditions. More details may be obtained from the study of high-resolution diffuse X-ray scattering measurements (Lal and Bhagavannarayana, 1989), which is not the main focus of the present investigation. It is worth mentioning here that the observed scattering due to point defects is of short range order. Because the strain due to such minute defects is limited to the very defect core, the long range order could not be expected.

Figure 6.3(b) shows the DC for the SR-grown LPZ crystal recorded under identical conditions as that of curve Figure 6.3(a). As seen in the figure the DC contains a single peak having FWHM value of 13 arc s which is less than that of curve in Figure 6.3(a) which belongs to the SEST-grown crystal. One may also observe that the scattered X-ray intensity along the tails of the DC of SR-grown crystal is quite low in comparison to that of SEST-grown crystal revealing that the former one contains lesser number of point defects or their clusters showing the better crystalline perfection of SR-grown crystal.

### 6.4.3 Etching study

The chemical etching technique is the simplest characterization technique that can be best employed to study the defect structure of a single crystal. How-

ever, the success of this technique lies in the efficiency of the chemical etchant to sense the dislocation site selectively. Subsequently, etch pits are formed at the dislocation centers on those faces at which the additives are bound, which is able to develop some of the features such as growth hillocks, etch spirals, rectangular etch pits, etc. on the surface. Figure 6.4(a) represents etch pit patterns produced on the (010) face of the conventional SEST grown LPZ crystal. Etch pits of pyramidal shape were observed and the calculated etch pit density (EPD) was  $8.2 \times 10^2 \text{ cm}^{-2}$ . The etch pits did not disappear upon continuous etching, suggesting that the pits were due to dislocations. In utilizing single crystals for NLO applications it is essential to grow single crystals containing a reduced dislocation density (Senthil Pandian 2010). Figure 6.4(b) represents the etch pits observed for SR method grown LPZ on the (010) face and EPD was  $5.3 \times 10^2 \text{ cm}^{-2}$ . In SR method grown LAM crystal the size of the etch pit is large compared to conventional method grown LAM. Such observations were reported on  $\langle 100 \rangle$  directed DGZC,  $\langle 001 \rangle$  directed TGS,  $\langle 101 \rangle$  and  $\langle 100 \rangle$  directed KDP single crystals (Senthil Pandian, 2010; 2008; Balamurugan, 2008). The possible reasons for large size etch pits in SR crystal may be due to the crystalline perfection. When the crystal was etched in an etchant the etch pit occurred more quickly in the less impurity content region. In the conventional SEST, certain dislocations have a tendency to nucleate at growth sector boundaries. The possible reasons for lower EPD of SR method grown crystal is the avoided faceted growth so that the growth sector boundaries are minimized. Hence the dislocations which are associated with growth sector boundaries are absent in the SR method grown crystal. Decrease in etch pits is associated with more systematic packing of the atoms/molecules, the strains formed during growth could be less though the growth rate is more in SR method (Senthil Pandian, 2008). This is the reason for low dislocation density

in SR method grown LPZ crystal. Less number of EPD in SR method grown LPZ shows that the quality of the crystals grown by SR method is better than conventional method grown crystals.

#### 6.4.4 Dielectric studies

The dielectric properties of the optical materials are interconnected with electro-optic properties of the crystal (Boomadevi and Dhanasekaran, 2004), particularly when they are non-conducting in nature. Studies of the temperature and frequency dependence of dielectric properties can unveil useful information about structural changes, defect behavior and transport phenomena (Lin et al., 2001). The variation of dielectric constant ( $\epsilon_r$ ) as a function of frequency with different temperature is shown in Figure 6.5(a). The values of dielectric constant are higher at the low frequencies, slightly decrease as frequency increases and increase with the increase in temperature. The dielectric constant of materials is due to the contribution of electronic, ionic, dipolar and space charge polarizations which depend on the frequencies. At low frequencies, all these polarizations are active (Rajesh, 2009; Ramesh Babu, 2006). The space charge polarization is generally active at low frequencies and high temperature. The dielectric loss curve as shown in Figure 6.5(b) clearly indicates that the grown crystal has negligible loss for entire range of characterized frequency, which indicates that crystal is almost free from the structure defect as observed from the HRXRD. In order to get the reproducibility above the experiment was repeated several times and the same results were obtained. The reproducibility was observed clearly. The temperature dependence of the dielectric properties of the LPZ crystal at 1 kHz of frequency are illustrated in Figures 6.6(a) and (b). As shown in both figures, it is observed that the values of dielectric constant and dielectric loss increase with the increase in temperature.

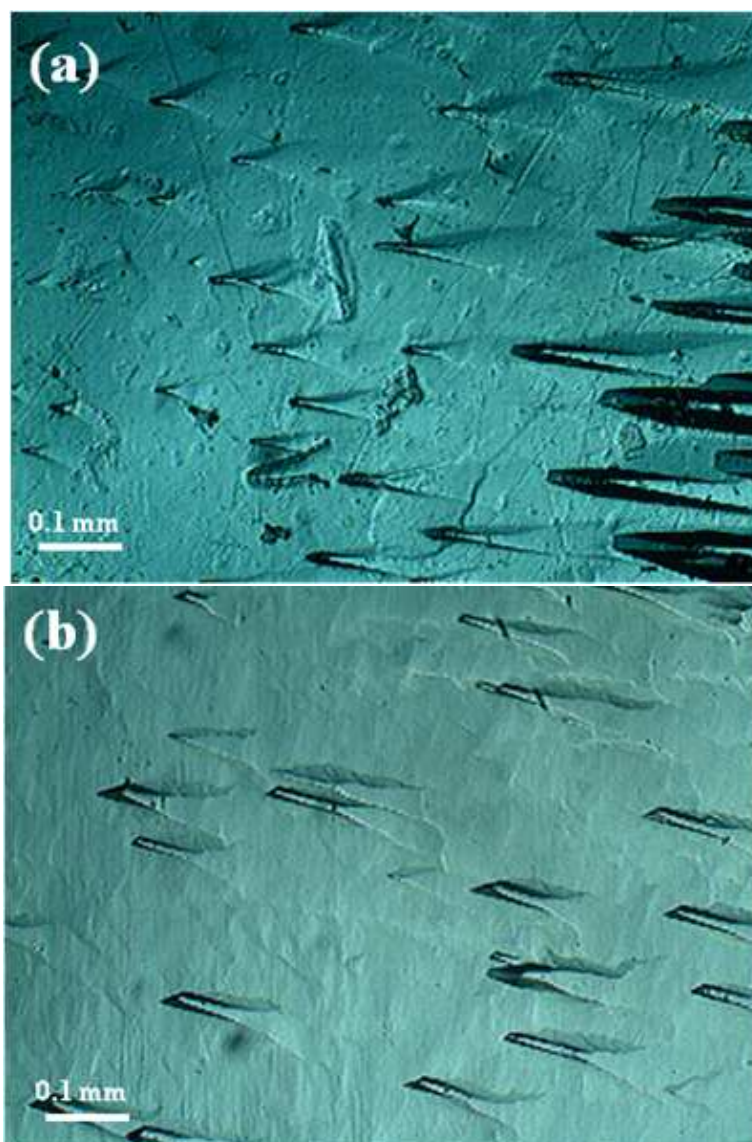


**Figure 6.4** Etching study on (010) face of LPZ crystals grown by (a) conventional and (b) SR methods.

From Figure 6(a), the dielectric constant has a higher value (SR-10.49, SEST-8.39) in the higher temperature region (140 °C) and it then decreases (SR-7.39, SEST-4.20) with the applied lower temperature (40 °C). Dielectric loss obtained in the present study for the SR method grown LPZ crystal and the conventional method grown LPZ crystal are shown in Figure 6(b). In the SEST grown LPZ crystal, the dielectric loss has a value of 0.30 at 80 °C. But in SR method grown LPZ crystal the dielectric loss has a value of 0.24 at 80 °C. The low value of dielectric loss indicates that the SR method grown LPZ crystal contains minimum defects which is in agreement with the HRXRD results with low FWHM value. The present study, in effect, shows that high dielectric constant and low dielectric loss is obtained for the crystal grown by SR method compared to the crystal grown by conventional method. These results clearly indicate that the crystal grown by SR method has higher quality than the crystal grown by conventional method.

#### 6.4.5 Piezoelectric measurement

A piezoelectric substance is one that produces an electric charge when a mechanical stress is applied. The piezoelectric property is related to the polarity of the material (Ge Wenwei et al., 2008). Without poling the crystal the piezoelectric measurement was carried out for the grown crystals. The output was measured directly from oscilloscope which gives the  $d_{33}$  coefficient in units of pC/N. The obtained  $d_{33}$  value for the conventional SEST and SR method grown LPZ crystals are 0.23 pC/N and 0.54 pC/N respectively. Approximately 2 times higher  $d_{33}$  value has been obtained for the SR method grown LPZ crystal than the conventional method grown LPZ grown crystal. Higher crystalline perfection may be the reason for the higher piezoelectric values of the SR method grown LPZ crystals.

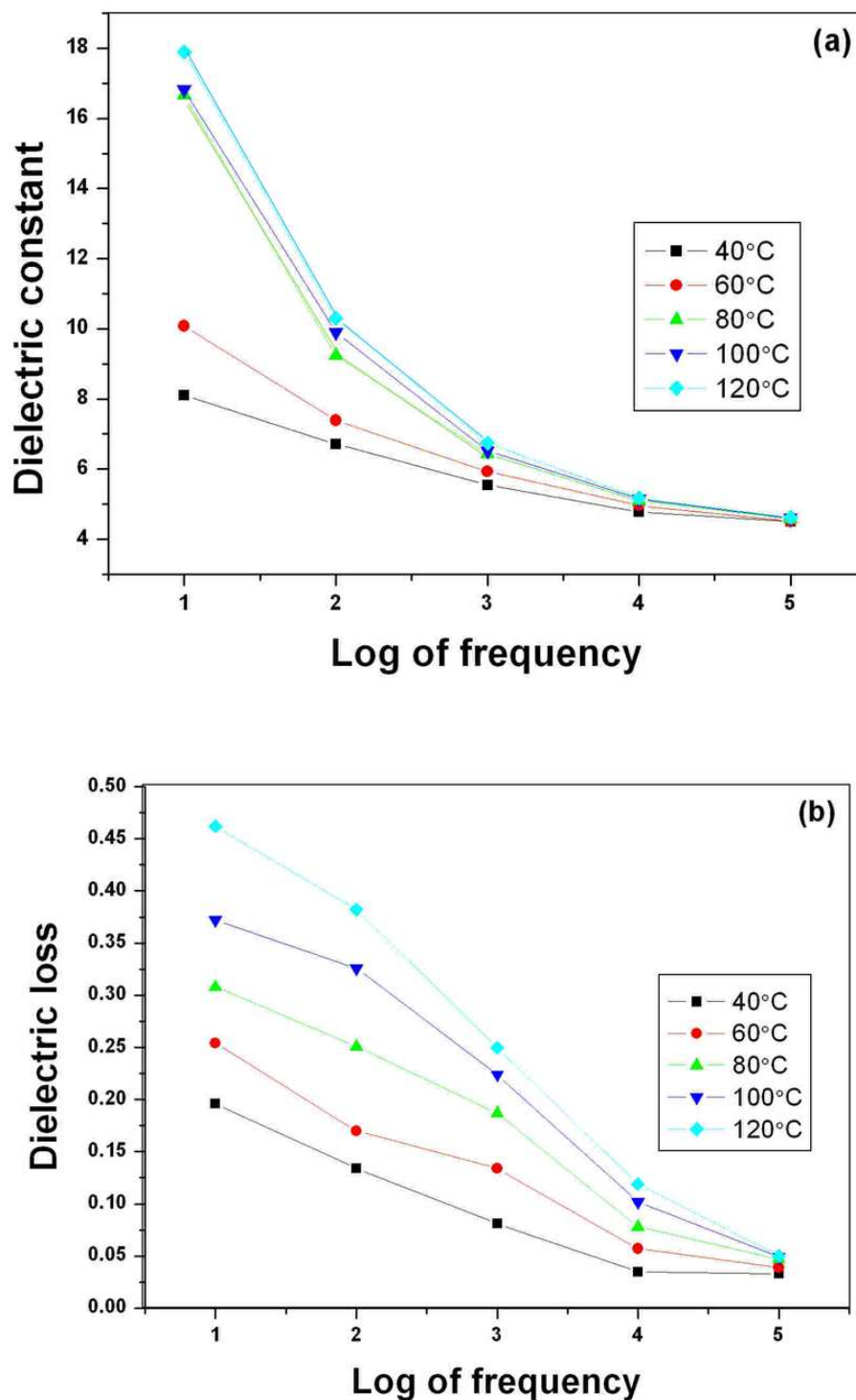


**Figure 6.5** (a) Dielectric constant and (b) dielectric loss as function of frequency with temperature for SR-grown LPZ crystal.

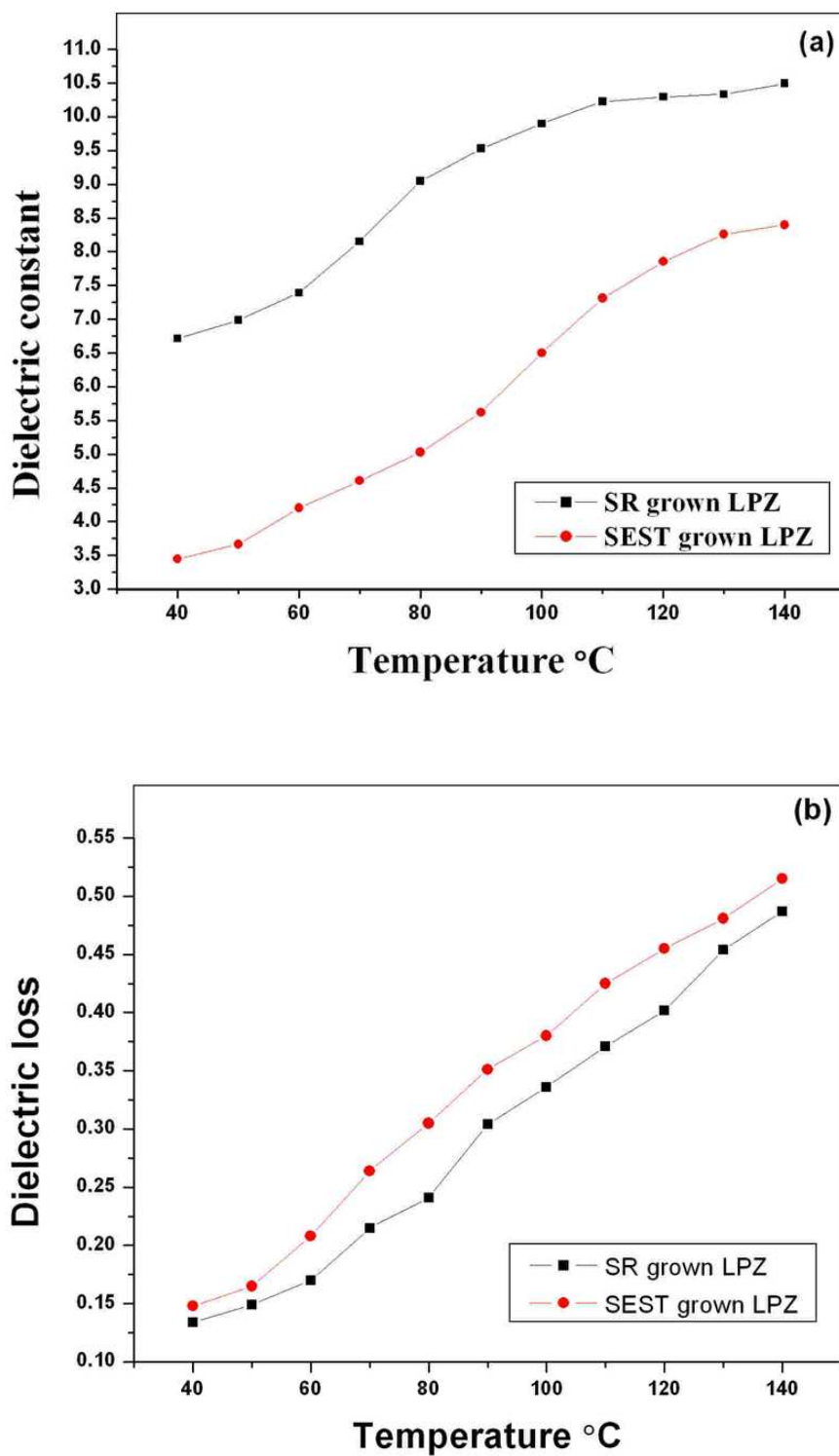


**Figure 6.6** (a) Dielectric constant and (b) Dielectric loss curve of LPZ crystals grown by conventional and SR method at 1 kHz frequency.

#### 6.4.6 Transmittance spectral studies

A good optical transmittance is very desirable in an NLO crystal since the absorptions, if any, in an NLO material near the fundamental or the second harmonic of a Nd:YAG laser, 1064 and 532 nm respectively, will lead to loss of conversion efficiency of SHG. Also the UV range from 200 to 400 nm is very important for the realization of SHG output in this range using diode laser. In order to find the transmission range to know the suitability for optical application, the recorded optical transmission spectra were recorded and shown in Figure 6.7. It is observed that the crystals have good transmission in the entire visible and IR region. The lower UV cut off wavelength is at 230 nm. The transmittance of the SR method as grown LPZ crystal of the thickness 10 mm is  $\sim 71\%$ . The improvement in the percentage of transmission may be attributed to the reduction of scattering from point and line defects of the crystal. Reduced transparency in the lower wavelength region reflects the incorporation of impurities that may be potentially coming from the slow dissolution of the borosilicate glass by the growth solution. In the case of conventional SEST, the transmission is nearly  $\sim 60\%$  for the 1 mm thick sample and  $\sim 35\%$  for as grown 4 mm thick sample. Usually the transmitted light intensity decreases when the optical path increases. In order to confirm the reproducibility, the transmittance studies were repeated several times using different parts of the grown crystals and the same results were observed. The absence of absorption of light in the visible region is an intrinsic property of all amino acids (Pritula, 1993). Absence of absorption in the region between 230 and 1100 nm shows that this crystal could be used for optical window applications.

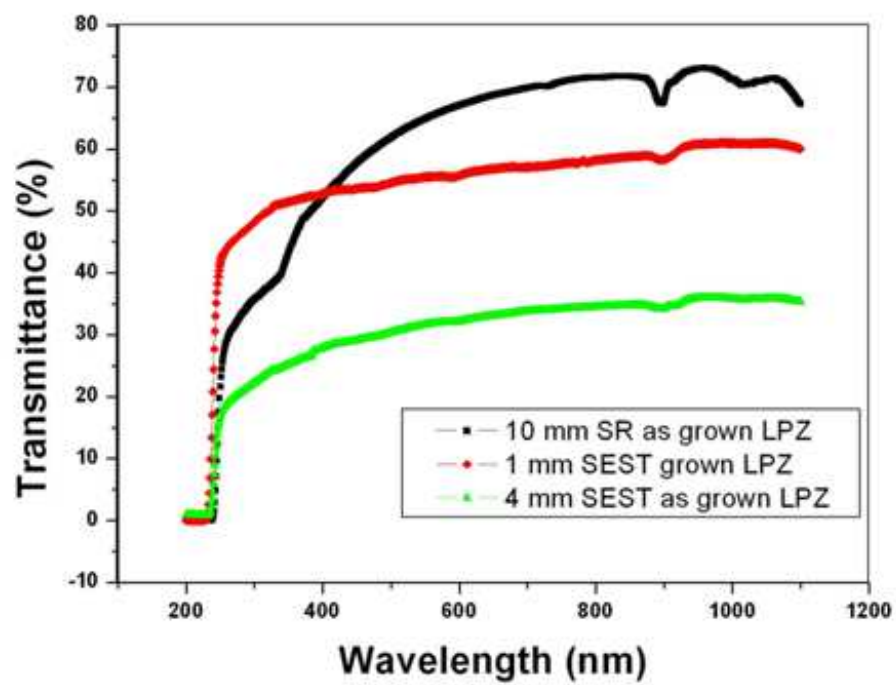
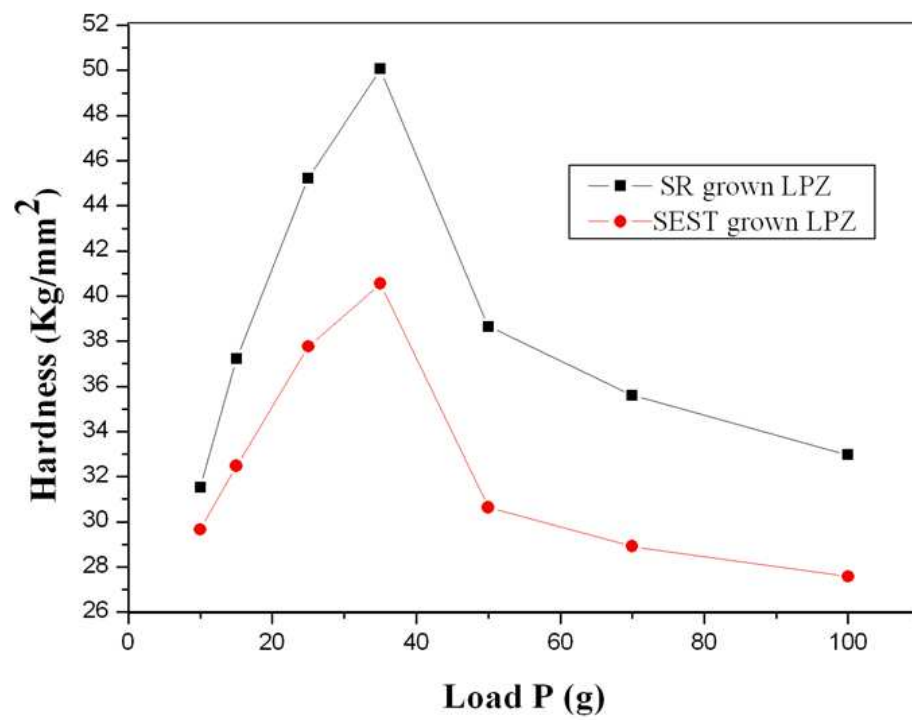


Figure 6.7 UV-Visible analysis of LPZ.

### 6.4.7 Measurement of microhardness

As the hardness properties are related to the crystal structure of the material, microhardness studies have been carried out to understand the plasticity of the crystals. Also, the hardness of the crystal is dependent on the type of chemical bonding, which may differ along the crystallographic directions. Figure 6.8 shows the  $H_v$  of the grown LPZ crystals and the values were plotted as a function of applied load. The hardness of the SR method grown sample increases from 31.5 to 50.1 kg/mm<sup>2</sup> when increasing the load from 10 to 35 g. After the load reaches 35 g, the hardness decreases with increase of load and finally reaches the saturation level. Similar result was observed for the SEST grown LPZ crystals in which the  $H_v$  increases from 29.7 to 40.6 kg/mm<sup>2</sup> when increasing the load from 10 to 35 g. The  $H_v$  values decrease after load reaches to 35 g and it changes only slightly after that when increasing the load up to 100 g. For an indentation load of above 100 g, cracks were initiated on the conventional SEST and SR methods grown LPZ crystal surface, around the indentation. Due to the application of mechanical stress by the indenter, dislocations are generated locally at the region of indentation. Hence larger hardness value for the SR method growth LPZ crystal indicates greater stress required to form dislocation thus confirming greater crystalline perfection. The mechanical strength of the SR grown LPZ crystal reveals that the crystal has a good hardness and it is useful for any applications. An increase in the mechanical strength will have significant effect on fabrication and processing such as ease in polishing and less wastage due to cracking/breakage while polishing (Senthil Pandian, 2010). The high mechanical hardness contributes to attractiveness of the present compound in practical applications.



**Figure 6.8** Vickers microhardness analysis of LPZ.

### 6.4.8 SHG conversion efficiency

Quantitative measurement of the conversion efficiency of the crystal was determined using the powder technique developed by Kurtz and Perry (Kurtz and Perry, 1968). The SHG efficiency varies with the particle size of the powder sample (Porter et al., 2001). Samples were prepared by powdering LPZ grown by SR and SEST methods whose SHG was calculated with KDP as reference material. The intensity of SHG gives an indication of the nonlinear optical behavior of the material (Rajesh, 2009). From the SHG measurement it is found that the SR-grown LPZ possesses slightly enhanced SHG efficiency. The generation of the second harmonics was confirmed by green radiation of 532 nm in both conventional and SR method grown LPZ samples. The SHG conversion efficiency of the both crystals grown from the SR method and SEST is about the same as that of KDP. Other semi-organic material such as L-APCl, L-AHCl, L-AHBr and L-AHClBr were only 0.3 - 0.4 times that of KDP (Mallik, 2005; Pal et al., 2002).

## 6.5 Conclusions

Single crystal LPZ, a potential semiorganic NLO material, has been successfully grown by Sankaranarayanan-Ramasamy method. The size of the grown crystal is  $70 \times 20 \times 10 \text{ mm}^3$ . The cell parameter was confirmed and it agrees with the reported values. The HRXRD analysis confirms that the crystal grown by the SR method has good crystalline perfection compared to that by the conventional method. Etching study reveals that the EPD of the SR method grown LPZ crystal is less compared to the conventional method grown crystal. Dielectric study showed that the higher dielectric constant and lower value of dielectric loss are due to less defects present in SR method grown LPZ crystal. The SR method grown

LPZ crystal shows higher piezoelectric charge coefficient because of having better crystalline quality. Vickers microhardness measurement reveals that the crystals grown by the SR method have a higher hardness than those by the conventional method. The SHG conversion efficiency of both crystal samples is approximately equal to that of standard KDP. The study will be useful to grow large size single crystal with higher crystalline perfection, higher hardness and good optical quality for SHG applications.

## 6.6 Acknowledgements

The authors are thankful to Dr. G. Bhagavannarayana, Head of Material Characterization Division, National Physical Laboratory, New Delhi, for the HRXRD study, Dr. C.K. Mahadevan, Physics Research Centre, S.T. Hindu College, Nagercoil, for the dielectric measurement and Dr. Binay Kumar, Department of Physics and Astrophysics, University of Delhi, India, for piezoelectric studies. The authors are also very much thankful to Prof. K. Kishan Rao, Department of Physics, Kakatiya University, Warangal, for microhardness measurement and etching studies.

## 6.7 References

- Anandha Babu, G., Ramasamy, P., (2009). Synthesis, crystal growth and characterization of novel semiorganic nonlinear optical crystal: Dichlorobis(l-proline)zinc(II) Materials. **Chemistry and Physics** 113(2-3): 727.
- Balamurugan, S., Bhagavannarayana, G. and Ramasamy, P. (2008). Growth of unidirectional potassium dihydrogen orthophosphate single crystal by SR method and its characterization. **Materials Letters**. 62(24): 3963.

- Balamurugan, S., Ramasamy P., Sharma, S.K., Yutthapong Inkong and Prapun Manyum. (2009). Investigation of SR method grown  $\langle 001 \rangle$  directed KDP single crystal and its characterization by high-resolution X-ray diffractometry (HRXRD), laser damage threshold, dielectric, thermal analysis, optical and hardness studies. **Materials Chemistry and Physics**. 117(2-3): 465.
- Balamurugan, S., Ramasamy, P. (2008) Bulk growth of (101) KDP crystal by Sankaranarayanan-Ramasamy method and its characterization. **Materials Chemistry Physics**. 112: 1.
- Batterman, B.W., Cole, H. (1964). Dynamical diffraction of x rays by perfect crystals. **Reviews of Modern Physics**. 36(3): 681.
- Boomadevi, S., Dhanasekaran, R.(2004) **Journal of Crystal Growth**. 261(1): 70.
- Ge Wenwei, et al. (2008) Growth and characterization of  $\text{Na}_{0.5}\text{Bi}_{0.5}\text{TiO}_3\text{-BaTiO}_3$  lead-free piezoelectric crystal by the TSSG method **Journal of Alloys and Compounds**. 456(1-2): 503.
- Jiang, M.H., Fang, Q. (1999). Organic and Semiorganic Nonlinear Optical Materials. **Advanced. Materials**. 11(13): 1147.
- Jingran Su, Youting Song, Daofan Zhang and Xinan Chang. (2009). **Powder diffraction**. 24: 234.
- Kandasamy, A., Siddeswaran, R., Murugakoothan, P., Suresh Kumar, P. and Mohan, R. (2007). Synthesis, growth, and characterization of L-Proline Cadmium Chloride Monohydrate (L-PCCM) crystals: A new nonlinear optical material. **Crystal Growth and Design** 7(2): 183.

- Kurtz, S.K., Perry, T.T. (1968). A powder technique for the evaluation of nonlinear optical materials. **Journal of Applied Physics**. 39(8): 3798.
- Lal, K., Bhagavannarayana, G. (1989). A high-resolution diffuse X-ray scattering study of defects in dislocation-free silicon crystals grown by the float-zone method and comparison with Czochralski-grown crystals. **Journal of Applied Crystallography**. 22(3): 209.
- Lin, H.M., Chen, Y.F., Shen, J.L. and Chou, W.C. (2001). Dielectric studies of  $\text{Cd}_{1-x-y}\text{Zn}_x\text{Mn}_y\text{Te}$  crystals. **Journal of Applied Physics**. 89(8): 4476.
- Lydia Caroline, M., Kandasamy, A., Mohan, R. and Vasudevan, S. (2009). Growth and characterization of dichlorobis l-proline Zn(II): A semiorganic non-linear optical single crystal. **Journal of Crystal Growth** 311(4): 1161.
- Mallik, T., Kar, T. (2005). Optical, thermal and structural characterization of an NLO crystal, l-arginine perchlorate. **Journal of Crystal Growth**. 274(1-2): 251.
- Myung, S., Pink, M., Baik, M.H., Clemmer and David, E. (2005). DL-Proline. **Acta Crystallographica Section C** 61(8): o506.
- Pal, T., Kar, T., Xin Qiang, W., Guang Ying, Z., Dong, W., Xiu Feng, C. and Zhao He, Y. (2002). Growth and characterization of nonlinear optical material, LAHClBr - A new member of L-arginine halide family. **Journal of Crystal Growth**. 235(1-4): 523.
- Porter, Y., Kang Min, O.K., Bhuvanesh, N. S. P. and Shiv Halasyamani, P. (2001). Synthesis and characterization of  $\text{Te}_2\text{SeO}_7$ : A powder second-harmonic-generating study of  $\text{TeO}_2$ ,  $\text{Te}_2\text{SeO}_7$ ,  $\text{Te}_2\text{O}_5$ , and  $\text{TeSeO}_4$ . **Chemistry of Materials**. 13(5): 1910.

- Pritula, I.M., Veliknov and Yu, N. (1993). Proc. **SPIE**. 202: 3793.
- Rajesh, P., Ramasamy, P. and Bhagavannarayana, G. (2009). Effect of ammonium malate on growth rate, crystalline perfection, structural, optical, thermal, mechanical, dielectric and NLO behaviour of ammonium dihydrogen phosphate crystals. **Journal of Crystal Growth**. 311(16): 4069.
- Rajesh, P., Ramasamy, P. (2009). A study on optical, thermal, mechanical, dielectric, piezoelectric and NLO properties of unidirectional ammonium chloride added ammonium dihydrogen phosphate crystal. **Materials Letters**. 63(26): 2260.
- Rajesh, P., Ramasamy, P. (2009). Growth of dl-malic acid-doped ammonium dihydrogen phosphate crystal and its characterization. **Journal of Crystal Growth**. 311(13): 3491.
- Ramesh Babu, R., Vijayan, N., Gopalakrishnan, R. and Ramasamy, P. (2006). Growth and characterization of L-lysine monohydrochloride dihydrate (L-LMHCl) single crystal **Crystal Research and Technology**. 41(4): 405.
- Sankaranarayanan, K., Ramasamy, P. (2005). Unidirectional seeded single crystal growth from solution of benzophenone. **Journal of Crystal Growth**. 280(3-4): 467.
- Senthil, A., Ramesh Babu R., Balamurugan, N. and Ramasamy, P. (2009). Unidirectional growth of largest L-LMHCl dihydrate crystal by SR method. **Journal of Crystal Growth**. 311(3): 544.

- Senthil Pandian, M., Balamurugan, N., Bhagavannarayana, G. and Ramasamy, P. (2008). Characterization of  $\langle 010 \rangle$  directed KAP single crystals grown by Sankaranarayanan-Ramasamy (SR) method. **Journal of Crystal Growth**. 310(18): 4143.
- Senthil Pandian, M., Balamurugan, N., Ganesh, V., Raja Shekar, P.V., Kishan Rao K. and Ramasamy, P. (2008). Growth of TGS single crystal by conventional and SR method and its analysis on the basis of mechanical, thermal, optical and etching studies. **Materials Letters**. 62(23): 3830.
- Senthil Pandian, M., Ramasamy, P. (2009). Unidirectional growth of  $\langle 001 \rangle$  tetraglycine barium chloride (TGBC) single crystal by Sankaranarayanan-Ramasamy method **Journal of Crystal Growth**. 311(3): 944.
- Senthil Pandian, M., Ramasamy, P. (2010). Conventional slow evaporation and Sankaranarayanan-Ramasamy (SR) method grown diglycine zinc chloride (DGZC) single crystal and its comparative study **Journal of Crystal Growth**. 312(3): 413.
- Senthil Pandian, M., Urit Charoen In, Ramasamy, P., Prapun Manyum, Lenin, M. and Balamurugan, N. (2010). Unidirectional growth of sulphamic acid single crystal and its quality analysis using etching, microhardness, HRXRD, UV-visible and Thermogravimetric-Differential thermal characterizations. **Journal of Crystal Growth**. 312(3): 397.
- Uma Devi, T., Lawrence, N., RameshBabu, R., Selvanayagam, S., Helen Stoeckli-Evans and Ramamurthi, K. (2009). Synthesis, crystal growth and characterization of l-Proline lithium chloride monohydrate: A new semiorganic nonlinear optical material. **Crystal Growth and Design**. 9(3): 1370.

# CHAPTER VII

## CONCLUSIONS

In the present investigation, single crystal of inorganic (SA), organic (LAM, LAMD), and semi-organic (LPZ) crystals were grown by the conventional SEST and SR method. Identical samples prepared both the conventional SEST and SR method with similar orientation were subjected to HRXRD, etching study, dielectric measurement, piezoelectric measurement, UV-Vis NIR analysis, Vickers microhardness measurement and SHG conversion efficiency in order to determine their properties and the results were discussed.

An inorganic single crystal, (100) directed SA with 150 mm length and 35 mm diameter were grown by the SR method. Etch pit density was less in the SR method grown crystal compared to conventional method grown crystal. The Vicker's hardness value of SR method grown SA crystal was higher than that of the conventional slow evaporation method grown crystal. Full width at half maximum value of the SR method grown SA crystal, which was 5.5 arc s, showed that the crystalline perfection was extremely good. Full width at half maximum of the conventional method grown SA crystal contains two additional peaks, which were 13 and 18 arc sec away from the main peak and these two additional peaks correspond to two internal structural very low angle boundaries. The SA crystals grown by the SR method have 4% higher transmittance than the conventional method grown crystal. SA crystal decomposed at 219 °C. Investigations showed that the SR method grown SA crystal had better perfection than the conventional method grown SA crystal.

An organic single crystal, (011) directed LAM with an 18 mm diameter and 32 mm length were successfully grown by SR method. The cell parameter was confirmed and it agrees with the reported values. The HRXRD analysis showed that the crystal grown by the SR method had good crystalline perfection compared to the crystal grown by the conventional method. Etching study revealed that the EPD of the SR method grown LAM crystal was less compared to the conventional method grown crystal. Dielectric study showed that the higher dielectric constant and lower value of dielectric loss were due to less defects present in the SR method grown LAM crystal. The crystals have good thermal stability up to 158 °C. The transmittance of the SR method grown LAM crystal was 7% higher than the conventional SEST grown crystal. Vickers microhardness measurement showed that the crystals grown by the SR method have a higher hardness than crystals grown by the conventional method. HRXRD, chemical etching, dielectric constant, dielectric loss, optical transmittance and mechanical strength studies showed that the SR method was a capable method to grow crystals of good crystalline perfection with high optical quality and good mechanical stability.

An organic single crystal, (001) directed LAMD with A 65 mm length and 15 mm diameter were successfully grown by SR method. X-ray single-crystal diffraction confirms the lattice parameter of the LAMD grown crystal. Morphology investigation revealed face appearing on the SEST-grown LAMD crystal. The SR method grown crystal contained a very low angle boundary and the low FWHM values showed that the crystalline perfection was reasonably good. Dielectric study showed that the higher dielectric constant and lower value of dielectric loss were due to less defects present in the SR method grown LAMD crystal. The SR method grown LAMD crystal showed higher piezoelectric charge coefficient because of having better crystalline quality. Optical transmittance indicated that

the transmission region of the SR-grown LAMD crystal was from 320 - 1100 nm which was sufficient for its SHG efficiency and the transmittance was more than 80% with the UV cutoff at 320 nm. Vickers microhardness measurement revealed that the crystals grown by the SR method had a higher hardness than the conventional method. The SHG conversion efficiency of both crystal samples was approximately 1.4 times greater than that of standard KDP crystal. The study will be useful to grow unidirectional large size single crystal with higher crystalline perfection, higher hardness and good optical quality for SHG applications.

A semi-organic single crystal, (010) directed LPZ with the size of  $70 \times 20 \times 10 \text{ mm}^3$  were successfully grown by SR method. The cell parameter was confirmed and it agrees with the reported values. The HRXRD analysis confirmed that the crystal grown by the SR method has good crystalline perfection compared to the crystal grown by the conventional method. Etching study revealed that the EPD of the SR method grown LPZ crystal was less compared to the conventional method grown crystal. Dielectric study showed that the higher dielectric constant and lower value of dielectric loss were due to less defects present in SR method grown LPZ crystal. The SR method grown LPZ crystal showed higher piezoelectric charge coefficient because of having better crystalline quality. Vickers microhardness measurement revealed that the crystals grown by the SR method had a higher hardness than the conventional method. The SHG conversion efficiency of both crystal samples was approximately equal to that of standard KDP crystal. The study would be useful to grow large size single crystal with higher crystalline perfection, higher hardness and good optical quality for SHG applications.

## CURRICULUM VITAE

The author, Mr. Urit Charoen-In, was born on the 8<sup>th</sup> February 1981 in Borabu District of Mahasarakham Province, Thailand. In March, 2003, he obtained his Bachelor degree in Physics from the Department of Physics, Faculty of Science at Mahasarakham University, Mahasarakham. In May, 2003, he started his post graduate study at the education department and graduated in 2004. In May 2005, he continued his education, by pursuing his Doctoral's degree at the School of Physics, Institute of Science, Suranaree University of technology. His Ph.D. thesis was entitled **GROWTH OF SOME INORGANIC, ORGANIC AND SEMI-ORGANIC NONLINEAR OPTICAL CRYSTALS BY SANKARANARAYANAN-RAMASAMY METHOD AND THEIR CHARACTERIZATION** which was under the supervision of Assoc.Prof. Dr. Prapun Manyum. His Ph.D. study was supported by Mahasarakham University. Urit successfully obtained his Ph.D. degree in 2010.